Thèse de Doctorat de l'Université de Strasbourg

Ecole doctorale des Science Chimiques
Institut de Science et d'Ingénierie Supramoléculaire

présentée par Diana Lieber

Functional Assays for Screening Antibody Activity in Droplet-based Microfluidics

Pour obtenir le grade de

Docteur de l'Université de Strasbourg

Composition du jury

Prof. Andrew Griffiths :	Directeur de Thèse
Dr. Pierre Martineau :	Rapporteur
Prof. Michael Köhler :	Rapporteur
Prof. Jacques Haiech:	Examinateur

30 Novembre 2010

ACKNOWLEDGEMENTS

I would like to thank Prof. Andrew GRIFFITHS for giving me the opportunity to work in his laboratory and do my doctoral studies in the LBC group. Thank you for your sustained encouragement and motivation. Your never-ending enthusiasm was always a good example for me.

My thanks go to Dr. Christoph MERTEN for the supervision of my PhD and the assistance of my work with scientific knowledge and ideas. I also want to say thank you to everybody in our 'subgroup' for all the experience I could make.

It is a great honor for me that Dr. Pierre MARTINEAU, Prof. Michael KÖHLER and Prof. Jacques HAIECH agreed to participate in the evaluation of my doctoral thesis. I am sincerely and deeply grateful for their time and patience.

I acknowledge thankful the receipt of funding from the *Fonds der Chemischen Industrie* (Germany) and *Région Alsace* (France) which allowed me to carry out my doctoral studies decribed in this thesis.

I appreciated and enjoyed so much being in the aquarium with you guys. Many, many, many thanks for all the laughing and talking and throwing the little yellow ball. It was such fun with you, you made the hard times bearable. I also want to express my thanks to all members of the LBC lab. Thank you for all the things I learned, scientifically and personally. Working with you was a great experience that I never would want to miss.

Danke an meine Familie und meine besten Freunde, ohne EUCH wäre ich nicht so weit gekommen. Durch eure Unterstützung und Motivation, eure Kraft und Freude habe ich nie aufgegeben. Ich bin dankbar, dass ihr hinter mir steht und immer an mich glaubt.

Thank you, Ali, for going together with me a part of the way. From the bottom of my heart I wish you the strength for the rest of it.

» … HIER UND DA BEGREIFEN WIR ES UND LACHEN DARÜBER, WIE GERADE NOCH DIE BESTE WISSENSCHAFT UNS AM BESTEN IN DIESER VEREINFACHTEN, DURCH UND DURCH KÜNSTLICHEN, ZURECHTGEDICHTETEN, ZURECHTGEFÄLSCHTEN WELT FESTHALTEN WILL, WIE SIE UNFREIWILLIG-WILLIG DEN IRRTUM LIEBT, WEIL SIE, DIE LEBENDIGE – DAS LEBEN LIEBT! «

FRIEDRICH NIETZSCHE

» AUF WELCHEN STANDPUNKT DER PHILOSOPHIE MAN SICH HEUTE AUCH STELLEN MAG: VON JEDER STELLE AUS GESEHN IST DIE IRRTÜMLICHKEIT DER WELT, IN DER WIR ZU LEBEN GLAUBEN, DAS SICHERSTE UND FESTESTE, DESSEN UNSER AUGE NOCH HABHAFT WERDEN KANN... «

FRIEDRICH NIETZSCHE

» VOICI MON SECRET. IL EST TRES SIMPLE: ON NE VOIT BIEN QU'AVEC LE COEUR. L'ESSENTIEL EST INVISIBLE POUR LES YEUX. ... C'EST LES TEMPS QUE TU AS PERDU POUR TA ROSE QUI FAIT TA ROSE SI IMPORTANTE. ... LES HOMME ONT OUBLIE CETTE VERITE. MAIS TU NE DOIS PAS L'OUBLIER. TU DEVIENS RESPONSABLE POUR TOUJOURS DE CE QUE TU AS APPRIVOISE. TU ES RESPONSABLE DE TA ROSE ... «

ANTOINE DE SAINT-EXUPÉRY

» WHAT IF YOU SLEPT? AND WHAT IF, IN YOUR SLEEP, YOU DREAMED? AND WHAT IF, IN YOUR DREAM, YOU WENT TO HEAVEN AND THERE PLUCKED A STRANGE AND BEAUTIFUL FLOWER? AND WHAT IF, WHEN YOU AWOKE, YOU HAD THE FLOWER IN YOUR HAND? AH, WHAT THEN? «

SAMUAL TAYLOR COLERIDGE

Gewidmet meiner Oma
und meinen Groβeltern

Table of Contents

List of Abbreviations

Δct	cytoplasmic tail
µg	microgram
µL	microliter
ACE	Angiotensin I-converting enzyme
AChE	Acetylcholine Esterase
CCR5	C-C motiv chemokine receptor type 5
CD4	cluster of differentiation 4
d	day(s)
DMEM	Dulbecco's Modified Eagles Medium
DMP	dimorpholinophosphate
DMSO	dimethyl sulfoxid
DNA	deoxyribonucleic acid
E.coli	Escherichia coli
elec	Electric eel (*Electrophorus electricus)*
FBS	fetal bovine serum
g	gram
gp120	glycoprotein 120
h	hour
HEK	human embryonic kidney
lacZ	β-galactosidase
LB	Luria-Bertani
LB-AMP	Luria-Bertani-ampicillin
min	minutes
mL	milliliter
MLV	murine leukemia virus
mm	millimeter
mM	millimolar
ng	nanogram
o/n	over night

OD	optical density
PBS	phosphate buffered saline
PEG	polyethylenglycol
PFPE	polyfluorinated polyether
PMT	photomultiplier
x g	relative centrifugal force
rpm	rounds per minute
RPMI	Roswell Park Memorial Institute
s	seconds
tACE	truncated Angiotensin I-converting enzyme
VSV-G	vesicular stomatitis virus G-protein
w/v	weight per volume
w/w	weight per weight
X-gal	5-bromo-4-chloro-3-indolyl—galactopyranoside

ABSTRACT

High-throughput, cell-based assays require small sample volumes to reduce assay costs and to allow for rapid sample manipulation. However, further miniaturisation of conventional microtiter plate technology is problematic due to evaporation and capillary action. To overcome these limitations, we developed droplet-based microfluidic platforms in which cells are grown in aqueous microcompartments separated by an inert perfluorocarbon carrier oil. Furthermore, this system allowed for an automated analysis of individual compartments subsequent to an incubation period as required for high-throughput, cell-based assays.

In addition, we focused on the development of functional assays for screening antibody activity, e.g. neutralisation of HIV or the inhibition of ACE-1. Common high throughput approaches for antibody screening use phage display or hybridoma cells. Phage display is powerful but based on binding properties rather than neutralising effects. Hybridoma cells allow for direct screening of neutralising activity, but are very restricted in the number of clones that can be screened due to their generation and proliferation as required for conventional screens. The aim of this study was the development of novel screening technology with the ultimate goal of screening single antibody-releasing cells (hybridoma cells). This system should also allow for direct B-cell screening. Once established, this technology could be used for the screening/ selection of many more therapeutic antibodies.

GENERAL INDRODUCTION

HIGH THROUGHPUT SCREENING FORMATS: MICROTITER PLATE-, MICROARRAY-BASED AND MICROFLUIDIC SYSTEMS

In modern drug discovery, high throughput screening (HTS) has become a key activity. Over the last decade, the number of targets available for drug screening increased dramatically. Not only that new technologies such as combinatorial chemistry and automated synthesis have generated a huge amount of new molecules, but also major advances in genomics and proteomics fostered this variety. Therefore, HTS is a primary tool used in pharmaceutical and biotechnology companies to identify hit compounds in the early phases of drug discovery.

The acceleration of drug discovery is mainly achieved by miniaturisation, decreasing time and costs of compound screening. In early stages, HTS was perfomed in 96-well microtiter plates where libraries up to 100,000 molecules could be screened in one week (Pereira & Williams, 2007). Further miniaturisation of reaction volumes, using 384- and 1.536-well plates (multiples of 96) resulted in screening efficiencies of 100,000 compounds per day. 1,536-well plates offer a good balance between high throughput, low costs and reliability. This format even allows for use with mammalian cell-based assays (Maffia et al., 1999). Microplates with higher density (3,456 and 9,600 wells) provide a tool for ultra high throughput screening and enable to screen much more then 100,000 molecules per day. For example, bacterial (discrete compound library) and enzyme (combinatotial bead-based) screens could be performed successfully (Oldenburg et al., 1998).

A substantial feature of HTS is automation. Integrated robot systems, data processing and control software, liquid handling devices and sensitive detectors allow a fast data-collection process, while bioinformatics are used to store, process, analyse and access the enormous amount of data.

However, with the miniaturisation of screening assays several problems emerge such as capillary action, evaporation effects, cross-contamination, formation of foam and

bubbles (Berg et al., 2001). Moreover, this technology involves high instrument and maintenance costs limiting the accessibility for academic researchers.

HTS methods can be combined with microarray technology providing a miniaturised, system for biological and chemical processes. Microarray technologies involve for example: DNA microarrays, protein microarrays, antibody microarrays (Chaga, 2008), cellular microarrays (Chen & Davis, 2006), tissue microarrays and chemical compound microarrays.

The experimental set up of this method utilises probes (biological material or chemical compounds) immobilised in a 2D grid on a chip (solid support such as a membrane, a polymer or glass). Labeled targets (e.g. fluorescence or chemiluminescence) are extracted from the liquid media and retained on the chip by molecular hybridisation. The generated signal depends on the strength of the hybridisation and is measured by automated readout systems. The signal intensity and the position of the spot on the chip identify probe-target interactions.

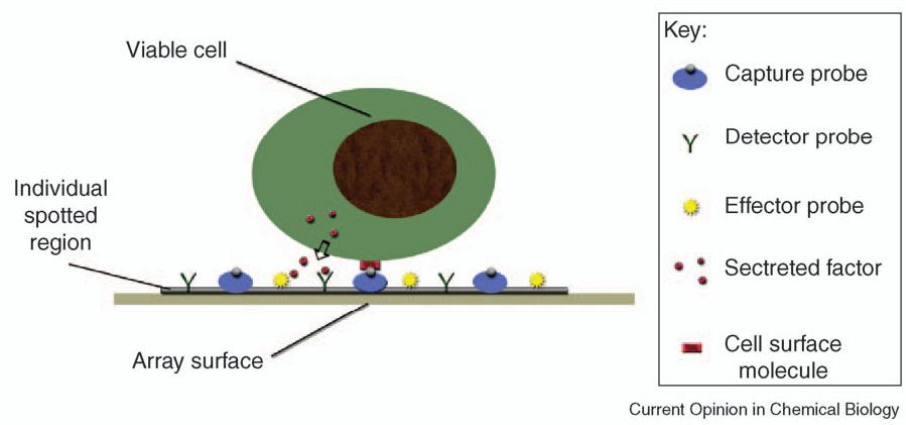

Figure 1: **Cellular microarray diagram.** Cellular microarrays can be printed with a few spots to thousands of spots per array. A spot can be small (< 10 microns in diameter) to large (> 500 microns in diameter), with the larger spots capable of capturing thousands of cells on a single spot. Each spot is printed with a single reagent, or mixtures of multiple reagents. Capture probes (antibodies, recombinant proteins), detector probes (antibodies, receptors) and effector probes (cytokines, antibodies, nucleic acids) are the different classes of reagents used to print cellular microarrays. (illustration from Chen & Davis, 2006; Figure 2)

More sophisticated arrays like cellular microarrays allow for the understanding of cellular behavior in response to defined signals. Analysis of cell populations for their

composition and phenotype can be performed on the single cell level (Chen & Davis, 2006, Figure 1).
Nevertheless, microtiter plates and microarrays exhibit limitations (evaporation of small liquid volumes and achievable speed of fluid dispensing) that can be overcome with fluidic systems. So called microfluidic chips offer a novel high througput screening technology. These systems are divided into one-phase and two-phase microfluidics and are explained in general in the following and for single cell analysis in the introduction of Chapter I.

Microfluidics allows for controlling and manipulating fluids in microchannels with dimensions on the μm scale. Such miniaturised systems deal with sample volumes of nanoliters, picoliters and femtoliters. The basic idea of microfluidic systems for biological, medical and chemical applications is the integration of many assay operations on a single chip. Miniaturisation of functional assays provides several advantages, like decreasing labor and costs and saving time as well as increasing throughput.
Microfluidic approaches for biological applications developed with the boom of genomics in the 1980s, the demand of microanalysis in molecular biology and the need for high throughout screening in drug discovery. Emerging methods, like molding techniques (Aumiller et al., 1974) and soft lithography (Xia & Whitesides, 1998) fostered integration of microfluidic technology into biological experiments. Especially the use of soft lithography in polydimethylsiloxane (PDMS) (McDonald et al., 2000) offered a cheap and simple way to fabricate sophisticated 3D microfluidic devices for biological and biochemical applications. PDMS is a chemically inert, transparent polymer and hence compatible with conventional optical detection methods. In addition, it is permeable for non-polar gases (O_2, N_2 and CO_2) being substantial for applications using living mammalian cells. Moreover, using PDMS, the fabrication of pumps, valves and mixers became possible (Figure 2; Thorsen et al., 2002). Because of its elastomeric nature these tools can be easily added to microchips by multilayer soft lithography.

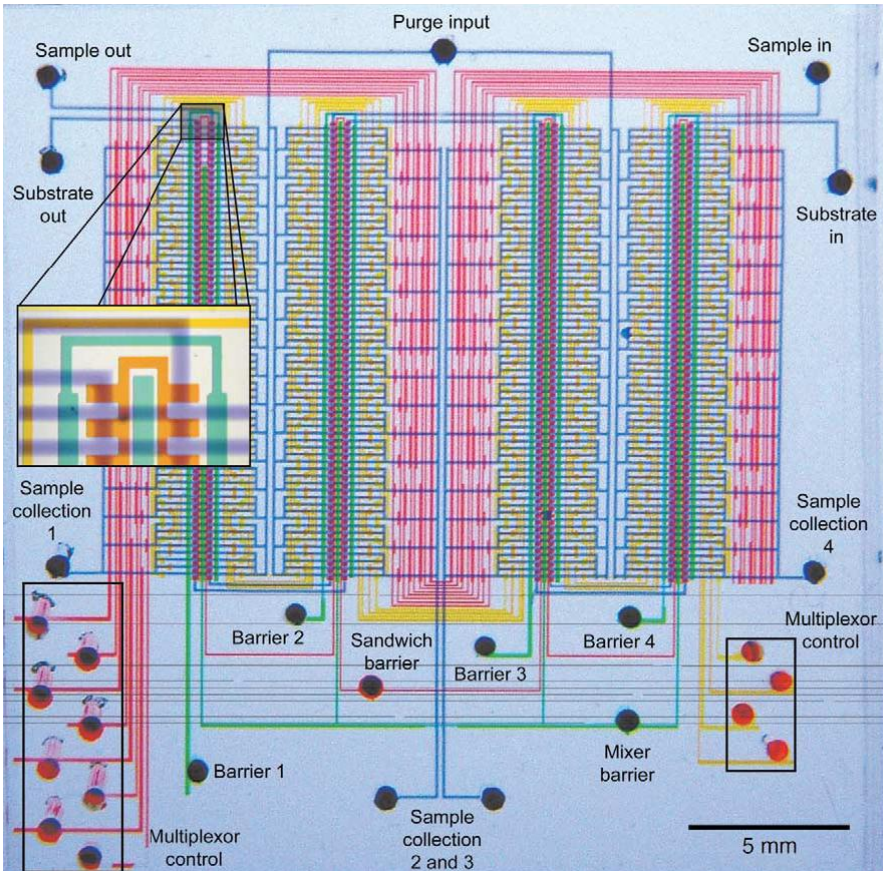

Figure 2: **Large-scale integration microfluidic chip.** The chip has 2056 active valves and 256 distinct sub-nanoliter reaction chamber. Valve and flow structures were filled with food dyes to visualize channels and sub-elements (Thorsen et al., 2002).

The physical properties of fluids on the microscale change fundamentally compared to macroscopic fluid movements. Usually, microfluidic technology is categorised into continues flow- and droplet-based systems. The current paragraph deals with continues flow-based, so called one-phase microfluidics is explained. Droplet-based (two-phase) systems are described below.

The flow in microfluidic channels is laminar and defined by the Reynolds number, Re:

$$Re = \frac{\rho \upsilon l}{\eta}$$

where ρ is the fluid density, υ the fluid velocity, l the channel length and η the viscosity of the fluid (Brody et al., 1996).

The Reynolds number expresses the ratio of inertial forces (mass acceleration or motion) to viscous forces (pressure due to shear stress). Laminar flow occurs at low Reynolds numbers, < 1. In microfluidic channels, Re << 1 are predominant and inertial forces are small enough to become irrelevant. Therefore, the flow in microfluidic devices is smooth, predictable and laminar. Through a straight circular pipe, the transition to turbulent flow occurs at Re between 2000 and 3000 (Squires & Quake, 2005). Reynolds numbers above 4000 refer to turbulent flow. In between, transition flows (laminar and turbulent) appear; this depends on factors, such as pipe roughness and flow uniformity.

Two important characteristics of laminar flow are: first, two parallel fluid streams do not mix convectively and second, dispersion of solutes along the channel is large due to parabolic flow pattern (Figure 3A, Song et al., 2003b).

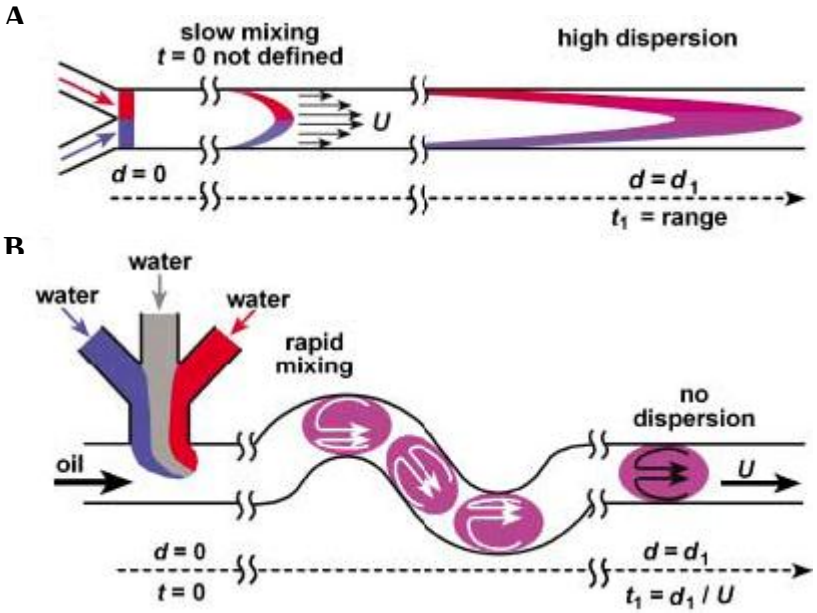

Figure 3: **Schematic comparison of flow in a single phase and droplet-based microfluidic system. (A)** Two aqueous reagents (read and blue) get in contact at d = 0 and t = 0. In laminar flow fluids show a parabolic flow profile (Taylor-Aris dispersion) and do not mix convectively. $t \neq d/U$. **(B)** Two aqueous reagents which are located in plugs mix rapidly and have low dispersion. t = d/ U. (Song et al., 2003b)

The parabolic flow profile of laminar flow, called after Taylor and Aris, causes high dispersion along the channel walls (Taylor, 1953; Aris, 1956; Figure 3A). In addition, without turbulences mixing only occurs due to diffusion (random Brownian motion of

individual particles in the fluid) but not advection (larger-scale motion of matter in the fluid). This can be overcome, when forming plugs from two liquid streams by injecting them into immiscible oil and moving them through winding channels, fluids are mixed and dispersion is eliminated (Figure 3B, Song et al., 2003b; Figure 4, Bringer et al., 2004). Comprehensive characterisation of mixing in droplets demonstrated that liquids merge by chaotic advection on a sub-millisecond scale (Figure 4, Bringer et al., 2004; Song et al., 2003).

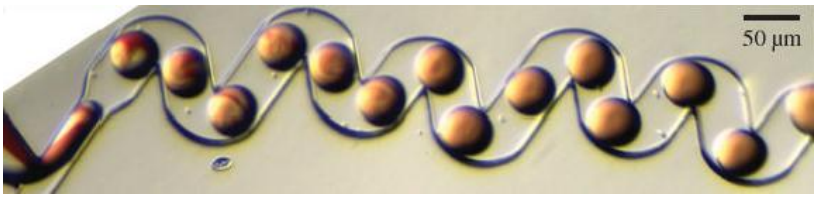

Figure 4: **Mixing by chaotic advection in droplets.** Microdroplets formed from two different colored fluids, moving through winding channels. Dispersion of liquids is low and mixing occurs in sub-millisecond regime (Bringer et al., 2004).

Over the last decade microfluidic applications were implemented globally into academic and industrial research. There is clearly a trend in commercial use of microfluidic systems (Haber, 2006). Most of the microfluidic applications are miniaturised versions of macroscale systems in areas like macromolecular or cellular analysis.

For example, Sanger DNA sequencing is a commonly used technique in molecular biology (Sanger et al., 1977). The integration of all three steps on one chip was demonstrated by Blazej et al., 2006. A hybrid glass-PDMS construction provided a bioprocessor for sequencing. On one device, thermo cycling reactors with a volume of 250 nL, affinity capture purification chambers, high-performance capillary electrophoresis channels as well as pneumatic valves and pumps were combined to perform complete Sanger sequencing from 1 fmol DNA. Accurancy of 99 % was demonstrated for up to 556 continuous bases (Figure 5; Blazej et al., 2006).

Polymerase chain reaction (PCR) is a method used to amplify DNA sequences (Saiki et al., 1985). In 1998, the first continuous-flow PCR chip was reported by Kopp et al., 1998. High speed amplification in 20 cycles was performed by passing DNA samples through a three temperature zone device. Tempered copper blocks kept well-defined

zones at 95 °C (DNA melting), 77 °C (primer extension) and 60 °C (primer annealing) (Figure 6).

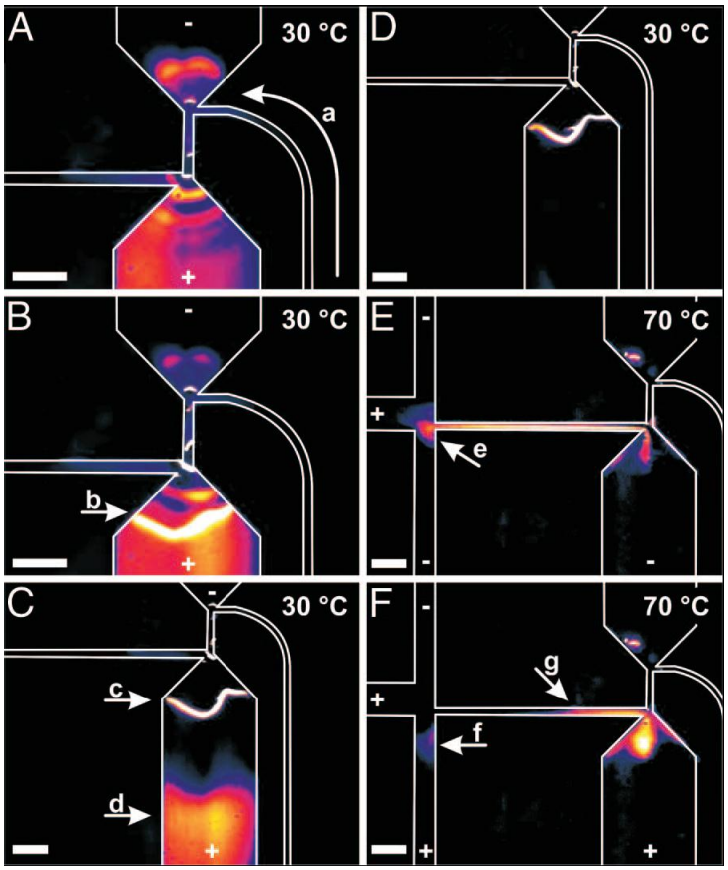

Figure 5: **On-chip Sanger sequencing.** False-color fluorescence images of the capture, purification, and injection steps. Cooler colors correspond to lower intensity; warmer colors to higher intensity. + and - indicate relative electric potentials. White bars are 300 μm. **(A)** Thermally cycled dye-terminator sequencing reagent, coming from the side channel (a), is pumped into the buffer-filled upper chamber. An electric field drives the sequencing mixture into the lower, capture-gel-filled chamber. **(B)** Fluorescently labeled DNA extension fragments selectively hybridize and concentrate at the gel/ buffer interface (b). **(C)** Desired extension fragments (c) are bound to the capture gel interface, and contaminants (d) continue to electrophorese out of the gel. **(D)** Purified and concentrated sample. **(E)** Extension fragments are released from the capture gel at 70 °C and injected into the channel junction (e). Pinching potentials constrain the plug size. **(F)** A ~1 nL sample plug is injected onto the separation capillary at (f), and reverse potentials pull out remaining material (g). (Blazej et al., 2006)

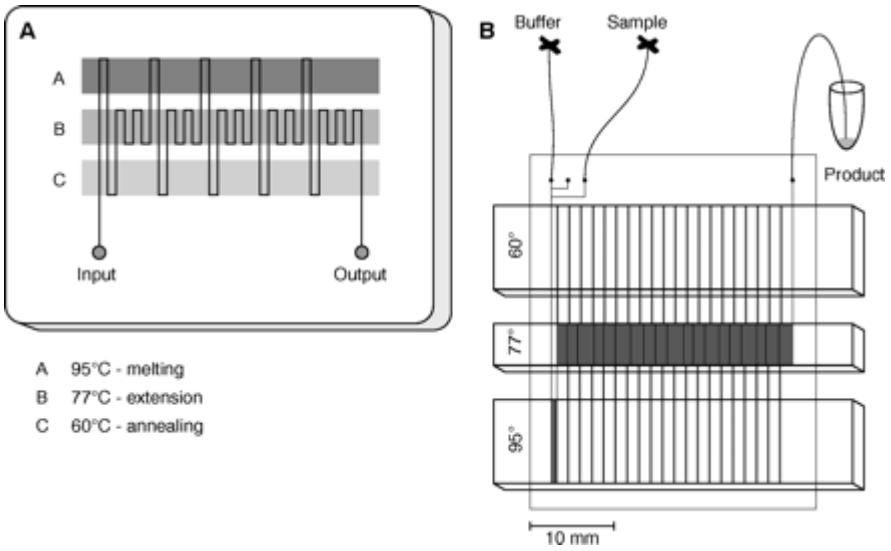

Figure 6: **On-chip PCR. (A)** Schematic of a chip for flow-through PCR. Three well-defined zones kept at 95°, 77°, and 60°C by thermostated copper blocks define the thermal cycling process. The sample is hydrostatically pumped through the channel. **(B)** Only two inlets are used: one injecting the PCR sample, the other bringing a constant buffer flow. The chip allows 20 identical cycles, except that the first one includes a threefold increase in DNA melting time. Product is collected at the outlet capillary. All three copper blocks are heated by heating cartridges, cooling fins passively cool the two blocks to 77° and 60°C. (Kopp et al., 1998)

Microfluidic systems have also a huge potential for use in biomedical applications and bioanalytics. Immunoassays for example have broad applications in medical diagnostics and pharma-biotech research. In this field miniaturisation is used to gain more information, in shorter time, without losing performance.

Immunoassays are routinely used in clinical practice to quantify blood analytes in patients. The development of a multi-antigen microfluidic immunoassay system offers an important step towards efficient and portable devices (Kartalov et al., 2006). Kartalov's system uses only 100 nL of a blood sample and can measure up to five clinically relevant analytes simultaneously. In addition, only 300 nL antibodies are needed to measure ten samples in one assay. The chip was used to demonstrate specific detection of C-reactive protein (CRP), prostate-specific antigen (PSA), ferritin and vascular endothelial growth factor (VEGF).

Commercial systems for immunoassay blood tests provide necessary tools in critical patient situations. Abbott Laboratories developed an automated hand-held blood analyser, i-STAT, for point-of-care diagnostics (Stephan, 2005). The system requires only two or three drops of blood to perform common panels of blood tests, including

blood gases, electrolytes, coagulation, haematology, glucose and cardiac markers (Abbott Diagnostics).

In contrast to one-phase microfluidics, in two-phase microfluidic systems, microcompartments are generated by using two immiscible fluids. Reagents are encapsulated into discrete water-in-oil droplets, thus enabling fast mixing within the drops and avoiding dispersion of liquids along the channel walls. In addition, utilisation of sub-nanoliter droplets is an excellent approach to open the way for high throughput conditions. Using microcompartments, such as aqueous drops or plugs, could facilitate the screening of large molecule ensembles on the order of 10^8 or higher (Huebner et al., 2008).

Between immiscible fluids, e.g. water and oil, surface tension is the driving force to form drops by minimising the interfacial area of the liquid, whereas viscous stresses (shear forces) operate in the opposite sense (Squires & Quake, 2005). Stability of droplet formation and droplet size can be estimated by balancing these two forces.

$$Ca = \frac{\upsilon \eta}{\gamma}$$

The capillary number (Ca), the ratio of υ (fluid velocity) multiplied by η (viscosity of the fluid) to γ (surface tension), is a relevant criterion to predict liquid stream breakup. Depending on the channel geometries, stable droplet formation occurs at moderate capillary numbers ($Ca = 0.05$), whereas at lower values ($Ca < 0.05$) droplet production becomes unstable and at higher capillary numbers ($Ca >> 0.05$) droplet break-up is reduced (jetting) (Abate et al., 2009).

During and especially after droplet formation the stability of droplets depends on the interfacial forces. Droplets tend to fuse in order to minimise the total interface and therefore decrease the state of energy. The generation of stable emulsions requires the addition of a surfactant in the carrier oil to decrease the surface tension and prevent droplet coalescence. A surfactant is an amphiphilic molecule which due to its nature adsorbs at the interface of immiscible liquids and stabilises generated droplets. Stabilisation by surfactants is limited to a maximum drop size. Drops which can not be

stabilised by a surfactant can be storaged in holding cartridges, such as a capillary or tubing when stably separated by immiscible oil spacers (Chen & Ismagilov, 2006). These big droplets which completely fill out the channels are usually called Plugs.

Using droplets or plugs, provides a system where each compartment functions as an individual microreactor allowing the linkiage of genotype and phenotype. In drug discovery, it is just as crucial to have a link between the activity and the structure in order to identify a potential compound. First, water-in-oil emulsions were generated by adding an aqueous solution to stirred mineral oil containing a surfactant (Tawfik et al., 1998). However, emulsions generated in bulk by homogenisation are quite polydisperse, droplets show a wide size distribution (Figure 7A; Miller et al., 2006). This is a disadvantage in drug discovery and HTS in general. Differences in the volume of microcompartments result in different distribution of reactants; inhibitor, enzyme and substrate concentrations are not identical, making quantitative readouts difficult. Moreover, further manipulations such as splitting or adding compounds are restricted in bulk emulsions. To overcome these limitations, highly monodisperse microdroplets (< 3 % polydispersity) with drop sizes ranging from 2 to 200 μm can be generated by a drop break-off technique (Umbanhowar et al., 2000; Figure 7B, Fallah et al., 2010, unpublished data).

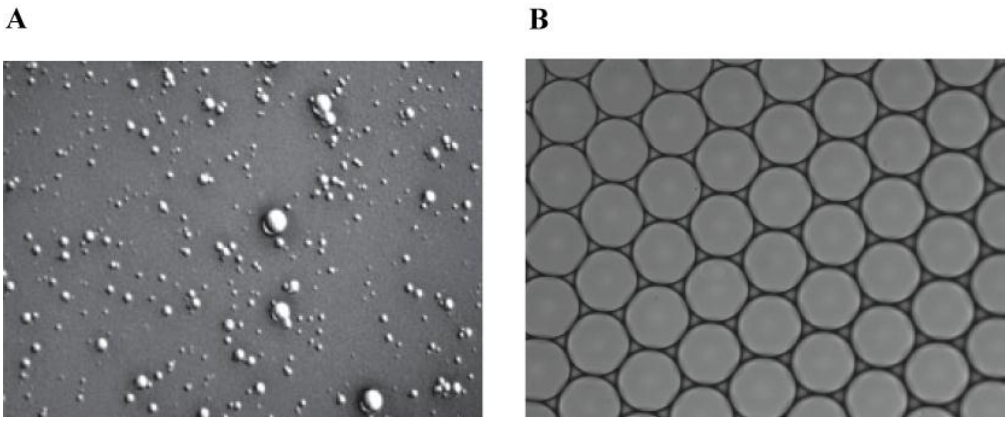

Figure 7: **Polydispersity of w/o emulsions. (A)** Differential interference micrograph of a emulsion produced by stirring. Droplet mean diameter of 2.6 μm (Miller et al., 2006). **(B)** Confocal micrograph of an emulsion generated with a droplet-based microfluidic device. Droplet mean diameter of ~ 17 μm (Fallah et al. 2010, unpublished data).

Using drop break-off in a microfluidic device, monodisperse droplets can be produced mainly by two different channels geometries. In a T-junction geometry, the aqueous

phase is orthogonally injected into the continuous oil phase resulting in dispersion and break-off (Thorsen et al., 2001; Figure 8A, taken from Mazutis, (PhD) 2009). Using flow-focusing, the aqueous phase (in the inner channel) and the oil phase (coming from two outer channels) are forced through a small nozzle resulting in droplet break up (Anna et al., 2003; Figure 8B, Joanicot & Ajdari, 2005).

After droplet generation at up to 10 kHz (Umbanhowar et al., 2000), drops can be controlled and manipulated in many different ways. In general, aqueous microdroplets can be mixed rapidly (Figure 9A; Song et al., 2003), they can be transported, incubated and stored in microfluidic channels (Figure 9B; Holtze et al., 2008) and subdivided in a T-junction (Figure 9C; Link et al., 2004). Moreover, droplets can be fused, either by active fusion after applying an electric field (Figure 9D (1); Ahn et al., 2006) or by passive fusion of droplets with low surfactant concentration (Figure 9D (1); Mazutis et al., 2009).

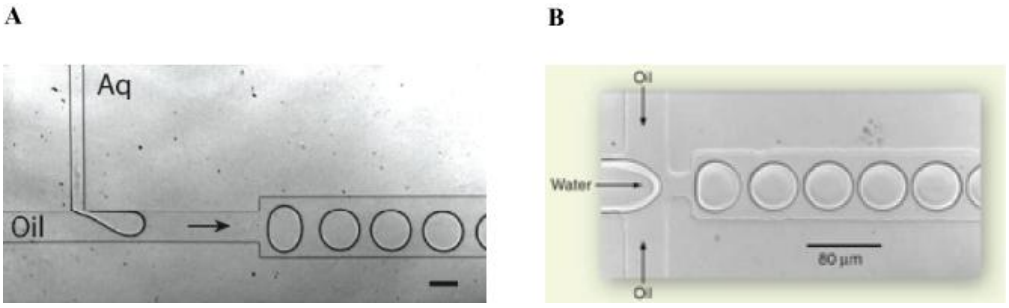

Figure 8: **Microfluidic chip for the generation of highly monodisperse w/o emulsions. (A)** Droplet production at a T-junction (Thorsen et al., 2001). Picture taken from Mazutis, (PhD) 2009. Flow indicated by black arrow. Scale bar 100 µm. **(B)** Droplet production by flow-focusing (Anna et al., 2003). Picture taken from Joanicot & Ajdari, 2005.

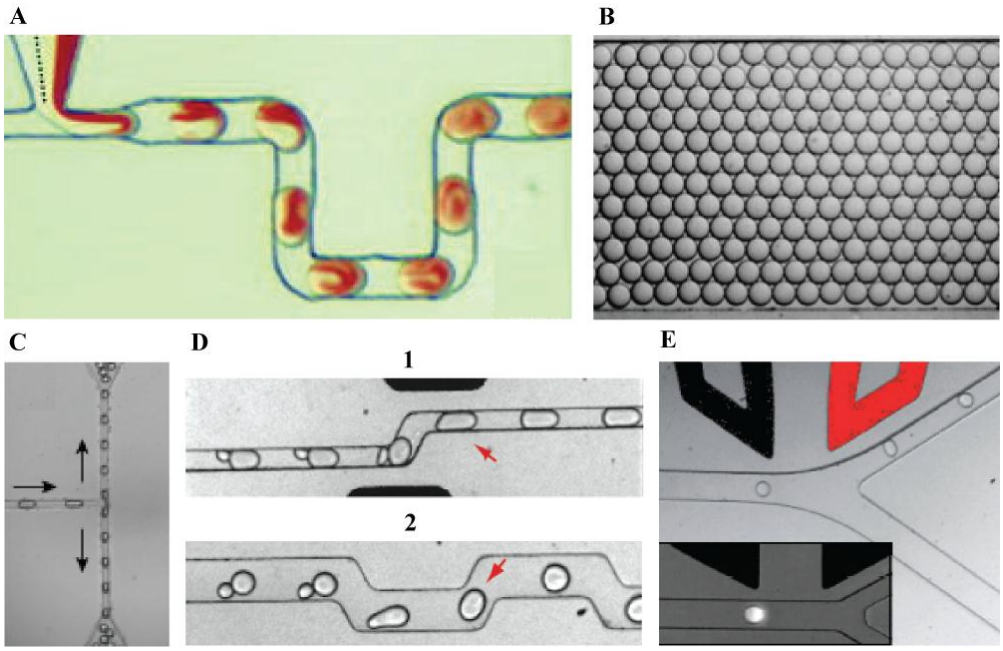

Figure 9: **Manipulation of microdroplets in microfluidic systems. (A)** Mixing in microcompartments, moving through winding channels. (Song et al., 2003) **(B)** Incubation of droplets in microfluidic channels. (Holtze et al., 2008) **(C)** Passive droplet break up in a T-junction. (Link et al., 2004) **(D)** Fusion of droplets with two different sizes. Pictures taken from Mazutis, (PhD) 2009. (1) Active fusion by an electric field. (Ahn et al., 2006) (2) Passive coalescence of drops. (Mazutis et al., 2009) **(E)** Fluorescence triggered sorting of droplets. An electric field is applied across the electrodes when the drops are fluorescent, therefore droplets flow into the upper channel. (Baret et al., 2009)

In this study fluorinated oils and surfactants were used. The hydrophobicity and lipophobicity of fluorocarbon liquids are attractive properties for their use in microfluidics as chemical compounds have low solubility (Li et al., 2006). Additionally, fluorinated carrier oils have, similar to PDMS, a high gas-permeability and are therefore suitable for cells-based assays (Lowe et al., 1998).

Droplet-based microfluics combines compartmentalisation, miniaturisation and monodispersity with a useful panel of different drop manipulation tools. Therefore it offers a potential approach, not only for chemical reactions, but also for high throughput screening and single cell analysis.

The use of drops in synthetic chemistry allows for controlled progression of the reaction. For example, in the synthesis of inorganic nano- and polymer particles which have many different applications, e.g. biomedical products, drug delivery, electronics and magnetics. Compared to conventional bulk synthesis, microfluidic emulsification

provides precise control of size, shape and morphology and generates particles with less than 5 % polydispersity (Li et al., 2009; Frenz et al., 2008).

Increasing throughput and efficiency is also an important feature in structural biology. In 2003, a microfluidic system for screening hundreds of protein crystallisation conditions inside 7.5 nL aqueous droplets was described by Zheng and co-workers. This system provides a less time-consuming procedure than manual screening and allows minimal use of reagents (Zheng et al., 2003). Crystals obtained during screening were large enough for traditional cryoprotection and X-ray diffraction data collection.

Performing polymerase chain reaction in microfluidics leads to faster throughput than batch PCR, as already described for continuous flow (Kopp et al., 1998). However, interactions of the channel walls with polymerases and DNA, resulting in cross-contamination, limited biocompatibility and high throughput (Schaerli et al., 2009). Performing PCR in microcompartments can overcome these problems. Schaerli and co-workers used nanoliter droplets, flowing through altering temperature zones for DNA denaturation, primer annealing and template extention. Using such a system high efficient amplification from a single DNA molecule per drop was achieved.

A very successful application of PCR in microdroplets is the commercialised Genome Sequencer FLX (454 Life Science Corporation, Roche). This next generation sequencing technology amplifies DNA fragments immobilised on beads in a one fragment – one bead fashion, performed in bulk emulsions (Margulies et al., 2005). This impressively shows the potential of microfluidics for industrial use. A few years later, RainDance Technologies performed multiplex PCR in droplet-based microfluidics to enrich target sequences for subsequent sequencing (Tewhey et al., 2009). The comparison with traditional singleplex PCR as well as the Roche 454 platform resulted in equally specific and sensitive data.

MONOCLONAL ANTIBODIES

Drugs created by biological processes (in contrast to chemical reactions), e.g. monoclonal antibodies, are reffered to as biologicals and provide a new class of medication. Even though research and production of biologicals is considerably more expensive than new chemical entities (NCE, small molecules) the market for new approved biologic drugs increased over the last years and is growing continuously. Not only that biologicals offer more precise therapies, better tolerance and good efficacy for specific diseases (e.g. cancer and rheumatoid arthritis), they also accelerate the drug discovery process by reducing the developmental period. Biolocicals include for example: monoclonal antibodies, growth hormones, insulin products, interferons and interleukin-2 drugs.

From the beginnings in the 1980s, monoclonal antibodies became the most successful biotech drugs in history, with 22 FDA (*Food and Drug Administration*, http://www.fda.gov) approved therapies, eight blockbusters currently in use, 200 products in the biotech pipelines and a global market of $ 40 billion in 2009.

The first Nobel Price in Physiology or Medicine (1901) was given to Emil Adolf von Behring for developing a serum therapy against diphtheria and tetanus. In 1940, Linus Pauling introduced the first instructive theory of antibody structure and process of formation (Pauling, 1940). Gerald M. Edelman and Rodney R. Porter elucidated the chemical structure of antibodies and discovered that immunoglobulins were composed of two heavy chains and two light chains; there are three domains in the molecule, two of them form binding sites for antigens and the third one links the two heavy chains together. In 1972, the Nobel Price in Physiology or Medicine was awarded jointly to Edelman and Porter for their work. Finally, the first complete protein crystal structure of an intact antibody was published by Harris and colleagues in 1992 (Harris et al., 1992; Figure 10). The therapeutic and diagnostic use of antibodies arose with discovery of their structure, in parallel to the development of hybridoma technology (Koehler & Milstein, 1975, Nobel Price in Physiology or Medicine in 1984 for theories concerning the specificity in development and control of the immune system and the discovery of

the principle for production of monoclonal antibodies) and advances in antibody purification (Gottschalk, 2009).

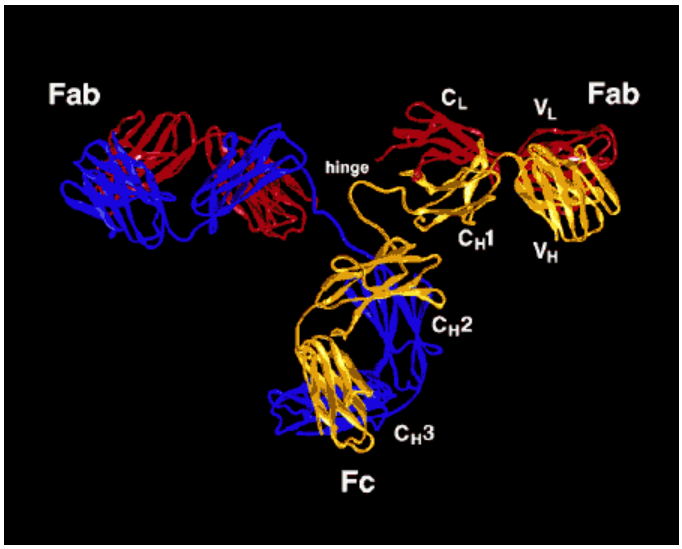

Figure 10: **Labeled ribbon drawing of the first intact antibody (IgG2A) ever crystallized.** The antibody is assymetric, reflecting its dynamic character. There are two local dyads in the molecule. One relates the heavy chains in the Fc, the other relates the constant domains of the Fabs. Fab: Fragment antigen binding. Fc: Fragment crystallisable region (interacts with cell surface receptors). C_H1, C_H2, C_H3: constant regions heavy chain. C_L: constant region light chain. V_H: variable region heavy chain, V_L: variable region light chain, hinge: proline-rich sequence between Fab and Fc to ensure mobility and flexibility of the two Fab arms. (http://www.antibodyresource.com/intactab.html)

.

An antibody is a glycosylated plasma protein (immunoglobulin, Ig) produced by immune cells to identify and neutralise foreign, invading objects, such as bacteria, viruses or toxins. B lymphocytes, a kind of white blood cells, release specific antibodies when activated by the presence of an antigen. All antibodies are typically made of basic structural units: two large heavy chains and two small light chains, the average molecular weight of a monomer is ~ 150 kDa. Antibodies exist in five different isotypes; IgA is a dimer, IgD, IgE and IgG are monomers and IgM is a pentamer. Due to different biological properties and functional locations the isotypes perform different roles and deal with different antigens within the body. Different biological effects of antibodies are e.g. virus and toxin neutralisation, direct antimicrobial activity, opsonisation and complement activation (Figure 11; from Casadevall et al., 2004). Antibody variability of up to 10^7 -10^9 different variants in each individual is achieved

by variable regions in each heavy and light chain, forming together a specific antigen recognition site.

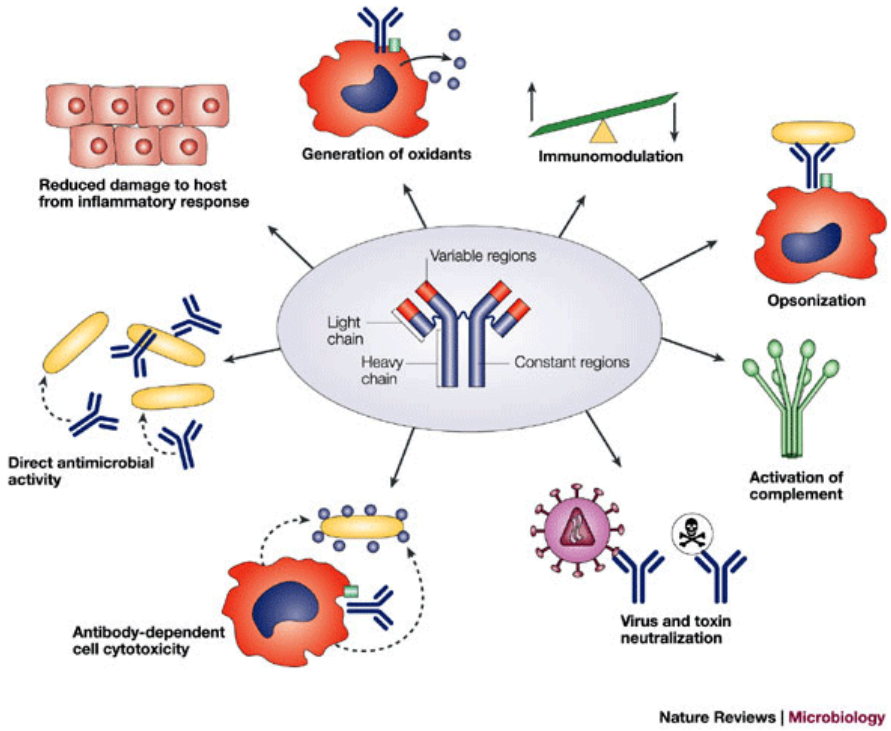

Figure 11: **The different biological effects of antibodies.** Toxin and virus neutralization, complement activation and direct antimicrobial functions such as the generation of oxidants are independent of other components of the host immune system, whereas antibody-dependent cellular cytotoxicity and opsonization depend on other host cells and mediators. (Casadevall et al., 2004; Figure 1)

Due to the technology development in the past 30 years, recombinant antibodies of today are genetically engineered molecules, designed for high specificity and functionality (Brekke & Sandlie, 2003). For example, rendering antibodies from non-human sources into molecules that are no longer recognised as foreign by the immune system (humanisation). Moreover, the ability to load antibodies with effector moieties such as enzymes, toxins, radionuclides or cytokines broadened their applications.

The progress in antibody research resulted in the first approved therapeutic monoclonal antibody (OKT-3), in 1986. OKT-3 is a murine IgG2a CD3 specific immunosuppressant drug to reduce transplant rejection, also called muromonab, and provided an important prototype of future monoclonal antibodies (Hooks et al., 1991).

SINGLE CELL ASSAYS

> *"I have been trying to think of the earth as a kind of organism, but it is no go. I cannot think of it this way. It is too big, too complex, with too many working parts lacking visible connections. The other night, driving through a hilly, wooded part of southern New England, I wondered about this. If not like an organism, what is it like, what is it most like? Then, satisfactorily for that moment, it came to me: it is most like a single cell."*
>
> (Thomas Lewis, 1974; The Lives of a Cell: Notes of a Biology Watcher)

In other words, the earth cannot be called an organism because of its invisible complexities, yet it can be compared to a single cell. With these thoughts, Thomas Lewis might have referred to the struggle of understanding the mechanisms of cells that are the smallest units of life in this world.

Today, many cell-based screening assays are performed in bulk using whole cell populations. Because of cellular heterogeneity, those assays only give averaged data and sometimes misleading information. For example, Toriello and co-workers measured siRNA knockdown of GAPDH gene expression of individual Jurkat cells using an integrated microfluidic bioprocessor (Toriello et al., 2008). Single cell analysis showed two distinct populations with partial (50 %) or complete (0 %) knockdown. These measurements differed fundamentally compared to the average result from 50 cells (21 %). These findings demonstrate that single cell analysis (SCA) is a crucial tool for studies on the expression of nucleic acids but also proteins or metabolites. Single cell analysis has major implications for the future of drug discovery processes; not only for the understanding how diseases originate (e.g. cancer starts with a single cell) or providing adequate time scales for cellular chemistry but also for diagnostics and high throughput screening of potent drug candidates.

Numerous methods for single cell assays have been established, they include capillary electrophoresis (CE), fluorescence imaging, flow cytometry (e.g. fluorescence-activated cell sorting, FACS), microarrays and microfluidics.

In single cell analysis by capillary electrophoresis, a cell is injected into a capillary and lysed (chemically, electrically or optically) inside. After microscale separation, the lysate content is chemically analysed by various detection techniques, such as fluorescence, amperometry (based on the oxidation and reduction of electroactive compounds) and chemiluminescence (Huang et al., 2008). Even though this method has a great potential, the limited range of analytes that can be measured and the many separately performed steps result in a time-consuming and low throughput process.

Fluorescence imaging of single cells is a method that requires prior *in vivo* or *in vitro* labeling of the molecule of interest. Mostly, single- or two-color imaging is used as simultaneous measurements are limited due to spectral overlaps. For example, levels and location of nearly 1000 different endogenously tagged proteins in individual human cancer cells could be measured with high temporal resolution (Cohen et al., 2008). Using CD (central dogma) tagging, a library of cell clones was constructed, each tagged for a different protein. Subsequently, these clones were used to study the dynamics of the protein response to a drug.

Fluorescence activated cell sorting (FACS) is the main application of flow cytometry. FACS uses tagged antibodies for staining characteristics of interest on the cell surface and/ or intracellular fluorescent molecules. Cells are separated by a rapidly flowing stream of liquid and the fluorescence signals can be measured individually. For example, this method was applied to profile phosphoprotein networks in single cancer cells (Irish et al., 2004).

CE, fluorescence imaging and FACS are well-established methods for single cell analysis, but they are limited in cell manipulation and their resulting information content. Therefore, these methods allow only little insight into the complexity of intracellular processes.

Microfluidic technology provides a great potential to overcome these limitations. Microfluidics offers unique advantages for single cell analysis, such as integration of many functions, e.g. cell culture, reagent delivery, separation and sorting. Moreover, this technology enables to mimic the natural physiological environment of cells, allowing gathering multiplex information on biochemical behaviors, like movement, differentiation, secretion, endocytosis and apoptosis (Huang et al., 2008).

Microfluidic systems deal with the manipulation of small amounts of liquids in channel with dimensions of ten to hundreds micrometers and provide a new approach for bio(chemical) analysis and synthesis (Whitesides, 2006). For example, Marcus and co-workers realised on-chip meassurment of gene expression in single cells. Cell capture, cell lysis, mRNA isolation, cDNA synthesis (by polymerase chain reaction, PCR) and cDNA purification were integrated on one microfluidic chip and allowed analysis of individual cells (Marcus et al., 2006). However, efficient single cell capture and manipulation still remains difficult. For example, technologies like laser capture microdissection and micropipette-based manipulators can hardly be integrated in microfluidic devices. In contrast, recent technologies like droplet-based encapsulation offer an alternative to overcome these problems. Also label-free methods for detection were reported to be compatible with the microfluidic system. For example, online mass spectrometry was used to analyse the chemical content of single microreactors (Fidalgo et al., 2009). Microfluidic technology provides integration and automation of many manipulations and detection functions in high throughput fashion applicable for single cell analysis.

Microarrays also offer the opportunity for single cell assays. By adopting the above described on-chip PCR technology (Marcus et al., 2006), Fluidigm Corporation was able to present the first commercialised microfluidic product for single cell analysis. Fluidigm Dynamic Array™ integrated fluidic circuits (IFC's) enable hundreds of individual cells to be tested for the expression of hundreds of genes in a few hours (http://www.fluidigm.com).

SCOPE OF THE THESIS

The purpose of this doctoral work was the development of advanced screening technology for monoclonal neutralising or inhibiting antibodies.

The first aim was to set up a two-phase microfluidic platform for cell-based assays. In two-phase microfluidic systems, aqueous drops serving as miniaturised reaction vessels (in nano- to picoliter scales) are generated within a continuous oil phase. This work aimed to establish and prove the basics of cell cultivation in microcompartments generated within microfluidic chips.

The second goal addressed the development and design of functional assays for screening inhibitory activities of monoclonal antibodies. The assays focused on inhibition of viral cell-entry or cell-cell fusion, respectively, and enzymatic reactions. Optimisation and feasibility for the combination with the microfluidic system were the main challenges.

CHAPTER I: MICROFLUIDIC PLATFORM FOR CELL-BASED ASSAYS

1 INTRODUCTION

1.1 CELL-BASED ASSAYS IN CONTINUES FLOW MICROFLUIDIC SYSTEMS

Cell-based assays are an inevitable instrument in drug development. Platforms that offer tools for cell culture, single cell analysis and high throughput are necessary technology for that purpose. Several groups demonstrated microfluidic systems for cell-based assays (Hung et al., 2005; McClain et al., 2003; Wheeler et al., 2003).

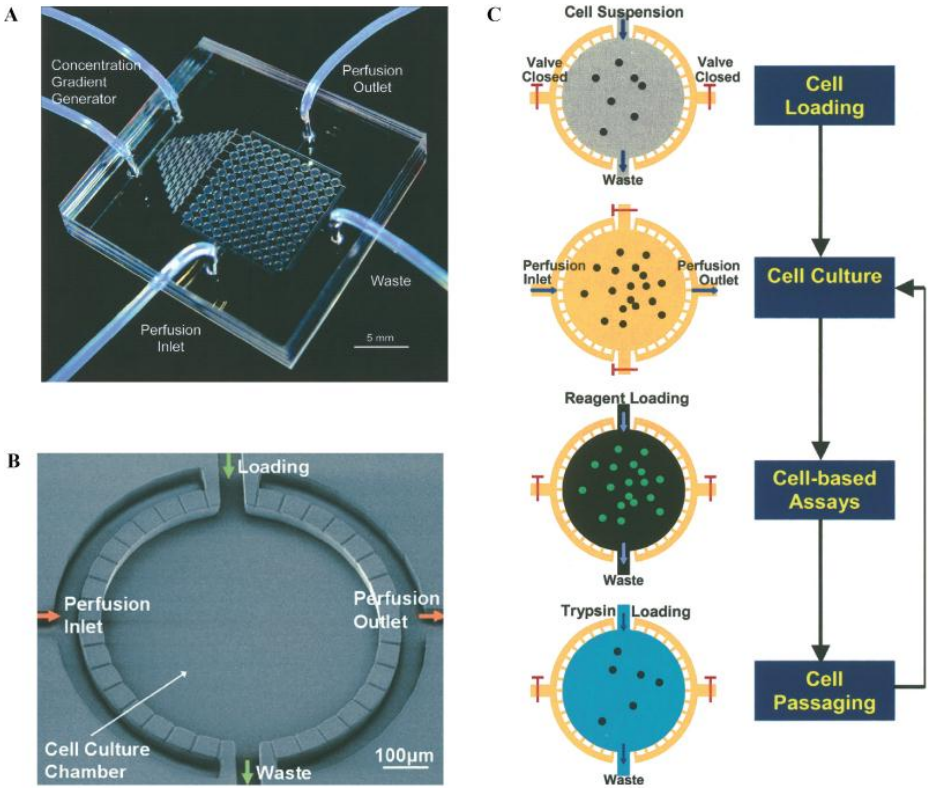

Figure 12: **(A)** Chip for microfluidic cell culture arrays. A 10 x 10 array of microchambers, fabricated on a 2 x 2 cm device. **(B)** Scanning electron microscopy picture of one unit of the arrayed device before bonding to a glass slide. Several perfusion channels surround the culture chamber. **(C)** Schematic representation of device option, closed valves are represented with the 'T' symbol. (Hung et al., 2005)

Hung and co-workers presented the first microfluidic cell culture array (Hung et al., 2005). They developed a device that potentially allows for 100 different experiments (Figure 12A) and combines a sterile microenvironment as well as long-term monitoring. The microchambers have the same dimensions as a well in a 1.536-well plate and through perfusion channels cells are provided with fresh medium (Figure 12B, red arrows). Using two additional ports, right-angled to perfusion inlet/ outlet, cells and reagents are loaded into the chamber to perform cell-based assays (Figure 12B, green arrows).

The information obtained from individual cells is essential in drug development. A microfluidic device to analyse single cells, especially the chemical composition of individual cells was reported by McClain and colleagues (McClain et al., 2003). Cells were hydrodynamically transported and separated within the device. After reaching the lysis intersection, cell membranes were disrupted by a high voltage electric field within < 33 ms. Subsequently, labelled analytes in the lysate were automatically injected into a separation channel, electrophoretically separated (in less than 2.2 s) and detected by laser-induced fluorescence (Figure 13). The rates for average cell analysis were 7-12 cells/ min.

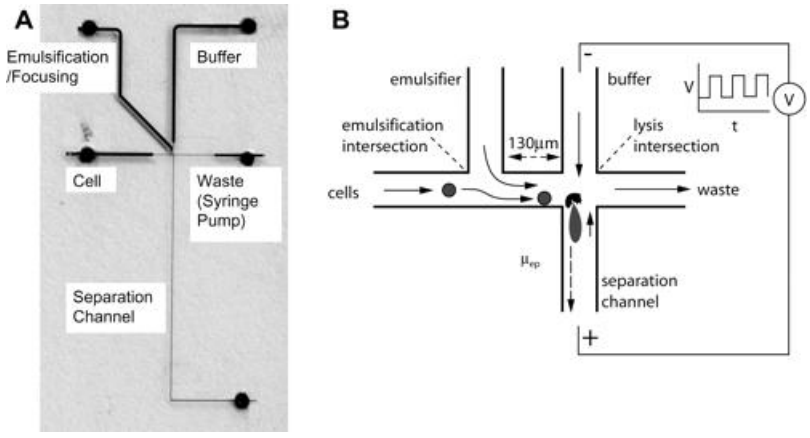

Figure 13: **Microchip used for high throughput chemical analysis of single cells. (A)** Image of the chip. **(B)** Schematic of the emulsification and lysis intersections for the microchip design shown in (A). The continuous arrows show the direction of bulk fluid flow and the dashed arrow shows the electrophoretic migration direction of the labelled components in the cell lysate (McClain et al., 2003).

Not only analysing the content of cells is of interest but also performing biological assays using single cells. Wheeler and co-workers presented a microfluidic device to

manipulate individual cells performing various assays (Wheeler et al., 2003). Using a T-junction a point of stagnation was created to isolate single cells. Then, drain channels were used to trap the cell and keep it positioned in the device (Figure 14B). Two small delivery channels allow supply with different reagents. Using this system viability assays and calcium flux experiments were performed, demonstrating potential applications for single cell analysis.

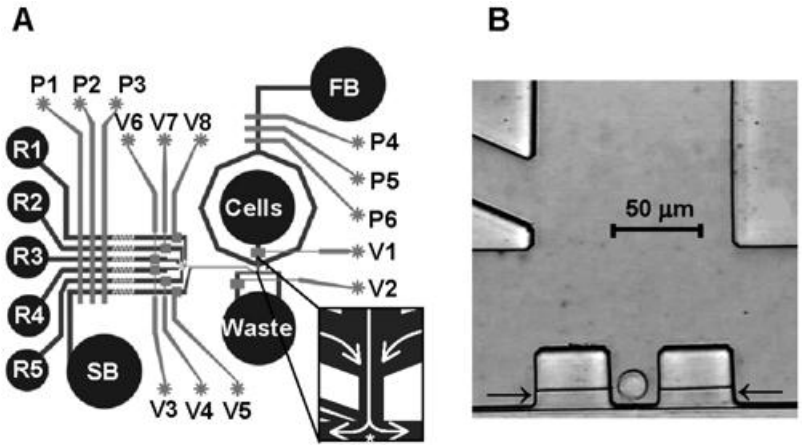

Figure 14: **Single-cell analysis device. (A)** Schematic of the device, fluidic channels are dark and control channels are bright. R1−R5 are reactant inlets, SB and FB are shield and focusing buffer inlets, respectively. Valves are actuated by applying pressure to control inlets V1−V8. Pumps are activated by actuating P1−P3 or P4−P6 in series. Inset: close up of cell trapping region, point of stagnation is formed at *x*. **(B)** Microscopic image of an individual Jurkat cell trapped in a cell dock. Drain channels on the dock are indicated by black arrows (Wheeler et al., 2003).

1.2 CELL-BASED ASSAYS IN DROPLET-BASED MICROFLUIDIC SYSTEMS

Aqueous microcompartments present a new opportunity for single cell analysis. Controlled and selective encapsulation of single cells has been reported (Tan et al., 2006; He et al., 2005). Relative quantification of protein expression in compartmentalised single cells was demonstrated by Huebner and colleagues. Expression of a yellow fluorescent protein (YFP) in individually encapsulated *E. coli* cells was detected to monitor bacterial growth and compared with bulk samples (cell density measured at 600 nm). Fluorescence measurements of the encapsulated cell population were found to be in agreement with absorbance measurements of the bulk

population. This demonstrates reliable monitoring and relative quantitation of proteins expressed by single cells in microdroplets (Figure 15; Huebner et al., 2007).

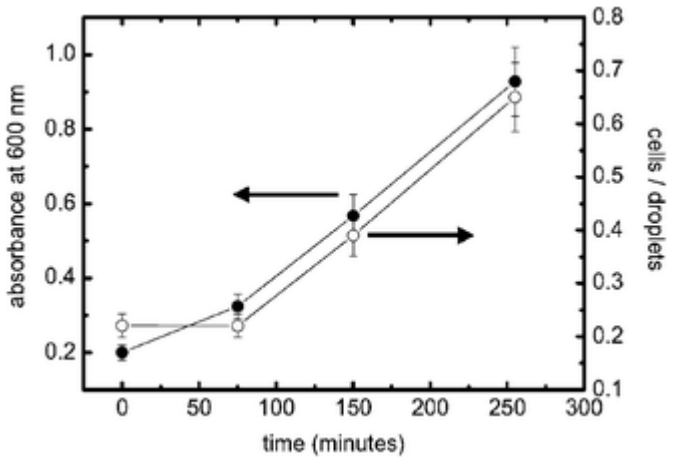

Figure 15: Growth curves of *E. coli* expressing YFP. Black circles: Bulk analysis. White circles: Analysis within microdroplets. Cell density in bulk and cell occupancy in droplets (number of cells/total number of droplets) show similar increase in level of expressed fluorescent protein over time. These results indicated that the measurement in droplets reflects the expression and growth state obtained in bulk experiments.

The feasibility of drug screening in droplet-based systems was investigated for antibiotic sensibility of resistant bacteria strains (Boedicker et al., 2008). Boedicker and co-workers tested methicillin-resistant *Staphylococcus aureus* for its sensitivity to different antibiotics (methicillin is an antibiotic of the penicillin class). Moreover, the minimal inhibitory concentration (MIC) of the antibiotic cefoxitin (CFX) was determined. In addition, using this platform, sensitive and resistant strains of *Staphylococcus aureus* could be distinguished within human blood plasma (Boedicker et al., 2008).

This Ph.D. work focused on establishing HTS assays for screening antibody activity by using antibody producing cells (hybridoma cells); therefore it seems essential to look at some historical and past achievements obtained from experiments combining compartmentalisation and antibody producing cells.

Nossal's and Lederberg's report from 1958, did not only support the clonal selection theory of antibody formation which was at the time only a theoretical prediction, it also was an impressive record of antibody production and screening for its functionality in

microdroplets (Nossal & Lederberg, 1958; Viret & Gurr, 2009). The original idea was to identify weather plasma cells could produce antibodies against two antigens. For this, rats were immunised 1:1 with two different *Salmonella* strains. Isolated plasma cells were incorporated into 100 nL to 1 pL microdroplets by free-hand micromanipulation (micropipette technique) and maintained under mineral oil for 4 hours to allow for substantial antibody concentration to be reached. One of the two *Salmonella* strains was introduced into the drops and the preparation was monitored by dark-field microscopy. The readout consisted in the capacity of the produced antibody to abolish the motility of every single bacterium. It turned out that none of the examined cells showed duel reactivity which was the first evidence for the clonal selection theory.

Usually, screening of monoclonal antibodies involves hybridoma cell generation (Chapter II, Introduction) as long-term culture of B-cells is impossible. Discovering a single monoclonal antibody requires retrieval of an individual hybridoma from polyclonal mixtures of cells producing antibodies with a variety of specificities (Love et al., 2006). Conventional screening of hybridoma cells is performed in microtiter plates and takes up to ten days to obtain detectable antibody concentrations for analysing assays. In 2006, Love and co-workers presented a soft lithography method based on microengraving resulting in arrays of microwells with 50 μm (or 100 μm) in diameter and a depth corresponding to a final volume of ~ 100 pL to 1 nL. This system allowed identification, recovery and clonal expansion of monoclonal hybridoma cells within less than 12 hours in a high throughput fashion (> 100.000 individual cells). They followed two approaches for secreted antibody detection, first covalent immobilisation of a secondary antibody on the glass slide or second covalent attachment of the antigen on slides. In comparison, the second approach showed higher sensitivity to variations in the number of cells per well and the amount of secreted antibody (Love et al., 2006).

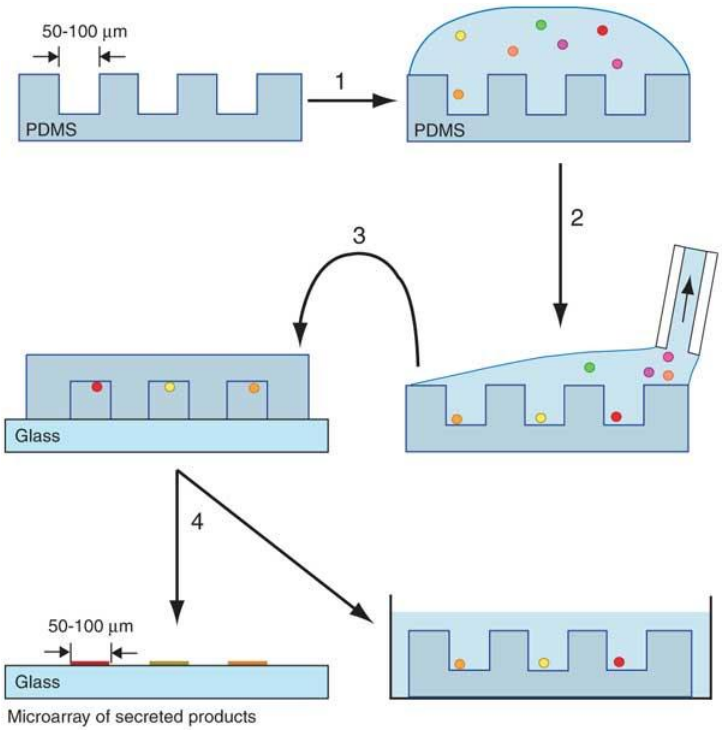

Figure 16: **Schematic diagram for the preparation of engraved arrays of secreted antibodies from a mixture of cells. (1)** Cell suspension is deposited onto a PDMS array of microwells. **(2)** Cells are allowed to settle into the wells, then the excess medium is removed by aspiration. **(3)** The array is placed in contact with a pre-treated solid support (secondary Ab or antigen treated) and incubated for 2–4 h. **(4)** The microwells are removed from the solid support and placed in a reservoir of medium for later manual retrieval of positive cells from the microwells.

A collaborating group (David Weitz's laboratory, Harvard University) demonstrated that detectable antibody concentrations can be obtained from single hybridoma cells encapsulated in monodisperse microdroplets generated using a microfluidic system (Köster et al., 2008). Hybridoma cells were encapsulated into 33 pL droplets, remaining fully viable for at least 6 hours. After 6 h on-chip incubation, the emulsion was broken and an ELISA test was performed to determine the concentration of secreted antibodies in the supernatant. After just six hours of incubation, detectable antibody concentrations similar to those after incubation of hybridoma cells in bulk were obtained (Figure 17). This shows that microdroplets could serve as assay reactors small enough to directly obtain detectable antibody concentrations from single antibody releasing cells, either hybridoma or even B-cells.

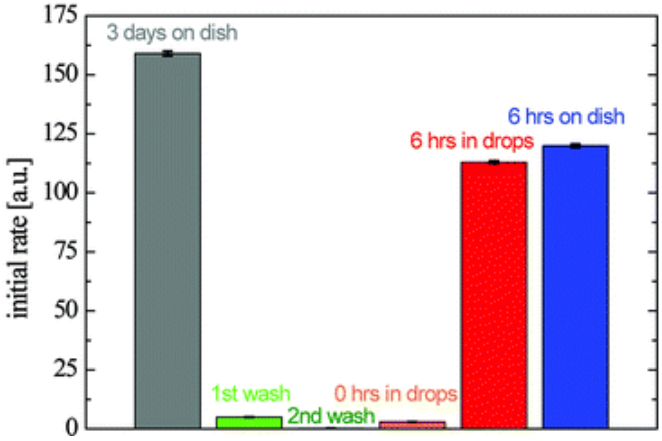

Figure 17: **Antibody production in drops.** Detection of antibodies by ELISA. Grey: after three days on culture dish. Light green: after first wash. Dark green: after second wash. Orange: encapsulated cells with no incubation time. Red: encapsulated cells after 6 h incubation. Blue: cells incubated for 6 h on a culture dish. (Köster et al., 2008). The x axis represents the initial slope as a measure of the relative antibody concentration.

2 MATERIAL & METHODS

2.1 SOFT LITHOGRAPHY (DESIGNS, MASKS, MOULDS & DEVICES)

Soft lithography is a technique for three-dimensional micro-fabrication (Whitesides et al., 2001). The process usually comprises **(1)** layout of patterns, **(2)** photomask printing, **(3)** template making and **(4)** stamp generation.

For the design of microfluidic structures a computer aided design software application (AutoCAD, Autodesk) was used **(1)**. These designs were then printed as a high-resolution dark field photomask (Selba S.A.); which is non-transparent for UV light **(2)**. To make a mould from this photomask, the design was printed on a silicon wafer (Siltronix) spin-coated with photoresist (SU-8 2075, MicoChem Corp.) using UV light (MJB3 contact mask aligner, SUSS MicroTec). In the process the pattern from the photomask was transferred onto the negative photorestist by polymerisation; exposed areas were cross-linked and remained after treatment with SU-8 developer (ethylene glycol monomethyl ether acetate, MicoChem Corp.) **(3)**. Then, a stamp was mould by pouring PDMS (polydimethylsiloxane) (Sylgard 184 silicone elastomer kit, Dow Corning Corporation), a two-component heat-curing system, onto the template. The curing agent and the base part of PDMS were mixed in a ration of 1:10 (w/w), degassed for several minutes and cross-linked for several hours at 65 °C. Afterwards, the silicon was peeled off the mould, inlets and outlets were punched with a biopsy needle (Harris Uni-Core biopsy punch, Electron Microscopy Sciences) and the structured side of the PDMS slab was bound to a 50 x 75 x 1 mm glass slide (Fisher Bioblock) using oxygen plasma (Plasma prep 2, Gala Instrumente). To provide hydrophobic channels, they were treated with a commercial surface coating agent (Aquapel, PPG Industries) and immediately flushed with nitrogen gas to purge the liquid **(4)**.

2.2 OPTICAL SET-UP

The optical set-up (Figure 18) used for the detection of fluorophores inside the drops consisted of an Axiovert 200 inverted microscope (Carl Zeiss SAS) mounted on a vibration-dampening platform (Thorlabs GmbH). A light emitting diode (LED) 488 nm laser (blue, 25 mW, Newport-Spectraphysics) and a solid-state 532 nm laser (green, 25 mW, Newport-Spectraphysics) were fixed on the platform. Both laser beams were combined using a laser beam combiner (LM01-503-25, Semrock Inc.) and shaped into a ~10 μm x ~150 μm wide line or a ~20 μm wide spot, respectively, using a beam expander (two lenses, Thorlabs GmbH). Afterwards, the focused beam was guided to the side camera port of the microscope. Inside the microscope the laser light was reflected up onto an LD Plan Neofluar 40x/ 0.6 microscope objective (Carl Zeiss SAS) and focused in the channel of the micofluidic device. A Phantom v4.2 digital high-speed camera (Vision Research) was mounted on the top camera port of the microscope to capture digital images during droplet production, re-injection and fluorescence measurement. To protect the camera from reflected laser light a bandpass filter (562/ 40, BrightLine, Semrock Inc.) was positioned in front. Emitted light from fluorescent droplets was collected by the objective and directed back along the path of the laser. Then, the emitted light was separated from the laser beam by a 488/532/638 nm-wavelength reflecting dichroic beam splitter (Di-T488/ 532/ 638-25x36x5.0, Semrock), filtered through two notch filters (NF01-488-25 and NF01-532U-25, Semrock) and diverted into two separate photomultiplier tubes (PMTs, H5784-20, Hamamatsu Photonics KK) by a single-edge dichroic beam splitter (FF562-Di02-25x36, Semrock). Reflected light passed through a bandpass filter (FF01-510/ 20-25, Semrock) and was collected in the Green PMT (fluorescein signal), whereas transmitted light was passed through another bandpass filter to the Orange PMT. The signal output from the PMT was analysed using a PCI-7831R Multifunction Intelligent data acquisition (DAQ) card (National Instruments Corporation) executing a program written in LabView 8.2 (FPGA module, National Instruments Corporation), which allowed the identification of droplets by peaks in fluorescence, as well as the width of each droplet. The data acquisition rate for the system was 100 kHz.

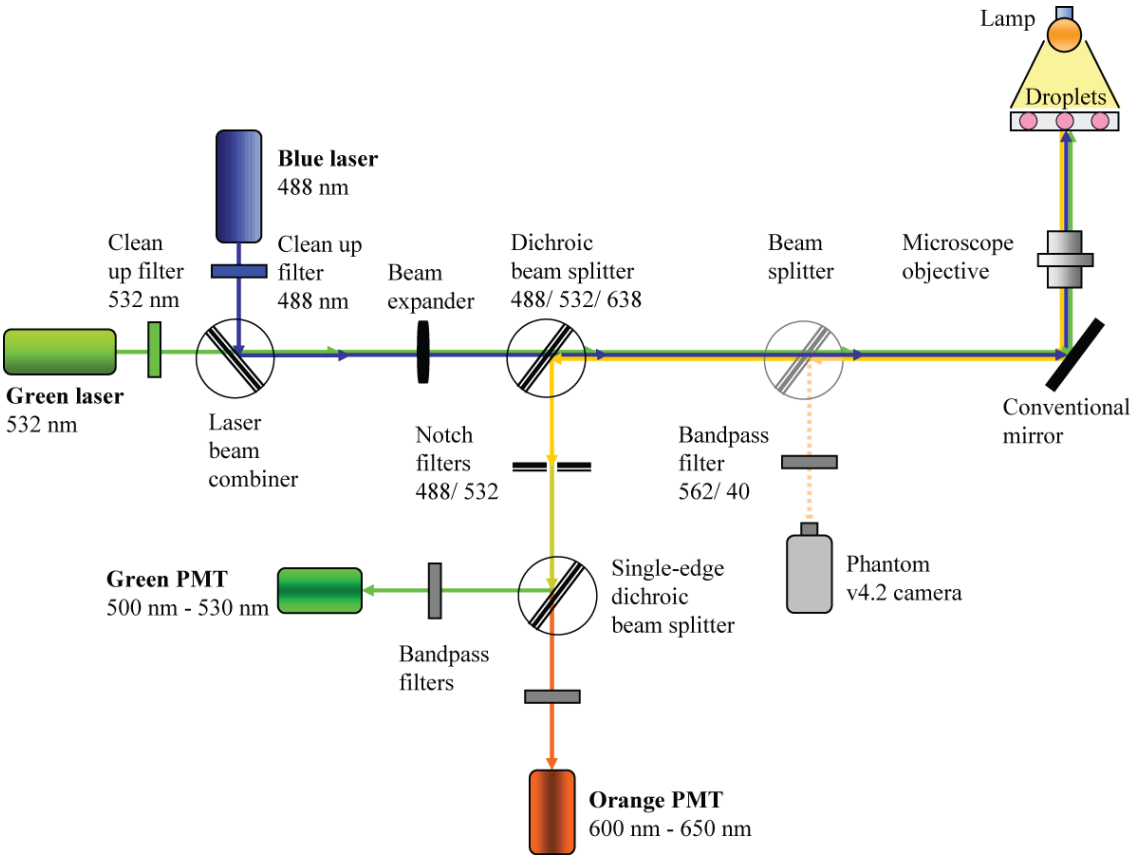

Figure 18: Optical set-up of droplet-based microfluidics station. Filter and splitters to direct specific wavelengths.

2.3 SYNTHESIS OF SURFACTANTS

To produce stable emulsion microdroplets, fluorinated surfactants were added to the fluorocarbon carrier oil. All surfactants tested in this work were based on a carboxy-polyfluorinated polyether (carboxy-PFPE) (Krytox FS(H), a commercial lubricant from DuPont) with different hydrophilic head groups. Before coupling Krytox to a head group, it was activated with $SOCl_2$ to obtain the electrophilic Krytox-chloride (Figure 19).

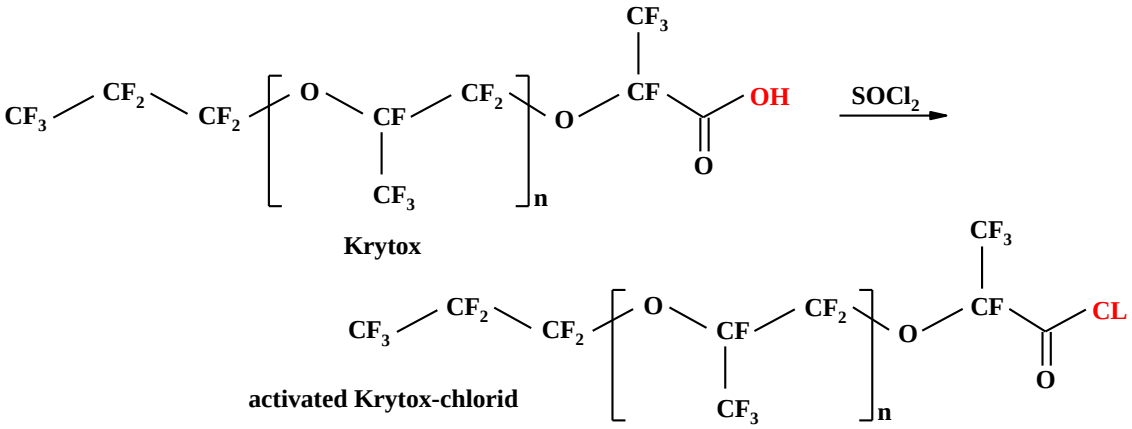

Figure 19: **Structure and acid activation of Krytox.** The resulting Krytox-chloride can be coupled to a hydrophilic head group.

Head groups that were used to synthesise surfactants by coupling with Krytox are poly-L-lysin (Figure 20), ammonium (Figure 21), dimorpholinophosphate (DMP) (Figure 22), Jeffamine® (Figure 23) and polyethylenglycol (PEG) (Figure 24).

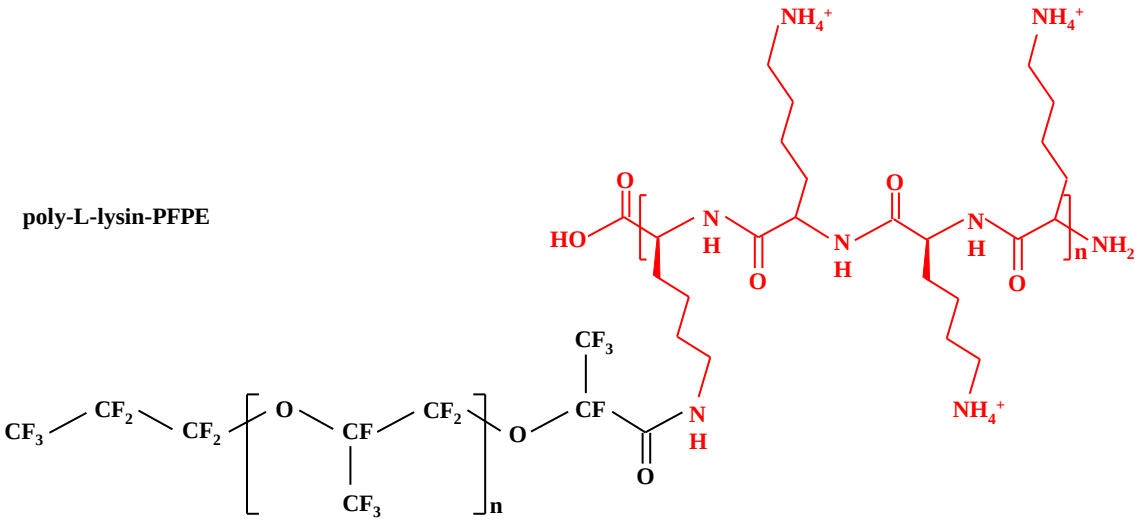

Figure 20: **Poly-L-lysin-PFPE.** Poly-L-lysine (15,000–30,000, Sigma) was reacted with Krytox FS(L) 2000 (Abdeslam el Harrak, unpublished data).

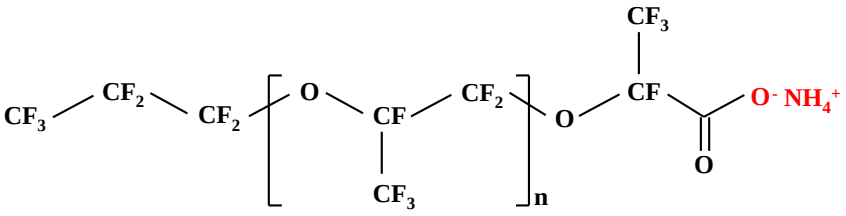

ammonium salt of carboxy-PFPE

Figure 21: Ammonium salt of carboxy-PFPE. To obtain an ammonium carboxylate perfluoropolyether surfactant, activated Krytox-chloride (Krytox FS(L) 2000) was reacted with NH_4OH_2 as described in Johnston et al. (1996).

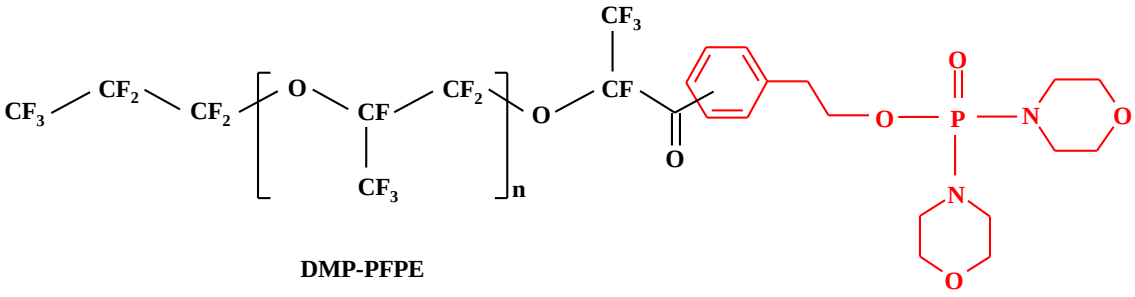

DMP-PFPE

Figure 22: DMP-PFPE. In a first step of the DMP head group synthesis, the aromatic alcohol PhEtOH (Aldrich) was phosphorylated by $POCl_3$ (Fluka). Then, the product was reacted with morpholine (Fluka) and $(Et)_3N$ (Sigma-Aldrich) in THF (Fluka) on ice. The resulting hydrophilic DMP was coupled to water/cyclohexane/isopropanol extracted Krytox FS(H) 4000 by Friedels-Craft-Acylation (Abdeslam el Harrak, unpublished data).

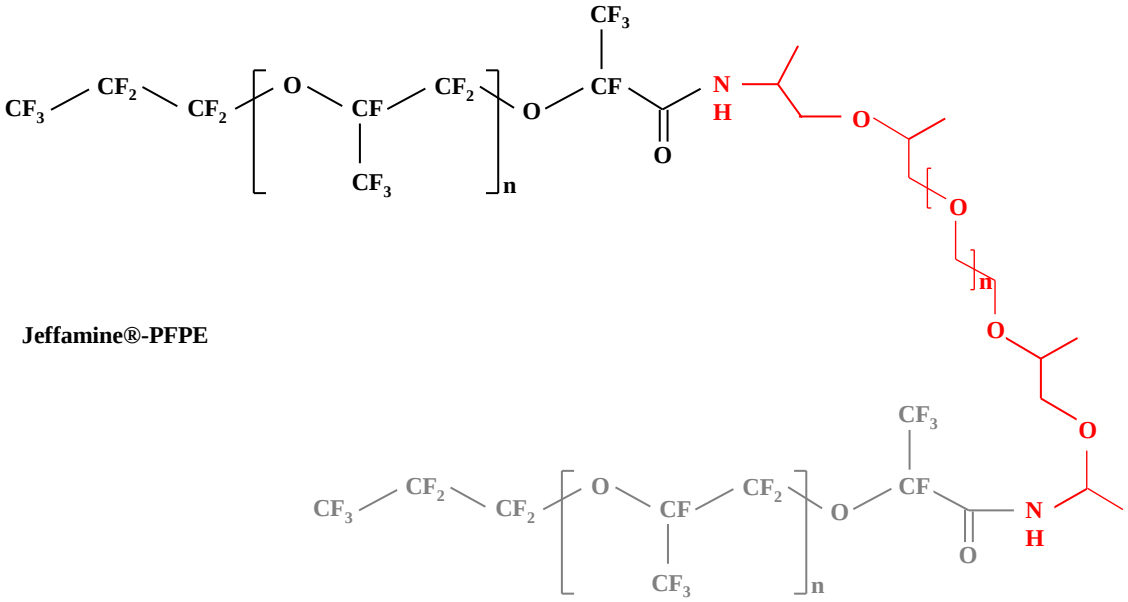

Jeffamine®-PFPE

Figure 23: Jeffamine®-PFPE. Reaction of Krytox FS(H) 4000 with Jeffamine® ED-900® (Sigma-Aldrich) resulted in a mixture of Jeffamine molecules coupled to either one or two Krytox molecules (Abdeslam el Harrak, unpublished data).

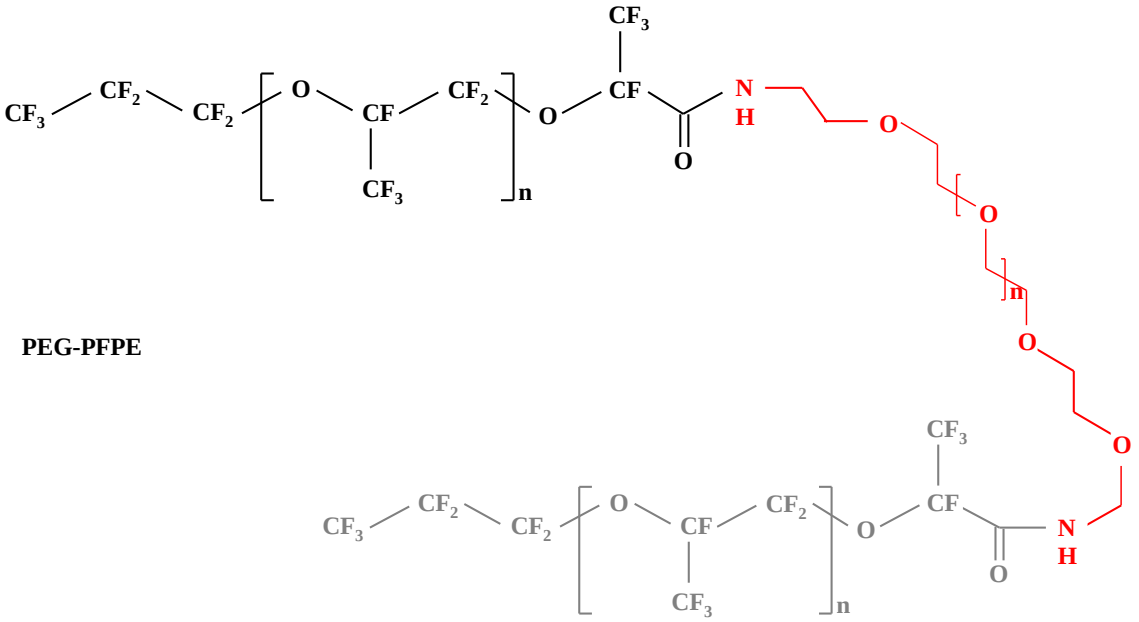

Figure 24: **PEG-PFPE.** The oligomeric perfluorinated polyether was coupled to the biocompatible PEG with a stable peptide bond. The synthesis resulted in a surfactant mixture containing triblock and diblock copolymers (Holtze et al., 2008).

2.4 BIOCOMPATIBILITY OF FLUORINATED OILS & FLUORINATED SURFACTANTS

Before using the fluorinated surfactants for cell encapsulation experiments, they were tested for their cell biocompatibility. To do so, 0.5 % (w/w) of the surfactants was each dissolved in fluorocarbon oil (FC40, 3M) (Figure 25). A 100 µL suspension of HEK293T cells (1.5 x 10^6 cells/ mL in fresh medium) or hybridoma tACE-4E3 cells (0.5 x 10^6 cells/ mL in fresh medium) respectively, was seeded on top of a layer of FC40 in the presence and absence of the tested surfactant and incubated at 37 °C within a water-saturated atmosphere (5 % CO_2). Bright-light images were taken with a Leica DMIRB microscope after 0 h, 24 h and 48 h. In addition, the PEG-PFPE surfactant (Chapter I, 2.3, Figure 24) was tested in combination with HFE-7500 oil (3M), a hydrofluoroether (Figure 26).

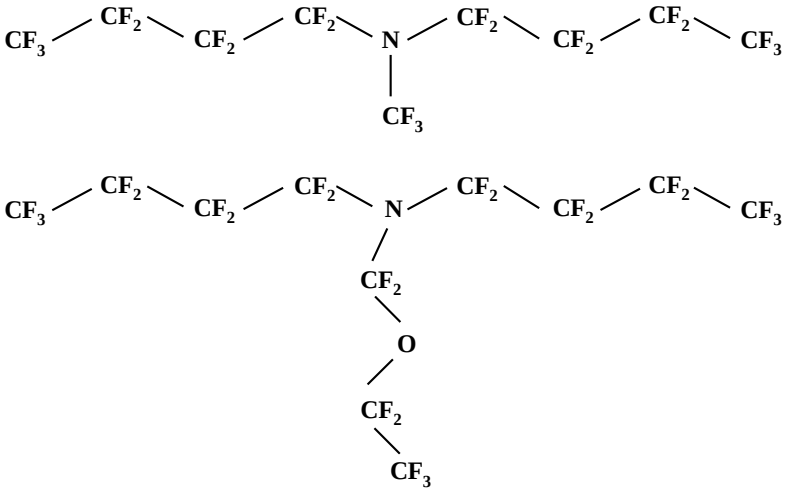

Figure 25: Chemical structure of FC40 oil. The fluorocarbon oil is a mixture of perfluoro-tri-n-butylamine and perfluoro-di-n-butylmethylamine.

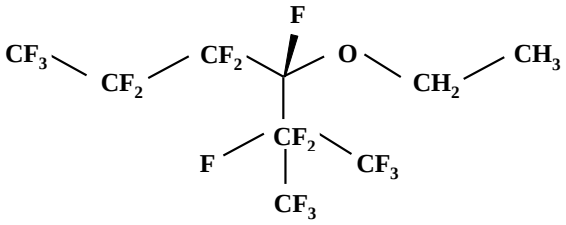

Figure 26: Chemical structure of HFE-7500 oil. The hydrofluoroether is a 3-ethoxy-1, 1, 1, 2, 3, 4, 4, 5, 5, 6, 6, 6 - dodecafluoro-2-(trifluoromethyl)hexane.

2.5 ENCAPSULATION OF MAMMALIAN CELLS & EGGS OF *C. ELEGANS* INTO AQUEOUS MICROCOMPARTMENTS

To investigate the cell recovery from and viability in microcompartments, Jurkat cells and HEK293T cells were encapsulated into 660 pL drops (corresponding to a spherical diameter of 100 µm ± 1.7 %) and 660 nL plugs. In addition, eggs of *C. elegans* were encapsulated into plugs.

Drops are aqueous microcompartments which are stabilized by surfactants and therefore prevented from uncontrolled coalescence. However, with increasing size drops become more unstable, therefore the maximum size of droplets is limited. In order to encapsulate several thousand cells into individual microcompartments plugs were used. Plugs are aqueous microcompartments stored in a holding cartridge, stably separated by immiscible oil and hence not requiring any surfactant.

Cells in drops. The cell density with in the syringe was adjusted to 2.5 x 10^6 cells/ mL and cells were stirred at 200 rpm by using an 8 mm magnetic stir-bar (Roth) in a 5 mL polyethylene syringe (Fisher Bioblock). By using a syringe pump (PHD 2000, Harvard Apparatus) at a flow rate of 1000 µL/ h, the cell suspension was injected via PTFE tubing (polytetrafluorethylene, 0.56 mm/ 1.07 mm internal/ external diameter, Fisher Bioblock) into the microfluidic device (Figure 27).

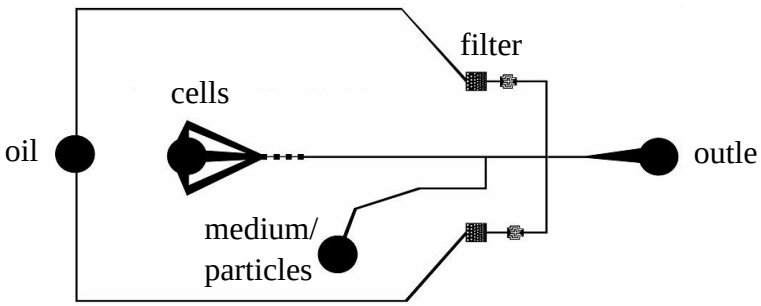

Figure 27: **Microfluidic device used for cell encapsulation.** Channel dimensions were 75 µm x 100 µm at the nozzle.

Within the device an additional stream of sterile medium was added with the same flow rate as the cells, resulting in a 1:1 on-chip dilution and a final density of 1.25 x 10^6 cells/ mL at the nozzle. Drops were generated by flow focusing (Anna et al., 2003) of the aqueous stream (2000 µL/ h), containing the cells, and a perfluorinated oil (FC40) stream (4000 µL/ h), containing 0.5 % (w/w) DMP-PFPE. The drop volume of 660 pL was calculated by dividing the flow rate by the drop frequency (determined by using a Phantom v4.2 high-speed camera).

Cells in plugs. To prepare the plugs, the cell density was adjusted to 5 x 10^6 cells/ mL and cells were stirred at 510 rpm within a 1.8 mL cryotube (Nunc) by using an 8 mm magnetic stir-bar. Subsequently, 660 nL plugs of this cell suspension (containing around 3300 cells each) and FC40 were aspirated (at 500 µL/ h) into PTFE tubing in an alternating fashion using a manually operating syringe pump.

***C. elegans* in plugs.** Eggs of *C. elegans* were encapsulated into plugs as described above for cells. To obtain the eggs, approximately hundred worms were lysed with

20 % alkaline hypochlorite solution. After several minutes, the worms had disintegrated and released the eggs, which are bleach resistant. Subsequently, the eggs were pelleted at 130 x g for 5 min and resuspended in a cryotube in M9 minimal medium (Sigma) supplemented with *E. coli* OP50 (10 % w/v of pelleted bacteria) serving as food source. For each sample, 20 plugs were loaded before the tubing was sealed (by clamping microtubes to both ends) and were incubated at room temperature.

2.6 Incubation, Recovery & Re-cultivation of Encapsulated Cells

Cells in drops. For each sample, 500 µL of emulsion were collected within a 15 mL centrifuge tube through a punched sealing and incubated within a CO_2 incubator (5 % CO_2, saturated with H_2O) at 37 °C. After different incubation times, 250 µL of the emulsion were transferred into a new centrifuge tube and broken by the addition of 15 % 1H,1H,2H,2H-Perfluoro-1-octanol (Aldrich). For re-cultivation, 10 mL semi-conditioned medium supplemented with 30 % fetal bovine serum were added to the cells. Then, after mixing and 3 min incubation (to allow sedimentation of the oil phase), 8.5 mL of the supernatant were transferred into a 25 cm^2 culture flask and the cells were incubated for 2 d within a CO_2 incubator (5 % CO_2, saturated with H_2O) at 37 °C, before imaging with bright-field microscopy.

Cells in plugs. For each sample, 30 plugs were loaded before the tubing was sealed (by clamping microtubes to both ends) and were incubated within a CO_2 incubator (5 % CO_2, saturated with H_2O) at 37 °C. After different incubation times, the plugs were infused into a 25 cm^2 culture flask and the oil was extracted using a syringe. For re-cultivation of cells recovered from plugs, 4 mL semi-conditioned medium supplemented with 30 % fetal bovine serum were added to the cells. Then, the cells were incubated for 2 d within a CO_2 incubator (5 % CO_2, saturated with H_2O) at 37 °C, before imaging with bright-field microscopy.

2.7 LIVE/DEAD STAIN

To determine recovery and viability of cells after encapsulation into microcompartments, cells were stained with a LIVE/DEAD Viability/Cytotoxicity Kit for animal cells (Invitrogen Kit L-3224). The kit uses a dual-fluorescence assay, consisting of calcein acetoxymethyl ester (calcein-AM), staining live cells green, and ethidium homodimer-1, staining dead cells red. The assay was carried out according to the manufactures instructions (1 µM calcein-AM and 1 µM ethidium homodimer-1 (EthD-1) in Dulbecco's Phosphate-Buffered Saline (DPBS)).

Cells in drops. For LIVE/DEAD stain, 10 mL staining solution were added to the recovered cells instead of semi-conditioned medium. The suspension was mixed and after 3 min of incubation (to allow sedimentation of the oil phase), the supernatant was transferred into a 25 cm^2 culture flask and incubated for 1 h at room temperature in the dark.

Cells in plugs. Instead of semi-conditioned medium 4 ml staining solution were added to the recovered cells and the samples were incubated in a 25 cm^2 culture flask for 1 h at room temperature in the dark. When using adherent cells, the staining solution was additionally supplemented with 0.25 g/l trypsin to break up cell clumps.

After staining, live and dead cells were counted manually under a microscope (Leica DMIRB) with a UV light source (LEJ ebp 100). For each sample within a 25 cm^2 culture flask, 30 fields of view (each corresponding to ~ 4.2 mm^2) were evaluated to calculate the total number of living (green stain) and dead (red stain) cells. To calculate the percentage of recovered cells (n_R), the following equation was used:

$$n_R = \frac{100 * \left(n_L * \left(\frac{A_{\text{T25 culture flask}}}{A_{\text{microscope field of view}}}\right)\right)}{n_0} + \frac{100 * \left(n_D * \left(\frac{A_{\text{T25 culture flask}}}{A_{\text{microscope field of view}}}\right)\right)}{n_0}$$

where n_L and n_D correspond to the average number of living, and dead cells respectively, counted per field of view in the microscope. $A_{T25\ flask}/\ A_{field\ of\ view}$ is the magnification factor (with A = area and T25 flask = 25 cm^2 culture flask) and the initial number of encapsulated cells is indicated by n_0.

2.8 ON-CHIP DILUTION

To obtain emulsions either with individual cells per drop or emulsions in which all droplets are occupied, on-chip dilution experiments were performed. The occupancy rate of the drop depends on the cell density and the drop size. To determine the corresponding average number of cells per drop (λ), Jurkat cells were encapsulated into 660 pL drops and CRL-2153 hybridoma cells (cell line producing monoclonal antibodies against human immunodeficiency virus 1 (HIV-1) gp120) were encapsulated into 480 pL drops, 2120 pL drops and 5960 pL drops, respectively, (as described in Chapter I, 2.5). The cells were diluted on-chip by bringing together two channels containing the cell suspension and sterile medium, respectively. The overall aqueous flow rate was kept constant at 2000 µL/ h by using two syringe pumps, while the relative flow rates of cell suspension and medium were varied. Table 1 summarises the channel dimensions, the resulting drop sizes (calculated by dividing the flow rate by the drop frequency) and the cell density in the syringe for the determination of λ for either single cells per drop or 100 % occupied drops.

Tested dilution factors were 1 (cells suspension 2000 µL/ h, medium 0 µL/ h), 1.33 (cells suspension 1500 µL/ h, medium 500 µL/ h), 2 (cells suspension 1000 µL/ h, medium 1000 µL/ h), 4 (cells suspension 500 µL/ h, medium 1500 µL/ h) and 8 (cells suspension 250 µL/ h, medium 1750 µL/ h). The number of cells per drop was determined by evaluating movies taken with a high-speed camera (Phantom v4.2) mounted on a microscope. For each dilution, 120 drops were analysed to determine the number of cells per drop. The average number of cells per drop (λ) was calculated by dividing the total number of cells counted by the number of evaluated drops.

channel dimensions: depth x width	*75µm x 100µm (1x)*	*225 µm x 100 µm (3x)*	*225 µm x 200 µm (6x)*
drop size	480 pL (1x)	2120 pL (4.4x)	5960 pL (12.4x)
cell density in the syringe for single cells per drop	5 x 10^6 cells/ mL	1.66 x 10^6 cells/ mL	0.833 x 10^6 cells/ mL
cell density in the syringe for 100 % drop occupancy	30 x 10^6 cells/ mL	10 x 10^6 cells/ mL	5 x 10^6 cells/ mL

Table 1: **Parameters for on-chip dilution.** Dimensions of the channels, resulting drop size and cell density in the syringe to determine λ for single cells and 100 % occupied drops.

2.9 Re-injection of Emulsions

The emulsions were collected in open syringes (without the plunger being inserted) and incubated within a water-saturated atmosphere (37 °C, 5 % CO_2). After the desired incubation time, mineral oil was added to fill the syringe completely before inserting the plunger and re-injecting the emulsion together with 0.5 % w/w DMP-PFPE surfactant in FC40 (injected into the oil inlet to space out the drops) into a chip with the same design as for the encapsulation step (Figure 27). To avoid fragmentation of the drops, the flow direction was reversed compared to the encapsulation step (the emulsion was injected into the outlet to avoid branching channels).

2.10 On-chip Single Cell Analysis

For fluorescence readouts of individual samples, the *lacZ* gene was introduced into HEK293T cells by retroviral transduction as described elsewhere (Stitz et al., 2001). By transfecting HEK293T cells, MLV-VSV-G-*lacZ* particles were generated (Chapter II, 2.4.3), which were used to stably transduce fresh HEK293T cells (Chapter II, 2.4.4). Then, the cells were cultivated for 2 weeks before encapsulating them together with 1.7 mM fluorescein di-β-D-galactopyranoside (FDG, Euromedex) in drops. During the

encapsulation step, a laser beam (488 nm wavelength) was focused onto the channel of the PDMS chip to excite the fluorophors using an objective with a 40-fold magnification (Figure 28, downstream of the nozzle). Emitted light was diverted by a dichroic beam splitter, filtered and collected in the Green PMT to record the first fluorescence measurement (t_0). After re-injection the second fluorescence measurement (at t_i) was captured with the same optical set-up. All signals from the photomultiplier were recorded and analysed using an in-house program running in Labview (National Instruments).

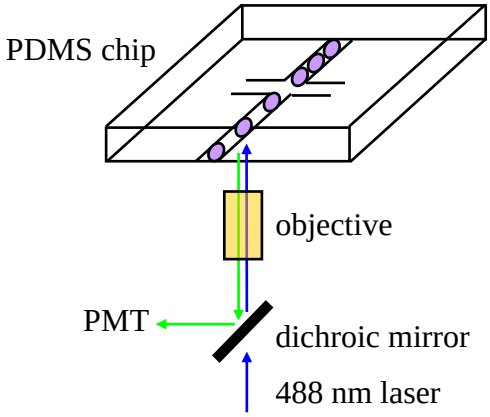

Figure 28: Optical set-up for fluorescence measurements. Fluorophores within the aqueous compartments are excited by a 488 nm laser. The emitted light is diverted by a dichroic mirror into a photomultiplier tube (PMT).

3 RESULTS

3.1 BIOCOMPATIBILITY OF CARRIER OILS & SURFACTANTS

A crucial step in the set-up of a droplet-based microfluidic platform for high-throughput cell-based assays was the identification of biocompatible surfactants used for droplet production.

The generation of stable droplets requires the addition of a surfactant to the carrier oil to decrease the surface tension thus preventing them from coalescence. However, for the encapsulation of living mammalian cells and incubation within droplets over several days, the surfactant not only had to ensure a long-term stability of the emulsion but as well must not interfere with cell viability. Several perfluoropolyether (PFPE) surfactants which differed only in their hydrophilic head group were synthesised and tested for their biocompatibility. A biocompatibility assay was performed by seeding HEK293T cells on top of a perfluorocarbon oil layer in absence and presence of four different surfactants. For evaluation of their biocompatibility microscopical bright-field images were taken at day 0, after day 1 and after day 2 (Figure 29).

In absence of any surfactant the cells remained intact and also proliferated (Figure 29A). In contrast, poly-L-lysine-PFPE (Figure 29B) and the ammonium salt of carboxy-PFPE (Figure 29C) mediated cell lysis. Therefore, these surfactants were not used for any further experiments. However, in presence of DMP-PFPE (Figure 29D) and Jeffamine®-PFPE (Figure 29E) good biocompatibility could be observed. Both surfactants did not affect the integrity of the cell membrane and even allowed for cell proliferation. On top of FC40, FC40/ DMP-PFPE and FC40/ Jeffamine®-PFPE the cells seemed to form aggregates. This could be explained by the fact that adherent cells need solid support and tend to interact with each other. Although, DMP-PFPE and Jeffamine®-PFPE showed sufficient and almost similar biocompatibility, stability tests revealed that DMP-PFPE dissolved in FC40 generated more stable emulsions than Jeffamine®-PFPE (data not shown). For this reason, DMP-PFPE was used for all following experiments in which a surfactant was required.

A

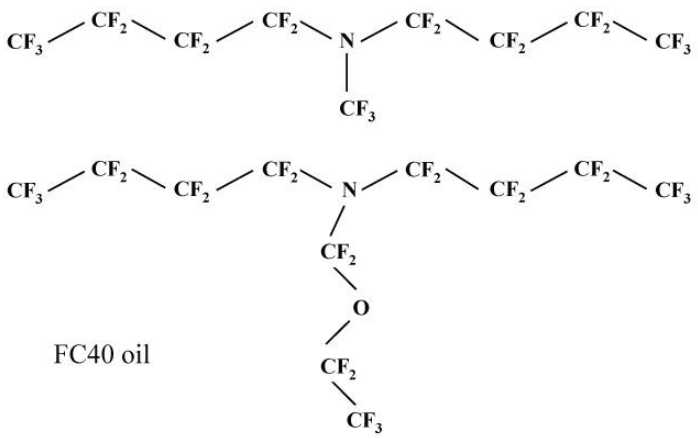
FC40 oil

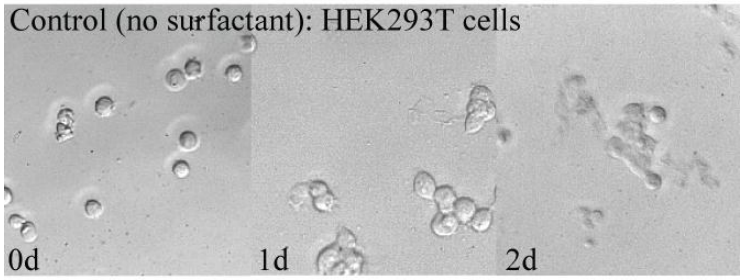
Control (no surfactant): HEK293T cells
0d
1d
2d

B

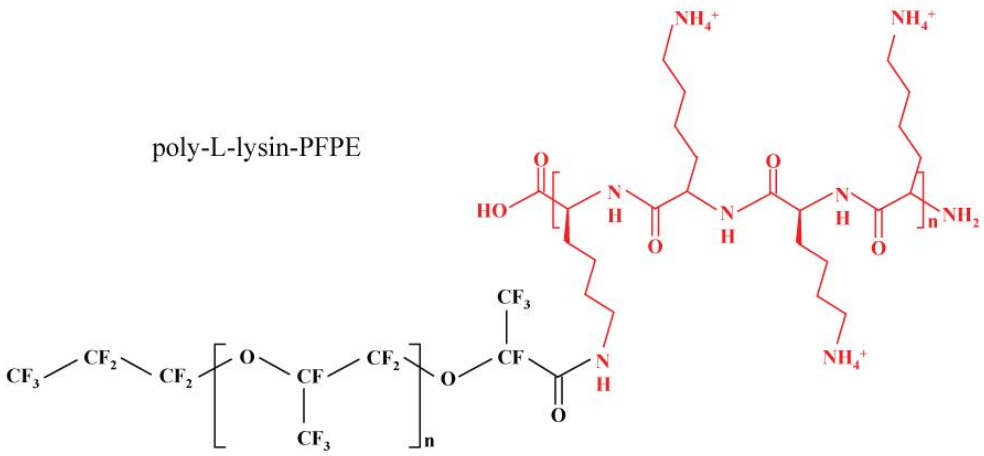
poly-L-lysin-PFPE

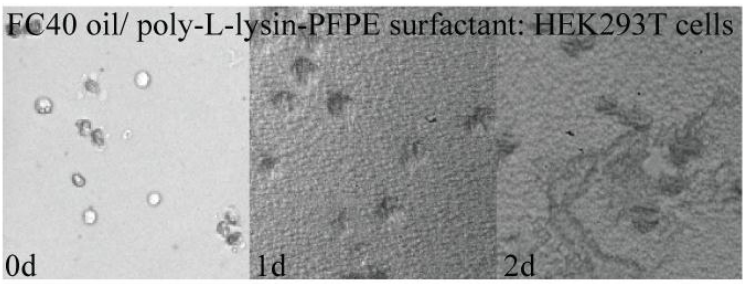
FC40 oil/ poly-L-lysin-PFPE surfactant: HEK293T cells
0d
1d
2d

C

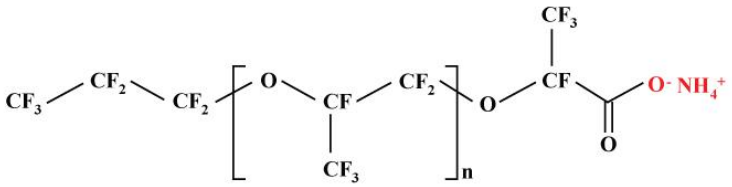

ammonium salt of carbonyl PFPE

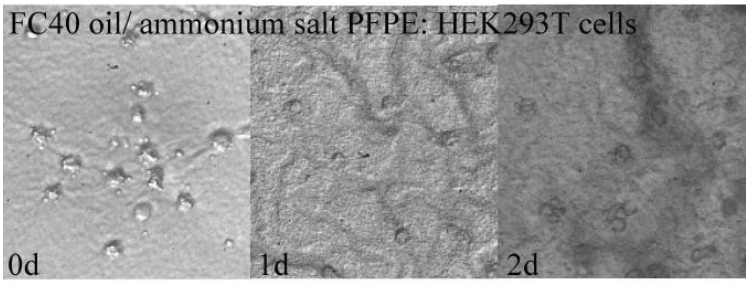

D

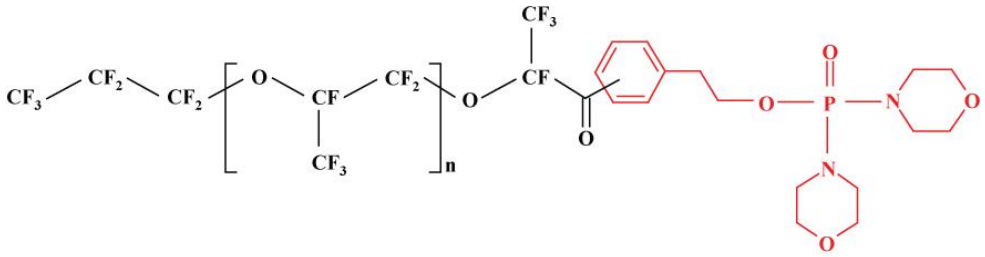

DMP-PFPE

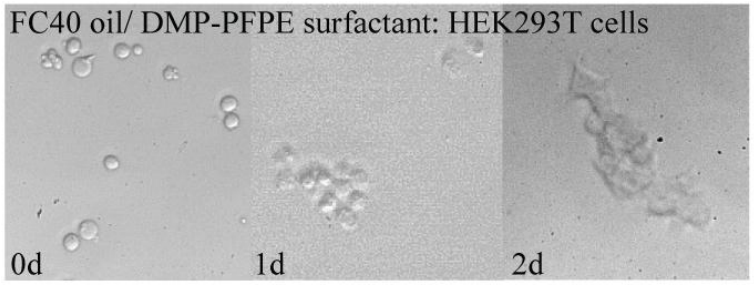

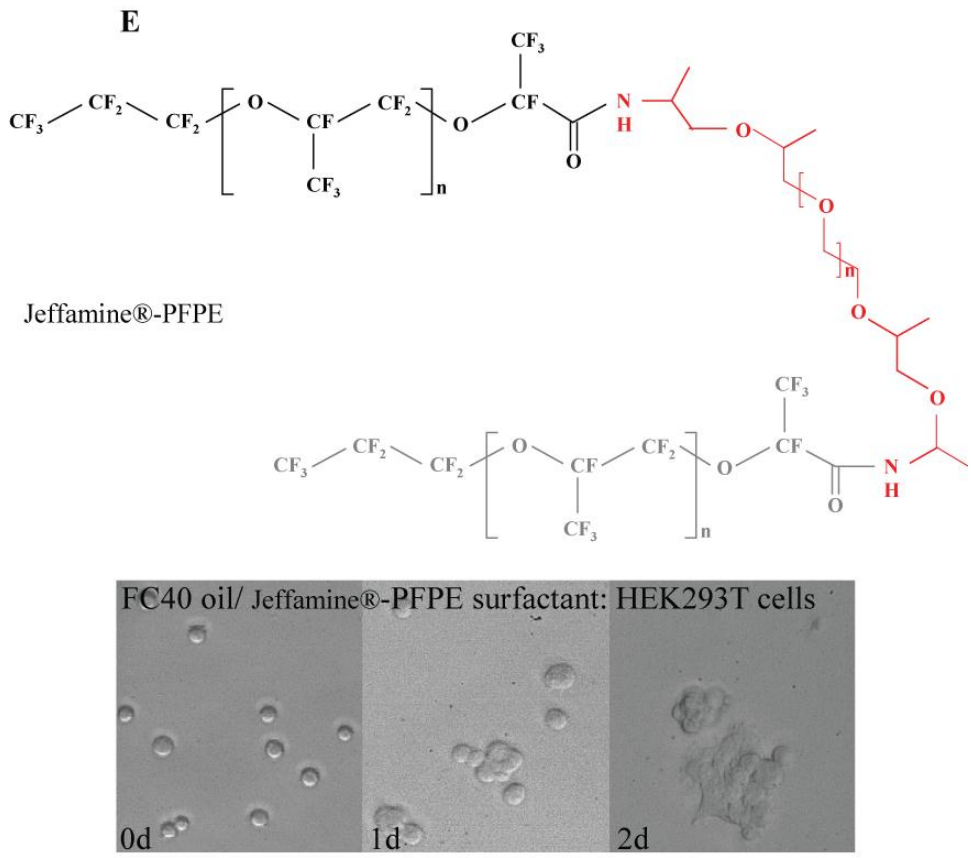

Figure 29: **Assay for the biocompatibility of surfactants.** HEK293T cells were incubated for 48 h on a layer of perfluorinated FC40 oil in the absence (control, **A**) or presence (**B**, **C**, **D** & **E**) of the indicated surfactant (0.5 % w/w).For each surfactant, the chemical structure and the results of the biocompatibility assay (microscopical bright-field images) are shown.

In addition, the biocompatibility of DMP-PFPE in comparison with another surfactant, PEG-PFPE, was determined for hybridoma cells (tACE-4E3 hybridoma cells, producing monoclonal antibodies against angiotensin I-converting enzyme). PEG-PFPE is a structural analogue of Jeffamine®-PFPE and differed only in three methyl side chains in the head group (compare Chapter I, 2.3, Figure 23 and Figure 24). Both surfactants were tested dissolved in two different fluorinated oils (0.5 % w/w), FC40 or HFE-7500 oil, respectively.

The same biocompatibility assay, as for HEK293T cells, was performed (Figure 30, for FC40 oil; Figure 31 for HFE-7500 oil). tACE-4E3 hybridoma cells on top of FC40 oil remained viable after 2 days of incubation (Figure 30A). The same result was obtained for hybridoma cells when DMP-PFPE (Figure 30B) or PEG-PFPE (Figure 30C), respectively, were dissolved in FC40.

A

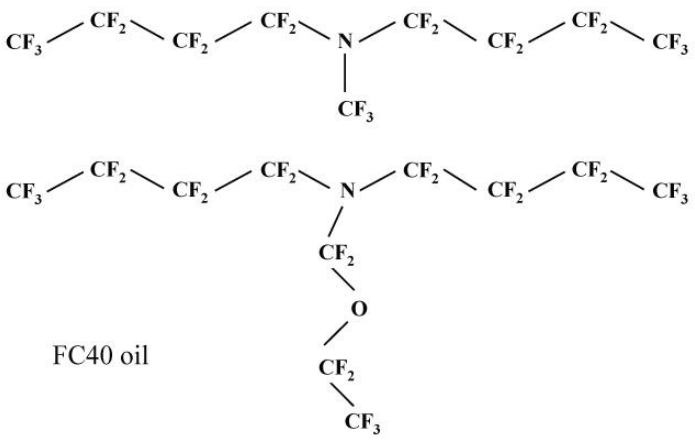
FC40 oil

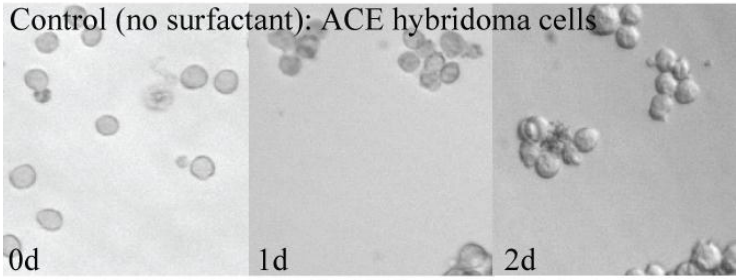
Control (no surfactant): ACE hybridoma cells
0d
1d
2d

B

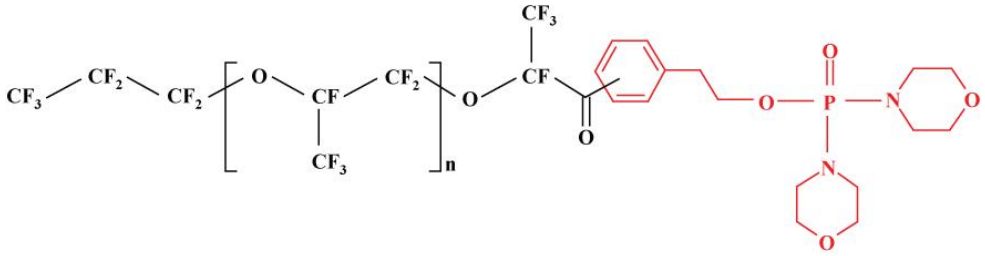

DMP-PFPE

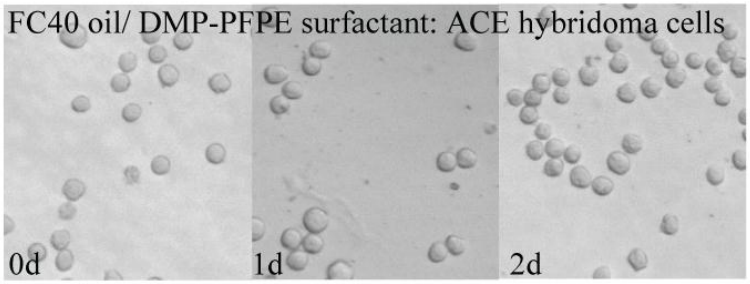
FC40 oil/ DMP-PFPE surfactant: ACE hybridoma cells
0d
1d
2d

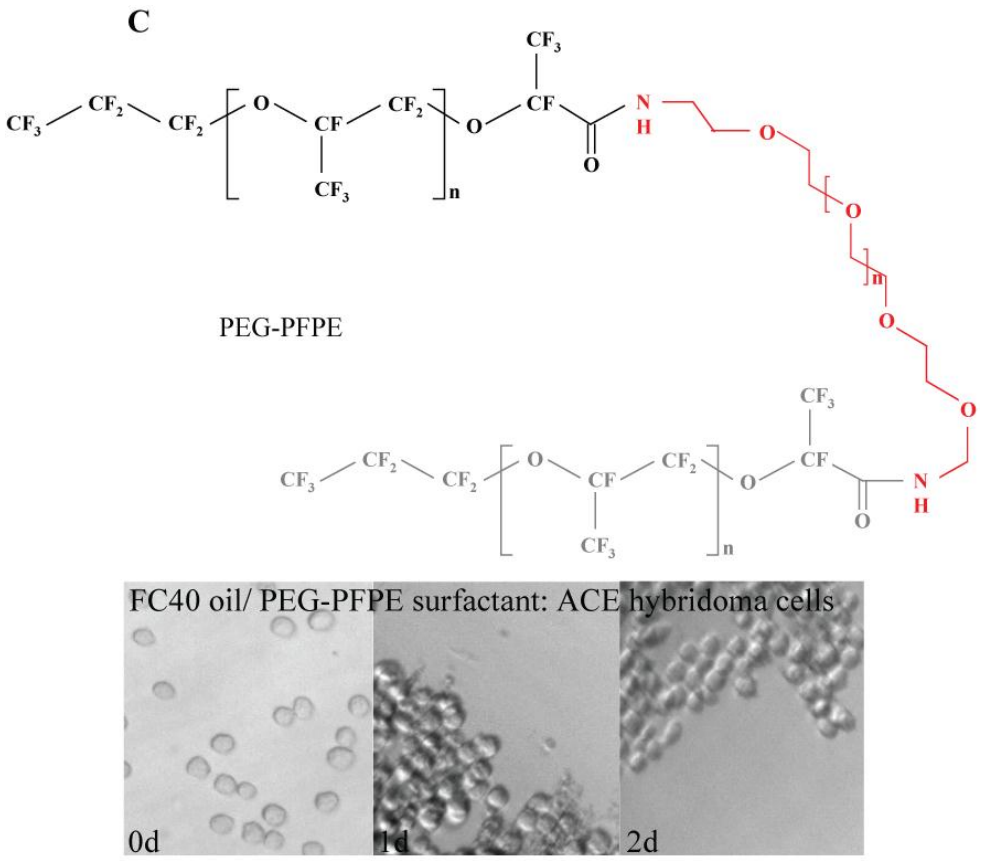

Figure 30: **Assay for the biocompatibility of surfactants.** Hybridoma tACE 4E3 cells were incubated for 48 h on a layer of perfluorinated FC40 oil in the absence (control, **A**) or presence (**B**, **C**) of the indicated surfactant (0.5 % w/w). For each surfactant, the chemical structure and the results of the biocompatibility assay (microscopical bright-field images) are shown.

In comparison, the absence of any surfactant as well as the presence of PEG-PFPE resulted in clustering of the cells. In contrast, ACE hybridoma cells on top of FC40/ DMP-PFPE did not aggregate. This effect was already observed for FC40, FC40/ DMP-PFPE and FC40/ Jeffamine®-PFPE when using HEK293T cells (compare Figure 29A, D, E). Even though, hybridoma cells are suspension cells, they also tend to interact with each other via adhesion molecules, potentially explaining their aggregation. The reason why this effect was not observed for FC40/ DMP-PFPE could be that DMP might affect the adhesion process between cells.

A

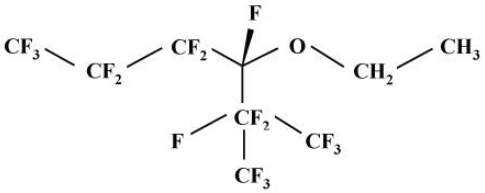

HFE-7500 oil

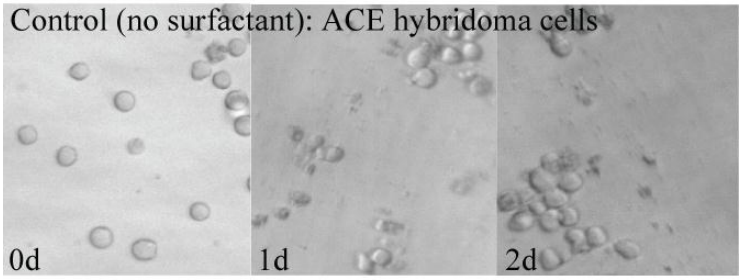

B

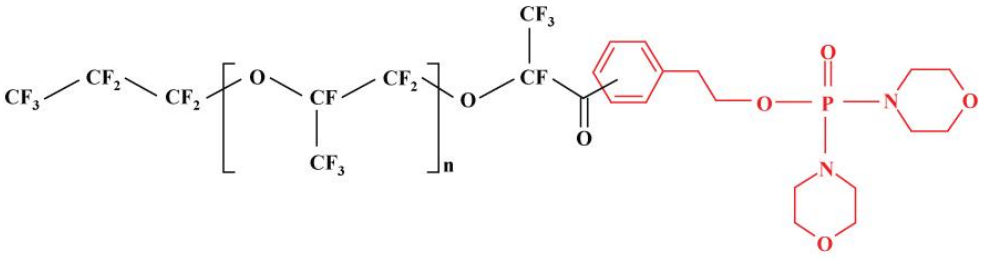

DMP-PFPE

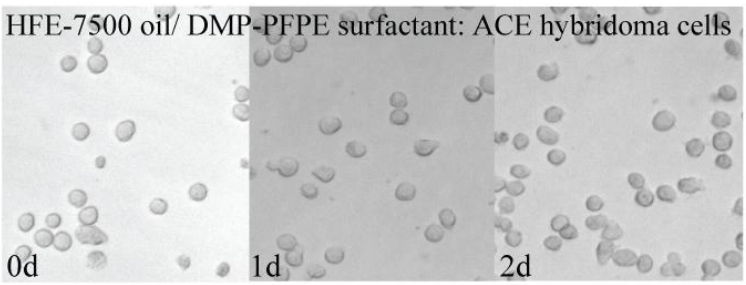

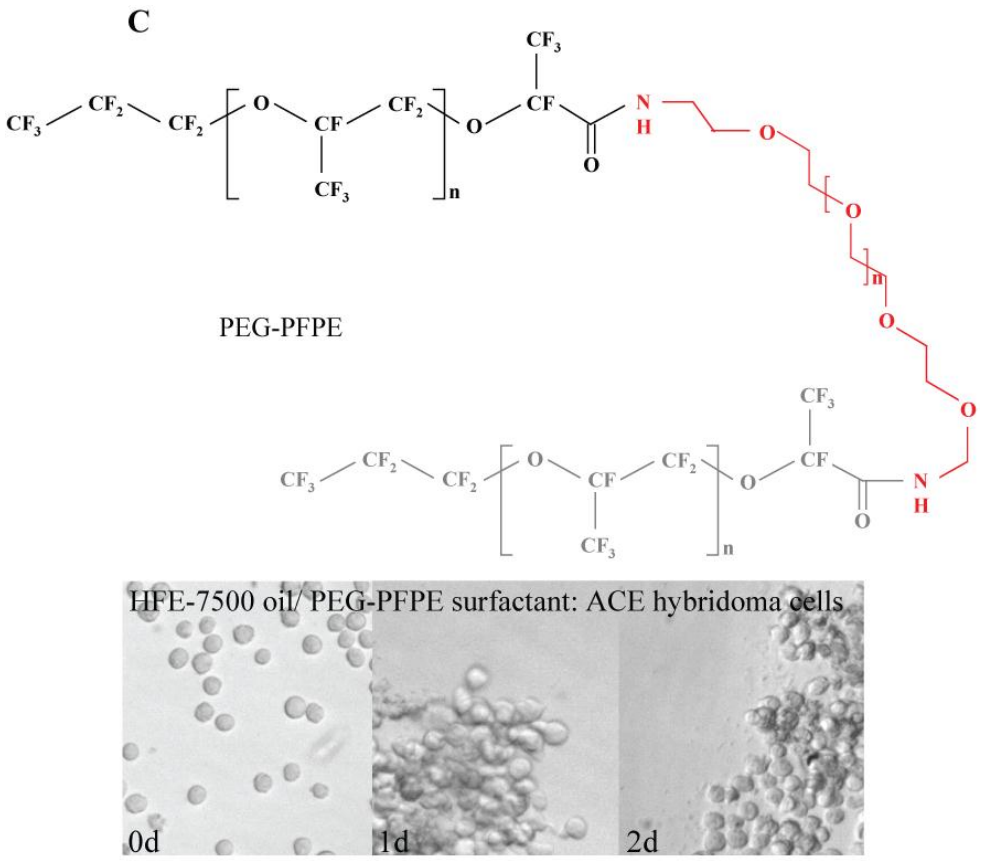

Figure 31: **Assay for the biocompatibility of surfactants.** Hybridoma tACE 4E3 cells were incubated for 48 h on a layer of perfluorinated HFE-7500 oil in the absence (control, **A**) or presence (**B**, **C**) of the indicated surfactant (0.5 % w/w). For each surfactant, the chemical structure and the results of the biocompatibility assay (microscopical bright-field images) are shown.

These results clearly showed that DMP-PFPE, but also PEG-PFPE dissolved in FC40 do not have any damaging effect on tACE-4E3 hybridoma cells.

Similar results were obtained for this cell line when using HFE-7500 as carrier oil (Figure 31). In absence and presence of DMP-PFPE and PEG-PFPE cells remained intact (Figure 31A, B, C). Once again, the clustering effect was observed for HFE-7500 (Figure 31A) and HFE-7500/ PEG-PFPE (Figure 31C) samples, but not for cells on top of HFE-7500/ DMP-PFPE (Figure 31B).

After identifying the biocompatibility of DMP-PFPE and PEG-PFPE in HFE-7500, the drop stability of both mixtures was tested. It turned out that PEG-PFPE dissolved in HFE-7500 results in more stable emulsions than DMP-PFPE (data not shown).

In summary, three surfactants, DMP-PFPE, Jeffamine®-PFPE and PEG-PFPE, biocompatible with both, adherent and suspension cells, could be identified. Stability tests showed that DMP-PFPE in combination with FC40 and PEG-PFPE together with

HFE-7500 generated also long-term stable emulsions. Therefore, PEG-PFPE dissolved in RFE-7500 oil could serve as alternative to DMP-PFPE solved in FC40.

3.2 ON-CHIP DILUTION

After the identification of biocompatible surfactants, the next goal of this study was to determine conditions that allowed for the encapsulation of a pre-defined number of cells per microcompartment. The aim was to provide the option of encapsulating single cells but also generating emulsions in which all drops contain at least one cell.

On-chip dilution experiments were performed to obtain emulsion with a maximum number of exactly one cell per drop and at the same time the lowest number of drops with multiple cells. The encapsulation step was performed on a PDMS chip with the design and channel dimensions indicated in Figure 27. From a continuous aqueous phase, 660 pL drops (corresponding to a spherical diameter of 100 μm ± 1.7 %) were created by flow focusing (Anna et al., 2003) with FC40 oil containing the biocompatible DMP-PFPE surfactant. The cell density of Jurkat cells in the syringe was adjusted to 5×10^6 cells/ mL and was changed by co-flow with a stream of sterile medium, resulting in different cell densities at the nozzle. By using two independent syringe pumps the overall aqueous flow rate was kept constant, while the relative flow rates of cell suspension and medium were varied. Cells were encapsulated into 660 pL droplets, of which 120 drops were evaluated. The probability (p) for the number of cells per drop (k) was plotted against k (Figure 32). The data was fitted to a Poisson distribution using the program OriginPro 8 and the following equation, where k is the number of cells per drop and λ is the average number of cells per drop:

$$p(x=k) = \frac{e^{-\lambda} * \lambda^k}{k!}$$

The evaluation of 120 drops was performed for five different cells densities in 660 pL drops (Figure 32). The number of cells per drop (k) was always in good agreement with a Poisson distribution, and high cell densities at the nozzle ($\geq 2.5 \times 10^6$ cells/ mL) made the encapsulation of multiple cells per drop highly likely ($p \geq 32.5$ %). In contrast, cell

densities of 1.25 x 10^6 cells/ mL and below resulted in low probabilities (p < 6 %) for the encapsulation of more than one cell per drop (while increasing the probability of finding drops without any cells inside). At the same time, the average number of cells per drop (λ) decreased from approximately 2 (at 5 x 10^6 cells/ mL) to below 0.5 (at ≤ 1.25 x 10^6 cells/ mL). Hence, the number of cells per drop could easily be regulated, even allowing for the compartmentalisation of single cells.

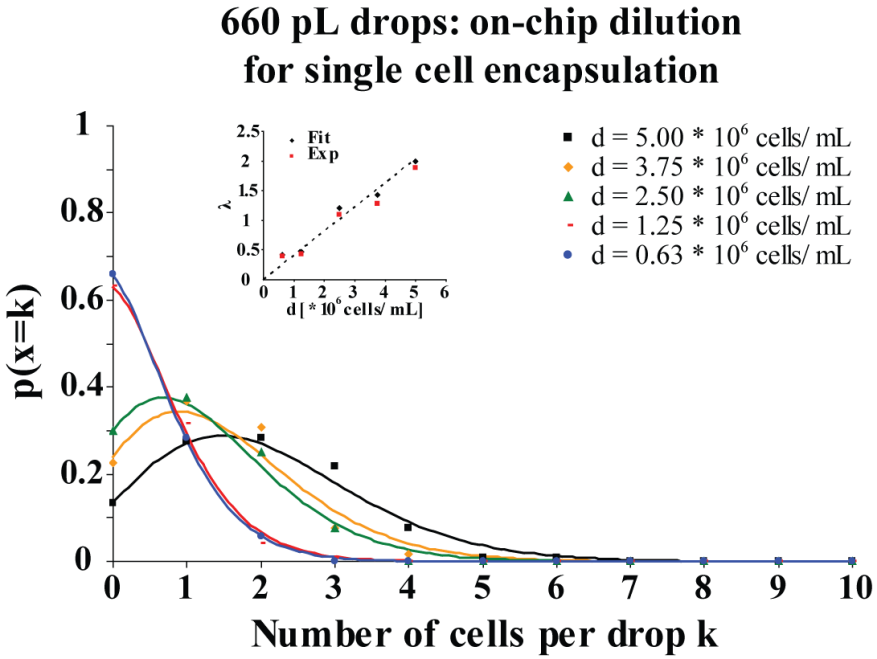

Figure 32: **On-chip dilution of the cell suspension allows for the controlled encapsulation of single cells (here: Jurkat cells).** The experimentally determined probability (p, y axis) for the number of cells per drop (k, x axis) is in good agreement with a Poisson distribution (colored lines) for various cell densities at the nozzle (resulting from on-chip dilution). **Inset:** The average number of cells per drop (λ) plotted against the cell density for the experimental data (Exp) and the Poisson distribution (Fit). The dashed line is the theoretical number of cells per drop according to the cell density only (assuming a homogeneously distribution).

To assess the efficiency of single cell encapsulation two values were taken in consideration, the percentage of single encapsulated cells and the probability for multiple encapsulated cells. Efficient single cell encapsulation corresponded to high values for single encapsulated cells and low values for multiple encapsulated cells. Taking these values into account (relative to each other), the most efficient cell density and the corresponding experimental average number of cells per drop (λ), under Poisson distribution conditions, could be determined.

For 660 pL drops, the best values were obtained at a cell density of 1.25 x 10^6 cells/ mL (Figure 32, red line). At this density, 31.67 % of the drops contained single cells and 5 % more than one cell. The experimental average number of cells per drop, λ, was 0.43 (Figure 32, insert). Therefore, the best conditions for single cell encapsulation for 660 pL drops were obtained by using a density of 1.25 x 10^6 cells/ mL at the nozzle. Figure 33 shows a sequence of digital images taken during encapsulation of single Jurkat cells under these conditions.

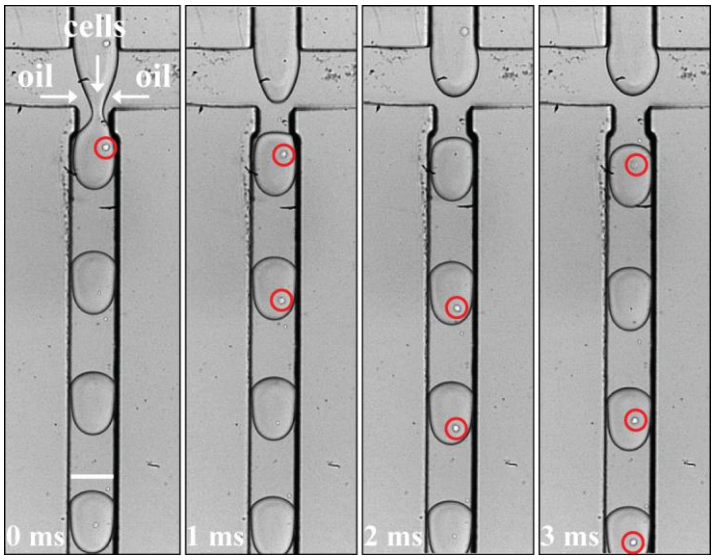

Figure 33: Encapsulation of single Jurkat cells into 660 pL droplets at a frequency of ~ 800 Hz. White arrows indicate the flow directions of the aqueous and oil phase. The white bar corresponds to 100 µm. Sequence of pictures taken during single cell encapsulation (cells are highlighted by red circles). The numbers at the bottom indicate the time intervals between the individual frames.

To explore the distribution of cells within drops of different size, on-chip dilution experiments were also performed for two larger drop volumes. The same microfluidic design as for 660 pL drops was used, with channel dimensions at the nozzle of 225 µm x 100 µm or 225 µm x 200 µm, respectively. This resulted in three- and six-times larger theoretical volumes. The actual measured volumes were 2120 pL and 5960 pL drops, corresponding to a spherical diameter of 160 µm or 220 µm, respectively. Hybridoma cells (CRL-2153, a cell line expressing monoclonal antibodies against HIV-1 gp120) were diluted on-chip allowing for single cell encapsulation. The cell density in the syringe was adjusted to 1.67 x 10^6 cells/ mL for 2120 pL drops and to 0.83 x 10^6 cells/ mL for 5960 pL drops. These numbers correlate with one third and one

sixth, respectively, of the cell density used for 660 pL droplets (where the cell density in the syringe was 5 x 10^6 cells/ mL). The probability (p) for the number of cells per drop (k) was evaluated for 120 drops, plotted against k and the data fitted to a Poisson distribution.

The resulting data for 2120 pL and 5960 pL drops were similar to the results obtained for single cells in 660 pL droplets (Figure 34). For both drops sizes, all curves for the different cells densities were in good agreement with a Poisson distribution.

For 2120 pL drops (Figure 34A), the encapsulation of two or more cells per drop was obtained with high probability ($p \geq 44.2$ %) at higher cell densities at the nozzle, $d \geq 0.83 \times 10^6$ cells/ mL. Lower cell densities, $d \leq 0.42 \times 10^6$ cells/ mL, resulted in low probabilities ($p \leq 5$ %) for the encapsulation of more than one cell per drop. At the same time, the probability of empty drops increased with decreasing cell densities, as already observed for 660 pL drops. Moreover, the best value for the ratio of single encapsulated cells (29.17 %) relative to multiple encapsulated cells (5 %) was obtained for a density of 0.42 x 10^6 cells/ mL. At this density, the experimental average number of cells per drop, λ, was 0.4 (Figure 34A, insert).

Using 5960 pL drops, the encapsulation of multiple cells per drop was highly likely ($p \geq 50.83$ %) at $d \geq 0.42 \times 10^6$ cells/ mL. On the other hand, cell densities $d \leq 0.21 \times 10^6$ cells/ mL resulted in lower probabilities of ≤ 10 % for the encapsulation of more than one cell per drop. As observed for 660 pL and 2120 pL droplets, the probability of empty drops increased with decreasing cell densities. Although, the best ratio of single encapsulated cells to multiple encapsulated cells was obtained for a density of 0.1 x 10^6 cells/ mL, the percentage of single cells was only 15 %. In comparison, for d = 0.21 x 10^6 mL the probability of single cells was more than twice as high (32.5 %), but the number of drops with multiple cells increased to 9.17 %. The values for the experimental average number of cells per drop, λ, were 0.2 for d = 0.1 x 10^6 cells/ mL and 0.55 for d = 0.21 x 10^6 cells/ mL (Figure 34B, insert).

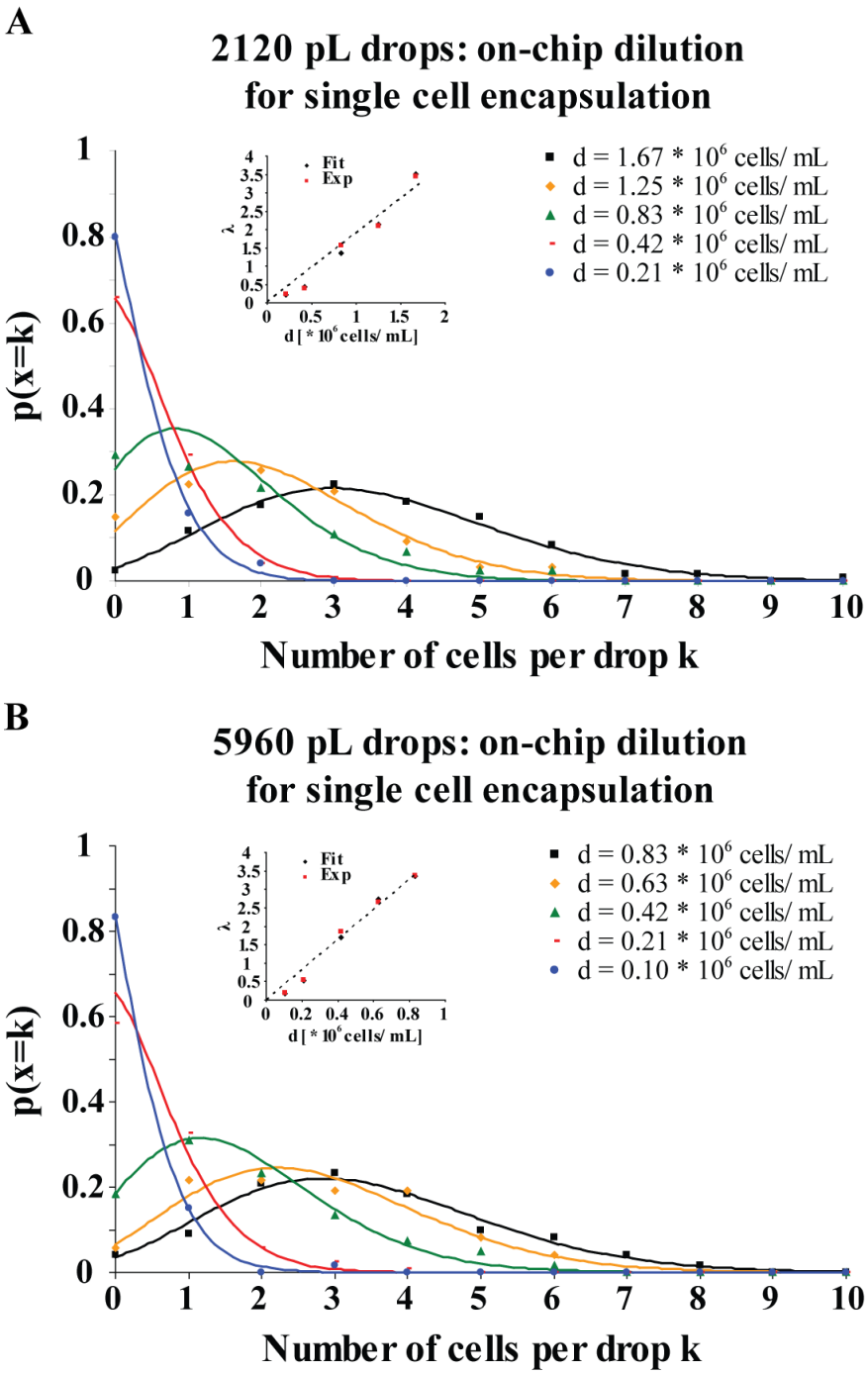

Figure 34: **On-chip dilution of suspension cells (here: hybridoma cells) to obtain single cells per drop. (A)** 2120 pL droplets resulting from channel dimensions of 225 µm x 100 µm at the nozzle, **(B)** 5960 pL drops generated in 225 µm x 200 µm channels at the nozzle.
The experimentally determined probability (p, y axis) for the number of cells per drop (k) as a function of k x axis) is in good agreement with a Poisson distribution (colored lines) for various cell densities at the nozzle. **Inset:** The average number of cells per drop (λ) plotted against the cell density for the experimental data (Exp) and the Poisson distribution (Fit). The dashed line indicated the theoretical number of cells per drop according to the cell density only (homogeneously distributed).

660 pL drops	*5 x 10^6 cells/ mL*	*3.75 x 10^6 cells/ mL*	*2.5 x 10^6 cells/ mL*	*1.25 x 10^6 cells/ mL*	*0.63 x 10^6 cells/ mL*
Empty drops	13.33 %	22.5 %	30 %	63.3 %	65.83 %
Single cells per drop	27.5 %	36.67 %	37.5 %	31.67 %	28.33 %
More than one cell per drop	50.83 %	40 %	32.5 %	5 %	5.83 %
λ	1.88	1.28	1.1	0.43	0.4
Ratio: single cells/ multiple cells	0.54	0.92	1.15	6.3	4.86

2120 pL drops	*1.67 x 10^6 cells/ mL*	*1.25 x 10^6 cells/ mL*	*0.83 x 10^6 cells/ mL*	*0.42 x 10^6 cells/ mL*	*0.21 x 10^6 cells/ mL*
Empty drops	2.5 %	15 %	29.17 %	65.83 %	80 %
Single cells per drop	11.67 %	22.5 %	26.67 %	29.17 %	15.83 %
More than one cell per drop	85.83 %	62.5 %	44.16 %	5 %	4.17 %
λ	3.46	2.1	1.57	0.4	0.24
Ratio: single cells/ multiple cells	0.14	0.36	0.6	5.8	3.8

5960 pL drops	*0.83 x 10^6 cells/ mL*	*0.63 x 10^6 cells/ mL*	*0.42 x 10^6 cells/ mL*	*0.21 x 10^6 cells/ mL*	*0.1 x 10^6 cells/ mL*
Empty drops	4.17 %	5.83 %	18.33 %	58.33 %	83.33 %
Single cells per drop	9.16 %	21.67 %	30.83 %	32.5 %	15 %
More than one cell per drop	86.67 %	72.5 %	50.83 %	9.17 %	1.67 %
λ	3.37	2.6	1.85	0.55	0.2
Ratio: single cells/ multiple cells	0.1	0.3	0.6	3.5	8.9

Table 2: Summary of data for on-chip dilution experiments for single cell encapsulation into 660 pL, 2120 pL and 5960 pL droplets.

The results for 2120 pL and 5960 pL drops confirmed the data obtained for 660 pL drops. Table 2 gives a summary of all data collected for on-chip dilution experiments for single cell encapsulation into 660 pL, 2120 pL and 5960 pL drops.
Comparing the values of λ for all three drop sizes leads to the conclusion that a value 0.4 and 0.5 is most efficient single cell encapsulation (~ 31.7 % single cells and ~ 5 % drops containing multiple cells). Consequently, the optimal cell density for efficient single cell encapsulation can be calculated according to the drop size. By dividing the desired value of λ by the drop size a first estimation for the cells density at the nozzle for efficient single cell encapsulation can be obtained. Subsequently, a fine tuning of the cell density and/ or the drop size is required to obtain a maximum number of drops hosting exactly one cell. The average number of cells per drop (λ) could be adjusted by on-chip dilution and the drops size could be varied by changing the flow rate of the aqueous phase in relation to the oil phase. Several facts could be the reason that a fine tuning is required: (1) Slight variations in the channel dimensions between devices could result in different average drop volumes. (2) Using different batches of surfactant, using a new or an older mixture of oil/ surfactant could influence the concentration of the surfactant in the oil and automatically affect the drop size. (3) Unintended variations in the pumping rate caused by the syringe pumps could affect the cell density at the nozzle and the drops size. (4) The encapsulation efficiency was typically less than 100 % due to some degree of settling and clumping of the cells within the syringe and/ or the channels and tubing, resulting in lower cells densities in the drops than initially set up in the syringe. Moreover, some cells were lost during the breaking process. And (5), the statistical error that occurs when cells are counted (both, before and after encapsulation) is around 10 % having an impact on the cell density in the syringe but also on the evaluation afterwards.

For some functional assays it is necessary to encapsulate single cells per drop, whereas other assay designs require emulsions with a drop occupancy rate of 100 %. To investigate and determine λ for this scenario, hybridoma cells were encapsulated into 480 pL, 2120 pL and 5960 pL drops. On-chip dilution experiment were performed in the same way as for single cell encapsulation with exactly same set up of microfluidic design, channel dimensions, carrier oil and surfactant, flow rates and dilution factors,

drop evaluation and statistical analysis. The only parameter which was changed was the cell density in the syringe as the aim was to generate emulsions which do not contain empty droplets.

Experimental data and curves of the Poisson distribution obtained from on-chip dilution experiments corresponding to emulsions where all drops host at least one cells were used to determinate λ and the average number of cells per drop (Figure 35).

The resulting curves were similar to the single cell encapsulation experiments. The encapsulation of multiple cells per drop was highly likely at high densities, whereas at low cell densities the probability for the encapsulation of more than one cell per drop decreased. At the same time, the probability of drops without any cells inside increased with decreasing cell densities.

Using 480 pL drops and cell densities at $d \geq 15 \times 10^6$ cells/ mL emulsions containing 100 % occupied droplets were generated (Figure 35A). When decreasing the cell density to $d = 7.5 \times 10^6$ cells/ mL, 9.17 % of the drops were empty and a further decrease to $d = 3.75 \times 10^6$ cells/ mL resulted in 54.17 % empty droplets.

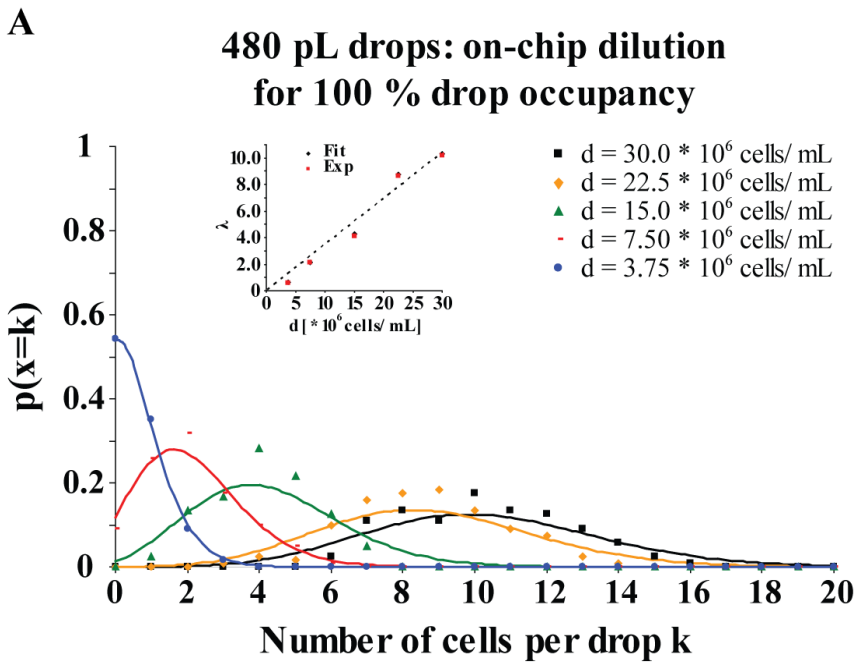

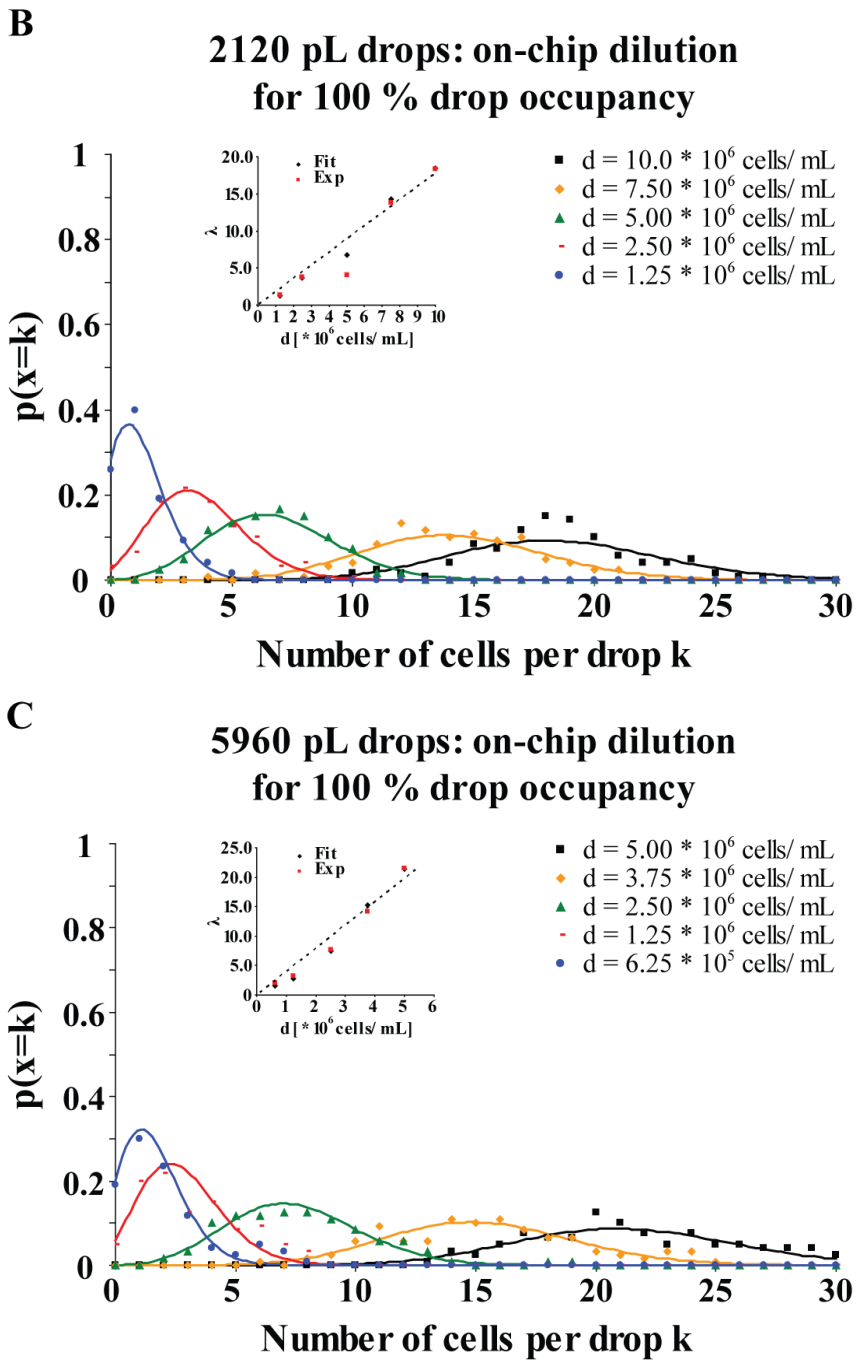

Figure 35: **On-chip dilution of suspension cells (here: CRL-2153 hybridoma cells) to generate emulsions in which all drops are occupied. (A)** 480 pL drops produced using a nozzle with a dimension of 75 µm x 100 µm, **(B)** 2120 pL droplets resulting from dimensions of 225 µm x 100 µm at the nozzle, **(C)** 5960 pL drops generated in 225 µm x 200 µm channels at the nozzle. The experimentally determined probability (p) for the number of cells per drop (k) is plotted against k and is in good agreement with a Poisson distribution (colored lines) for various cell densities at the nozzle. **Inset:** The average number of cells per drop (λ) as function of the cell density for the experimental data (Exp) and the Poisson distribution (Fit). The dashed line is the theoretical number of cells per drop according to the cell density only (homogeneously distributed).

For 2120 pL drops, cell encapsulation at densities of $d \geq 5 \times 10^6$ cells/ mL all droplets hosted one or more cells (Figure 35B). With lower cell densities ($d = 2.5 \times 10^6$ cells/ mL and $d = 1.25 \times 10^6$ cells/ mL) empty drops were generated with increasing probabilities (3.33 % or 37.2 %, respectively).

The production of 5960 pL drops, using $d = 2.5 \times 10^6$ cells/ mL resulted in 100 % drop occupancy (Figure 35C). At densities of $d = 1.25 \times 10^6$ cells/ mL, the occupancy dropped to 95 % and at $d = 0.63 \times 10^6$ cells/ mL further to only 62.8 % occupied droplets.

Table 3 gives an overview of the data obtained for on-chip dilution experiments for the generation of emulsions with an occupancy rate of 100 % for 480 pL, 2120 pL and 5960 pL drops.

480 pL drops	***30 x 10^6 cells/ mL***	***22.5 x 10^6 cells/ mL***	***15 x 10^6 cells/ mL***	***7.5 x 10^6 cells/ mL***	***3.75 x 10^6 cells/ mL***
Empty drops	0 %	0 %	0 %	9.17 %	54.17 %
One and more cells per drop	100 %	100 %	100 %	90.83 %	45.83 %
λ	10.2	8.7	4.1	2.1	0.6

2120 pL drops	***10 x 10^6 cells/ mL***	***7.5 x 10^6 cells/ mL***	***5 x 10^6 cells/ mL***	***2.5 x 10^6 cells/ mL***	***1.25 x 10^6 cells/ mL***
Empty drops	0 %	0 %	0 %	3.33 %	37.2 %
One and more cells per drop	100 %	100 %	100 %	96.67 %	62.8 %
λ	18.3	13.9	4.1	3.8	1.3

5960 pL drops	***5 x 10^6 cells/ mL***	***3.75 x 10^6 cells/ mL***	***2.5 x 10^6 cells/ mL***	***1.25 x 10^6 cells/ mL***	***0.63 x 10^6 cells/ mL***
Empty drops	0 %	0 %	0 %	5 %	37.2 %
One and more cells per drop	100 %	100 %	100 %	95 %	62.8 %
λ	21.5	14.2	7.7	3.2	2.0

Table 3: Summary of data for on-chip dilution experiments for generating emulsion containing no empty drops for volumes of 480 pL, 2120 pL and 5960 pL.

To determine λ, the average number of cells per drop, for which 100 % of the drops were occupied with cells, the cell occupancy for different cell densities was taken into account. For this purpose, the lowest cell density, for which still 100 % of the drops hosted a cell and the highest cell density for which empty drops were generated, were compared.

The results of this comparison were similar for the three different drop volumes. Cell densities resulting in λ values higher than 4 allowed, under Poisson distribution conditions, generated emulsions with 100 % cell occupancy (Table 3). In contrast, λ values lower than 4 resulted in emulsions with empty drops. Therefore, to obtain emulsions where all drops host cells values for λ above 4 should be chosen. Using such values for λ, the corresponding cell density could be estimated with consideration of the drop size. As described for single cell encapsulation, an approximate suggestion for the cell density at the nozzle could be given by dividing the desired value of λ by the drop size. Also here a fine tuning of the cell density and/ or the drop size is required to obtain emulsions with 100 % occupancy. The same facts should be taken into account as already mentioned for single cell encapsulation: (1) slight variations in channel dimensions, (2) different batches of surfactant, (3) variations caused by syringe pumps, (4) less than 100 % encapsulation efficiency and (5) the statistical errors of around 10 %.

3.3 CELL VIABILITY AND RE-CULTIVATION

After the identification of biocompatible surfactants and the ability to encapsulate pre-defined numbers of cells into droplets, the next step was to establish methods for storage of the compartmentalized samples within a CO_2 incubator and recovery of the cells from the compartments in a way that does not abolish cell viability. Moreover, the survival rates in microcompartments after encapsulation and incubation as well as the recovery rate were determined. In addition, subsequent re-cultivation of mammalian cells was demonstrated.

3.3.1 CELLS IN DROPS

Procedures allowing for the recovery of encapsulated cells had to be established. Addition of 15 % (v/v) 1H,1H,2H,2H-Perfluoro-1-octanol, to the emulsions mediated reliable breaking without an obvious impact on cell viability. This allowed for the determination of the recovery and survival rates of suspension (Jurkat) and adherent (HEK293T) cells for different incubation times within drops. For this purpose, cells were encapsulated at a density corresponding to an average of less than 1 cell per 660 pL drop (1.25 x 10^6 cells/ mL at the nozzle, resulting in a λ value of ~ 0.425 and single cells in ~ 31.7 % of all drops) and resulting emulsions were collected in 15 mL centrifugation tubes. After different incubation times at 37 °C under a 5 % CO_2 atmosphere saturated with water, the emulsions were broken and the cells were treated with a LIVE/DEAD stain to determine the total number (live and dead) of recovered cells and the survival rate (Figure 36).

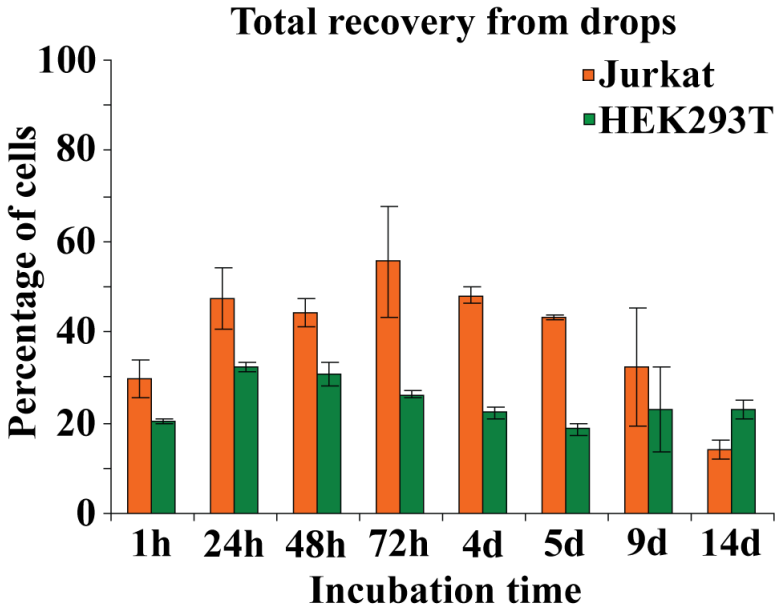

Figure 36: Recovery of cells encapsulated into 660 pL drops. The total number (live and dead) of recovered Jurkat (orange bars) and HEK293T (green bars) cells relative to the number of initially encapsulated cells. Error bars show the standard deviation of three independent experiments.

The recovery rate was defined as the total number of recovered cells divided by the number of initially encapsulated cells (equal to the aqueous flow rate multiplied by the

injection time multiplied by the cell density at the nozzle). For Jurkat cells (Figure 36, orange bars), the total recovery increased from 29 % after 1 h to more than 55 % after 2 days. This indicates some degree of proliferation within the drops, which is also supported by the fact that after 24 h the percentage of dead cells was lower than after 1 h (data not shown). During further incubation within drops, the recovery rates slowly decreased to just 14 % after 14 days. This decrease can be explained by the fact that dead cells ultimately disintegrate (after several days) and thus cannot be stained anymore. This effect is well known and was analysed in detail for bacterial cells (Villarino et al., 2000). However, early time points and the live stain are not affected by this phenomenon.

The total recovery rate for HEK293T cells (Figure 36, green bars) increased slightly from 20 % after 1 h to more than 30 % after 2 days. During further incubation within drops, the recovery rate slowly decreased to 23 % after 14 days. To confirm that recovered cells could also be re-cultivated after incubation (instead of stained), HEK293T cells incubated for 2 days within droplets were seeded in a tissue culture flask after breaking the emulsion. Two days later, microscopic analysis revealed normally proliferating cells with typical morphology (Figure 37).

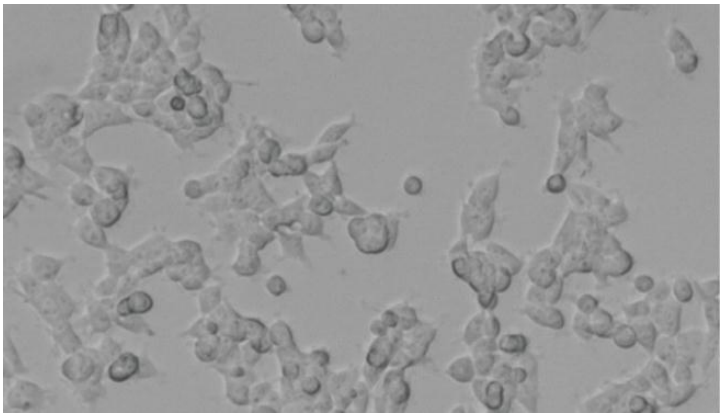

Figure 37: Re-cultivation of HEK293T after encapsulation into 660 pL drops. The bright-field image was taken after incubation for 48 h and re-cultivation for 2 days in a tissue culture flask.

To determinate cell viability in drops, survival rates were calculated. For this purpose, the total number of living cells was divided by the number of initially encapsulated cells (Figure 38).

During the first 4 days, the fraction of recovered viable Jurkat cells did not change significantly and was always in excess of 79 % (Figure 38, orange bars). Then, the percentage of live cells decreased from 71 % after 5 days to 32 % after 6 days and finally to 1 % after 14 days of encapsulation.

When repeating the experiments with adherent HEK293T cells, similar results were obtained (Figure 38, green bars). During the first 2 days, the fraction of recovered viable cells remained constant at more than 90 % before slowly decreasing to 58 % after 5 days and 39 % after 9 days. Finally, after 14 days of encapsulation, 28 % of the recovered cells were still alive. The longer cell survival compared to Jurkat cells is most likely explained by slower proliferation, resulting in slower consumption of the available nutrition, probably due to the lack of a solid support and the formation of clumps in which only the outer cell layer could proliferate.

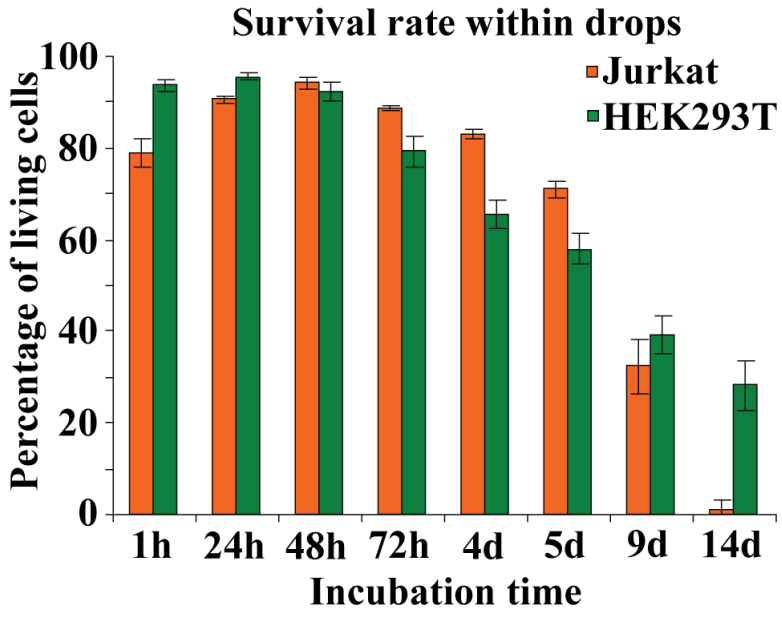

Figure 38: Cell viability of cells encapsulated into 660 pL drops. The percentage of viable Jurkat (orange) and HEK293T (green) cells recovered from emulsions was determined for the indicated time points. Error bars show the standard deviation of three independent experiments.

In an additional experiment, the effect of the cell density on the survival rates was assessed. For this purpose, five- and ten-fold higher densities of Jurkat cells were encapsulated than used initially. Comparison of the cell survival after 3 days showed that the cell density inversely correlated with the survival rate (Figure 39). Whereas

almost 90 % of viable cells were recovered by using the initial cell density, only 80 % and 68 %, respectively, survived for the 5- and 10-fold increased cell density. Insufficient gas exchange could be ruled out, since equally dense cultures in ordinary tissue culture flasks did not survive longer: using a density equal to 1 cell in a 660 pL drop (~ 1.5 x 10^6 cells/ mL), the number of viable Jurkat cells remained above 87 % for the first 2 days, before decreasing to 51 % after 4 days and 0 % after 9 days (data not shown). Therefore, it could be concluded that the encapsulated cells most likely die due to the lack of nutrition or the accumulation of toxic metabolites, but not because of compartmentalisation-specific factors such as the oil and surfactant.

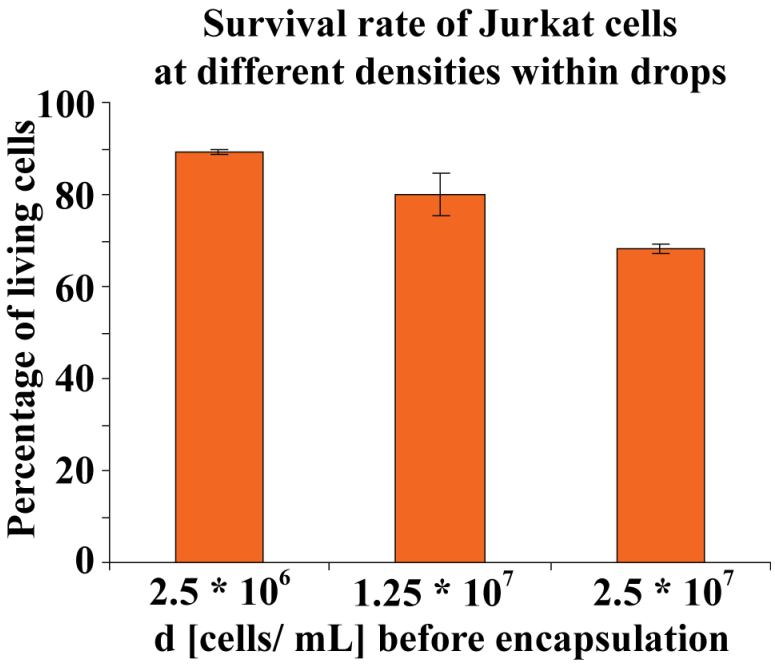

Figure 39: Cell viability at different densities of Jurkat cells encapsulated into 660 pL drops. The percentage of viable Jurkat cells was assessed for different densities after 3 days of encapsulation. Error bars show the standard deviation of three independent experiments.

3.3.2 CELLS IN PLUGS

In parallel to encapsulating cells into aqueous drops of a w/o emulsion, a system in which aqueous plugs spaced by immiscible oil within a length of tubing serve as a culture vessel, was established. This approach allows for the generation of aqueous microcompartments big enough to host small cell populations and even multicellular organisms. This cannot be achieved by simply increasing the drop size of a given

emulsion. First, the maximum size of a drop generated on a microfluidic chip is limited by the channel dimensions. Second, as the size of the drops increases, they become less stable, resulting in uncontrolled sample coalescence. These problems can be circumvented by alternately aspirating aqueous plugs and immiscible oil into a holding cartridge (e.g., a capillary or a length of tubing) (Chen and Ismagilov, 2006). This approach was used to encapsulate several thousand cells into single microcompartments. Due to the stable separation within the holding cartridge (the oil spacers cannot drain), plugs do not tend to fuse. Therefore, they do not require any surfactant.

First, holding cartridges made of different materials were assessed for their suitability to host living cells. For this purpose, 660 nL plugs were generated hosting 3300 Jurkat cells each. While gas-permeable PTFE tubing allowed the cells to survive for several days, the use of glass capillaries and vinyl tubing (all with an inner diameter of ~ 0.5 mm) resulted in cell death within 24 h (data not shown).

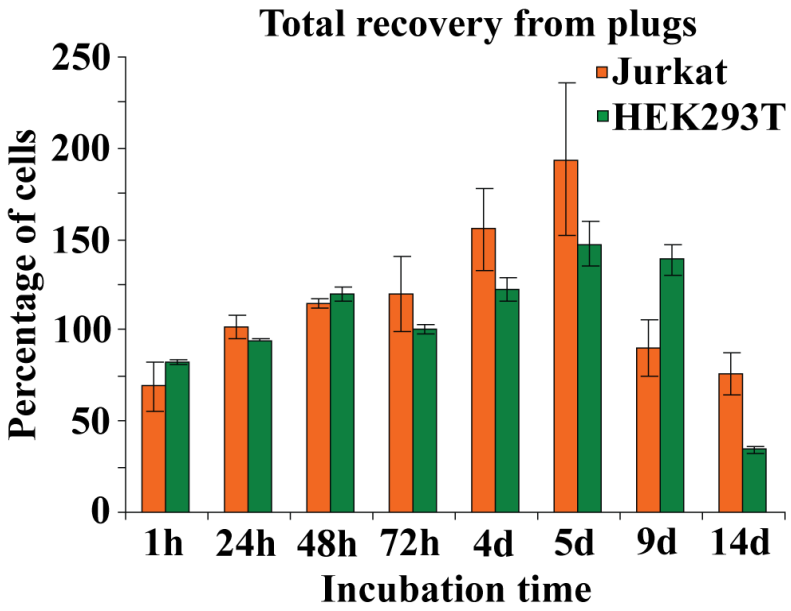

Figure 40: **Recovery of cells encapsulated into 660 nL plugs.** The total number of recovered Jurkat (orange) and HEK293T (green) cells relative to the number of initially encapsulated cells is shown for different time points. Error bars show the standard deviation of three independent experiments.

Second, the recovery rates were determined (Figure 40). For Jurkat cells the total number of recovered cells increased from 69 % after 1 h to 194 % after 5 days,

indicating roughly 1 - 2 cell divisions (Figure 40, orange bars). The recovery rate for HEK293T cells increased during the first 5 days from 83 % to ~ 147 % (Figure 40, green bars).

Re-cultivation experiments demonstrated the recovery of fully viable and normally proliferating HEK293T cells after 2 days of encapsulation (Figure 41).

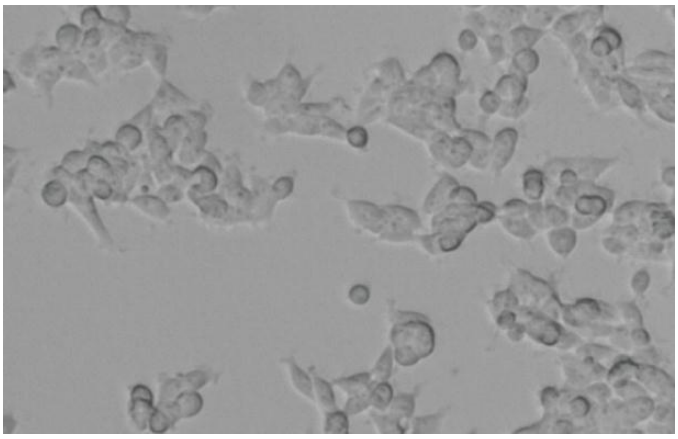

Figure 41: Re-cultivation of HEK293T after encapsulation into 660 nL plugs. The bright-field image was taken after incubation for 48 h and re-cultivation for 2 days in a tissue culture flask.

Third, the survival rates for suspension and adherent cells were assessed in plugs (Figure 42). LIVE/DEAD stains revealed that, when using PTFE tubing, the survival rate of Jurkat cells remained at ~ 90 % for the first 2 days, before decreasing gradually from 69 % after 3 days, to 38 % after 5 days, and finally to 6 % after 14 days (Figure 42, orange bars).

When repeating the experiments with adherent HEK293T cells, slightly different results were obtained. Here, the fraction of viable cells remained above 80 % for the first 4 days, before slowly decreasing to 31 % after 14 days (Figure 42, green bars).

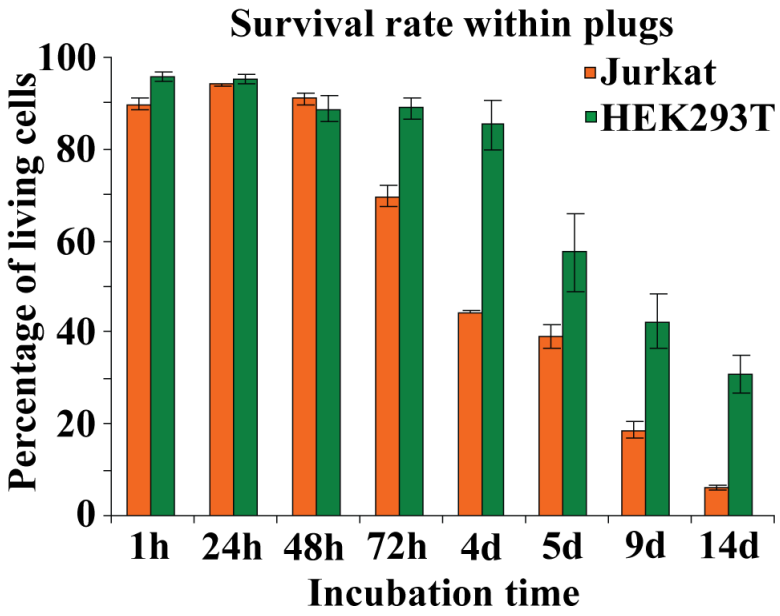

Figure 42: Cell Viability of cells encapsulated into 660 nL plugs. The percentage of viable Jurkat (orange bars) and HEK293T (green bars) cells recovered from plugs was obtained after incubation of the indicated time points. Error bars show the standard deviation of three independent experiments.

To assess the influence of the cell density on cell survival, experiments with five- and ten-times more Jurkat cells per plug were performed. Similar to droplets, an inverse correlation between cell density and survival was obtained. Whereas ~ 69 % viable Jurkat cells were recovered after 3 days when using the initial cell density, only 52 % and less than 1 % survived when encapsulating five- and ten-times more cells per plug, respectively (Figure 43). This massive decrease in cell survival is probably due to the fact that higher cell densities directly resulted in more cells per plug (even at the lowest density, all plugs were occupied), whereas, when encapsulating single cells into drops, the proportion of occupied drops was increased first (with a single cell in a drop still experiencing the same cell density).

In addition, plugs were analysed for possible evaporation during the incubation period. For this purpose, the mean length of the plugs over time was determined by measuring the size of 30 plugs for each time point using a digital slide gauge. To obtain the corresponding plug volumes, the mean length value was multiplied by the inner tube diameter. No significant decrease in size was observable, most likely due to the fact that the incubation step was performed in a water-saturated atmosphere (at 37 °C, 5 % CO_2) (Figure 44).

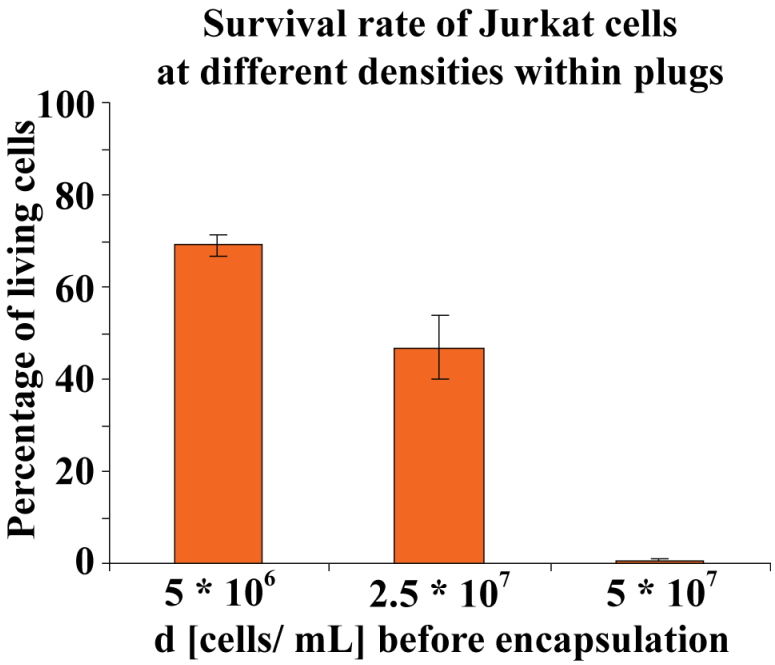

Figure 43: Cell viability at different densities of Jurkat cells encapsulated into 660 nL plugs. The percentage of viable Jurkat cells was determined for different densities after 3 days of incubation. Error bars show the standard deviation of three independent experiments.

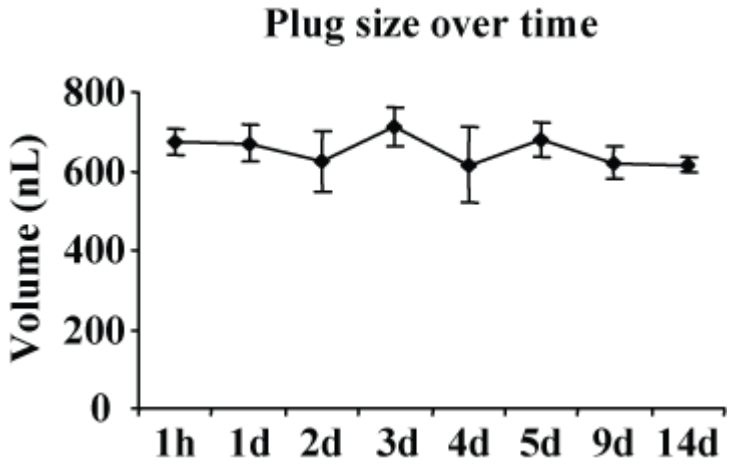

Figure 44: Mean size of plugs harboring HEK293T cells plotted against the incubation time. Error bars show the standard deviation of three independent experiments.

3.3.3 *C. ELEGANS* IN PLUGS

The possibility of encapsulating multicellular organisms into plugs was also investigated (Figure 45). For this purpose, individual eggs of the nematode *C. elegans* were encapsulated into the plugs and analysed under the microscope at different time points (Figure 45A). Whereas after 2 days hatched worms had already reached the

L2-L3 larvae stage (Figure 45B), 4 days of encapsulation resulted in the growth of adult worms and the birth of the next generation (L1 larvae) (Figure 45C). Longer encapsulation resulted in plugs hosting up to 20 worms, which finally died after 6 - 9 days. The passing of individual worms into adjacent microcompartments was never observed, even at high flow rates (up to 1000 µL/ h).

Figure 45: Growth of the nematode *C. elegans* within aqueous 660 nL plugs. (A) Eggs (black arrow) were encapsulated at room temperature. **(B)** The bright-field microscopical image after 2 days showed hatched worms in the L2–L3 larvae stage. **(C)** The bright-field microscopical image after 4 days showed larvae of the second generation of encapsulated worms (black arrows). Black bar indicates 100 µm.

3.4 ON-CHIP SINGLE CELL ANALYSIS

High-throughput, cell-based assays require the readout of individual samples after the incubation step (e.g., to screen the phenotype of individual cells within a heterogeneous population). For this purpose, microcompartments stored in a length of tubing or a reservoir have to be re-injected into an on-chip readout module subsequent to the incubation period.

To prove the feasibility of this approach, HEK293T cells were encapsulated within 660 pL drops, the resulting emulsions collected, and the samples incubated for 2 and 14 days. Subsequently, the emulsions were re-injected into a chip (same design as for the encapsulation step) and were analysed microscopically. During re-injection of the emulsion after 2 days of incubation, hardly any coalescence of individual samples was detectable (Figure 46A). After 14 d of incubation, some degree of coalescence was observable; however, the majority of drops (> 90 %) remained intact. Microscopical comparison of the drops at the time of cell encapsulation and re-injection revealed no obvious reduction of the drop size (Figure 46B). This indicates that the drops are not

subjected to significant evaporation during the incubation period (within a water-saturated atmosphere).

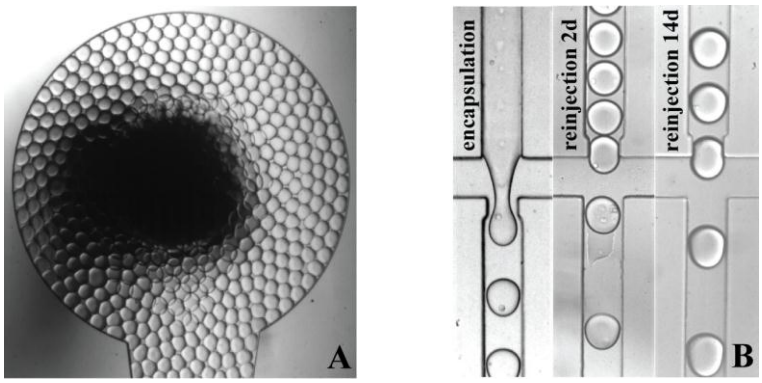

Figure 46: **Reinjection of emulsions after incubation. (A)** Bright-field image of the inlet during re-injection of an emulsion (drops containing HEK293T cells) after 2 d of incubation. **(B)** Bright-field images of individual drops during encapsulation and after reinjection (off-chip incubation for 2 and 14 d).

To demonstrate that the drops can be analysed individually after re-injection, HEK293T cells expressing a reporter gene were encapsulated into drops and a fluorescent readout was performed. For this, two weeks before the experiment, a population of HEK293T cells was incubated in bulk with viral particles (murine leukemia virus pseudotyped with the G protein of the vesicular stomatitis virus) having packaged the *lacZ* gene. The fraction of cells stably expressing the corresponding gene product (β-galactosidase) was ~ 13.9 %, as determined in an X-Gal assay (Stitz et al., 2001). During drop production, a fluorogenic substrate (1.7 mM fluorescein di-β-D-galactopyranoside, FDG) for β-galactosidase was co-encapsulated into the drops, and a laser beam (488 nm wavelength) was focused onto the channel (downstream of the nozzle, Figure 28). The emitted light was collected in a photomultiplier tube to record the fluorescence signal at t_0. This measurement was performed with the initial population of transduced HEK293T cells and a sample that had been diluted 1:9 with non-transduced HEK293T cells. At the time of encapsulation, no difference in the fluorescence signals was observable, and even drops without any cell showed the same signal intensity (data not shown). After an incubation time of 16 h at 37 °C, the emulsions were re-injected into the chip together with additional fluorinated oil (separately injected into the oil inlet to space out the drops) to repeat the fluorescence

measurement (at t_i; analysing 500 drops/ s). Plotting the maximum fluorescence intensity of the drops against the peak width (which corresponds to the drop size and therefore is a good indicator of coalescence) revealed different distinct populations (Figure 47C). Analysis of the peak width proved that even though populations with two-fold and three-fold higher volumes were observable, the majority of drops did not coalesce (> 93%). In terms of the fluorescence, two main populations with an ~ 35-fold difference in their intensity were obtained, as also confirmed by fluorescence microscopy in which the drops appeared to be either highly fluorescent or non-fluorescent (Figure 47A). Based on these observations, gates were set for the quantitative interpretation of the data (as routinely done in FACS analysis). Gates were set to solely analyse those drops that had not coalesced (corresponding to the populations with the lowest peak width). Based on the way the peak width was defined, fluorescence-positive drops appeared to be bigger (Figure 47B). Nonetheless, plotting the fluorescence against the peak width enabled non-coalesced drops to be clearly distinguished from coalesced drops for both species (positives and negatives). The use of gating led to the conclusion that ~ 5.08 % of all non-coalesced drops were fluorescence positive in the sample with non-diluted transduced cells. This number corresponds to ~ 12.7 % of the corresponding cell population when taking into account that only 40.0 % of the drops were occupied (as determined by microscopical analysis of the drops during the encapsulation step, data not shown). This value is in the same range as the fraction of positive cells determined in bulk (~ 13.9 %), by using a conventional X-Gal assay. For the diluted sample, 0.63 % positive drops were obtained, corresponding to 1.8 % of the cells (34.8 % of the drops were occupied). Compared to the non-diluted sample, the negative population showed lower fluorescence intensity. This is most likely due to the fact that all drops (even the ones without cells) contain traces of soluble β-galactosidase, resulting from the few dead cells within the syringe (during the encapsulation step). Since the diluted sample contains less enzyme in total, a lower background can be expected, too.

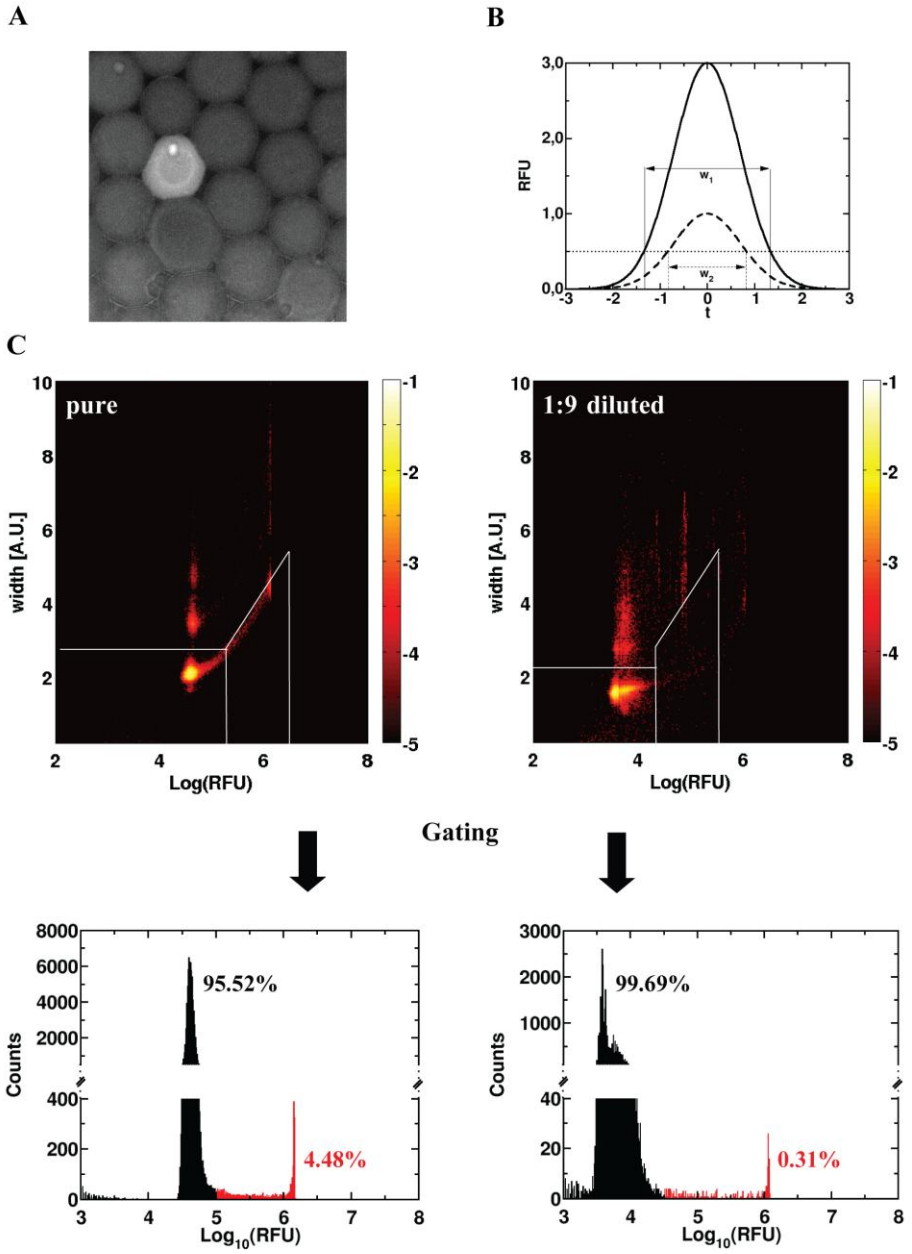

Figure 47: **Analysis of emulsions after incubation. (A)** Fluorescence-microscopic image of drops hosting *lacZ*-expressing HEK293T cells (converting the fluorogenic substrate FDG) after 16 h of incubation. **(B)** Influence of the fluorescence intensity (y axis) on the peak width (w). The peak width is defined as the time (t, x axis) for which a fluorescent signal above a certain threshold (dotted, horizontal line) can be measured (due to a drop passing the laser beam). Different fluorescence intensities of the drops (continuous and dashed peaks) result in different apparent peak widths (w1 and w2). **(C)** Fluorescence signals of drops after reinjection. **Upper panels:** fluorescence intensity (x axis) plotted against the peak width (y axis) for pure (left) and 1:9 diluted (right) transduced cells. The relative frequency of all events is color coded according to the bar on the right (numbers corresponding to the exponent of the frequency). White gates correspond to non-coalesced drops: left gate, drops considered as negatives; right gate, drops considered as positives. **Lower panel:** fluorescence intensity (x axis) plotted against the drop counts (y axis) of all events within the gates. Positive events are depicted in red, and negative events are depicted in black.

Another possible explanation would be the exchange of fluorescein between the drops. However, this seems to be unlikely, since for incubation periods of up to 24 h no significant exchange of fluorescein for the surfactants tested (including DMP-PFPE, the ammonium salt of carboxy-PFPE and Jeffamine®-PFPE; data not shown) was ever observed. The resulting 7.1-fold difference in terms of positive cells between the samples is in good agreement with the initial 1:9 dilution (assuming an accuracy of ± 10 % when counting the cultures in a Neubauer chamber before mixing leads to the conclusion that the effective ratio might have been as low as 1:7.4). In summary, these results clearly demonstrate the possibility of quantitatively analysing individual drops in a high-throughput fashion (the drops were analysed at a frequency of 500 Hz).

CHAPTER II: FUNCTIONAL ANTIBODY INHIBITION ASSAYS

1 INTRODUCTION

1.1 HUMAN IMMUNODEFICIENCY VIRUS

An infection with the human immunodeficiency virus (HIV) leads to the life-threatening acquired immunodeficiency syndrome (AIDS). In 1981, several reports about an increase in the number of cases of a rare lung infection, Pneumocystis carinii pneumonia (PCP), were published and reflect the actual beginning of the awareness of AIDS (Gottlieb et al., 1981a; Gottlieb et al., 1981b; Masur et al., 1981; Siegal at al., 1981). Two years later, several groups succeeded in the isolation and identification of the pathogenic agent that causes AIDS (Barré-Sinoussi et al., 1983; Popovic et al., 1984). Recently, in 2008, the Nobel Price in Physiology or Medicine was given to Luc Montagnier and Francoise Barré-Sinoussi for their discovery of the human immunodeficiency virus.

According to the World Health Organization Report in May 2010, an estimated 33.4 million people worldwide were living with HIV, 2.7 million have been newly infected with the virus, and 2 million died from AIDS (WHO, 2010). Therefore, HIV/ AIDS is the world's leading infectious killer and remains the leading cause of mortality worldwide.

HIV infects $CD4^+$ T-cells, macrophages and dendritic cells causing low levels of these cells, leading to failure of the immune system. HIV is an enveloped virus and belongs to the family of retroviruses, in particular to lentiviruses. The main characteristics of lentiviruses are the long incubation period and the fact that these viruses are able to replicate in non-proliferating cells, a unique feature within the retrovirus family.

HIV has an almost spherical shape with a diameter of around 120 nm (Figure 48, National Institute of Allergy and Infectious Diseases). The virus genome consists of two copies of single stranded RNA with each containing all three structural genes (gag, pol

and env) and all six regulatory genes (tat, rev, nef, vif, vpr, and vpu). The regulatory genes are responsible for controlling the steps during viral replication by activation of HIV expression, enhancement of virion release, efficient viral spread and disease progression (HIV Sequence Compendium 2008). All structural genes are produced as precursor polyproteins which are processed by the viral protease (PR). The gag genes encode for the viral capsid proteins NC (nucleocapsid, tightly bound to viral RNA), CA (core capsid) and MA (matrix protein). The pol proteins are PR (protease), RT (reverse transcriptase, containing DNA polymerase and RNA H activity), and IN (integrase). The env gene encodes for the surface envelope glycoprotein gp120 (SU) and the transmembrane glycoprotein gp41 (TM) which determine the viral tropism.

The viral genome also contains functional sequences. The long terminal repeat (LTR) is found on each end of the viral RNA is used by the integrase to insert the HIV DNA into the host genome. In addition, retroviruses feature a 5' ψ sequence representing a packaging signal for encapsidation of the retroviral RNA during replication.

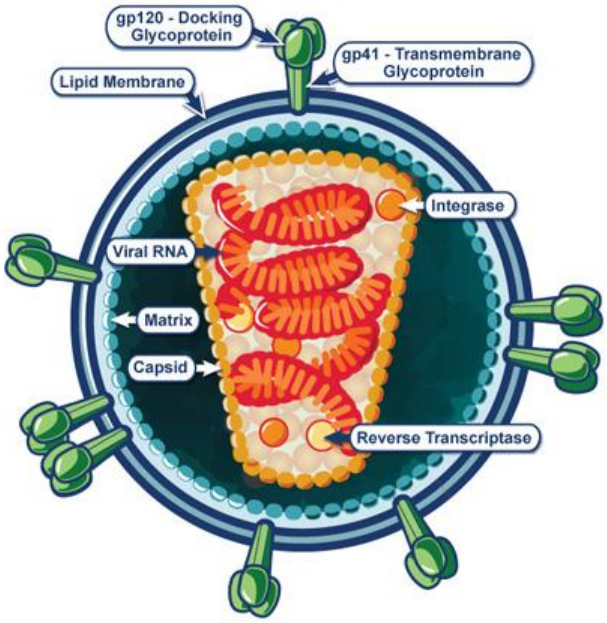

Figure 48: **Structure of HIV.** The viral RNA is bound to the nucleocapsid protein. This complex interacts with the enzymes reverse transcriptase and integrase and is surrounded by the core capsid protein and the matrix protein. The virion is enveloped by an outer membrane which is derived from the infected cell and contains the two glycoproteins gp120 and gp41. (National Institute of Allergy and Infectious Diseases (NIAID)).

1.1.1 VIRAL CELL-ENTRY AND LIFE CYCLE

The life cycle of HIV starts with the viral cell-entry process (Figure 49; National Institute of Allergy and Infectious Diseases).

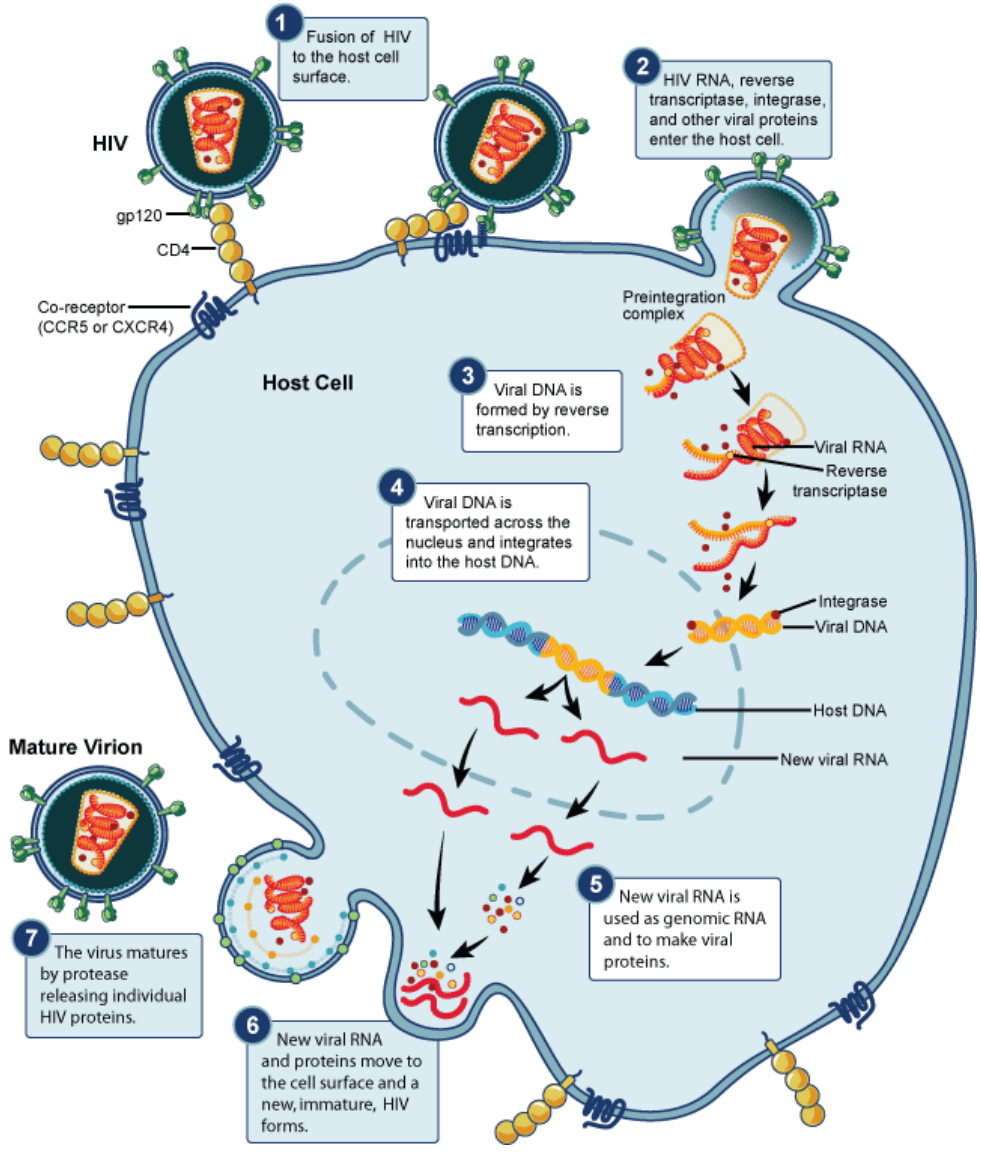

Figure 49: **Life cycle of HIV.** Gp120 interacts with its receptor CD4 and its co-receptor, usually CCR5 or CXCR4 (1). The viral content is released into the cytosol (2). Viral RNA is reverse transcripted into DNA by the enzyme Reverse Transcriptase (3). Then, the viral DNA is transported into the nucleus and integrated into the host cell DNA by Integrase (4). Afterwards, new viral RNA is transcribed and new viral proteins are translated (5) which are moved to the cell surface to form an immature particle (6). Ultimately, the virion matures by proteatic cleavage of the precursor proteins (7). (National Institute of Allergy and Infectious Diseases (NIAID)).

First, the trimeric gp120/ gp41 complex strongly interacts with the CD4 receptor and the co-receptor (CCR5 or CXCR4) on the surface of immune cells (mainly T-helper cells) (Figure 49, 1). In the next step, the HIV RNA, bound to various enzymes (RT, IN), is injected into the host cell (Figure 49, 2). Subsequently, reverse transriptase is converting the viral single stranded RNA into double stranded DNA (Figure 49, 3) which is then transported across the nucleus membrane and integrated by the integrase into the host cell genome (Figure 49, 4). From this integrated viral DNA new viral RNA and structural proteins are produced to assemble new particles (Figure 49, 5). After expression of the gag/ pol genes in the cytosol and the env proteins in the secretory pathway, all required compounds move to the cell surface, associated with the inner membrane and immature virions begin to bud from the host cell (Figure 49, 6). Finally, maturation occurs by the HIV proteases cleaving the polyproteins and release individual functional HIV proteins and enzymes (Figure 49, 7).

1.1.2 FUSION INHIBITORS

Part of this study focused on HIV fusion inhibitors, in particular neutralising antibodies. At the moment, there is no vaccine or cure for HIV/ AIDS available. The only way to prevent HIV infection is avoiding contact with the virus. Post-exposure prophylaxis guidelines were established and are believed to reduce the risk of seroconversion (development of specific antibodies against HIV detectable in the blood serum) to HIV (Cardo et al, 1997). An experimental HIV vaccine was reported to cut for the first time the risk of infection (story from BBC NEWS, 2009). Although, post-exposure prophylaxis and the experimental vaccine seem promising, both provide only incomplete protection. The most successful treatment so far is based on highly active antiretroviral therapy (HAART). This therapy consists of a combination of at least three drugs from two different drug classes. Currently, antiretroviral medications are classified into four major drug types: reverse transcriptase inhibitors, protease inhibitors, integrase inhibitors and fusion/ entry inhibitors. One of the most efficient and first approved compound for HIV treatment was azidothymidine (AZT), a reverse transcriptase inhibitor which was, at the time, a major breakthrough in AIDS therapy (Fischl et al., 1987).

Fusion/ entry inhibitors, so called new class inhibitors, offer treatment options to patients that are resistant to other therapies. Therefore, this drug class is a field of intensive research.

Since the 1990s, there were several reports that synthetic C-peptides, peptides modeling the C-helical region of HIV-1 gp41, show various degree of antiviral activity. Since then, these potent fusion inhibitors and their mechanism are under continuous investigation (Jiang et al., 1993; Wild et al., 1994; Judice et al, 1997; Koshiba & Chan, 2003; Seo et al., 2005). The C-peptide DP-178 (Fuzeon, T-20) showed the highest inhibitory activity and is broadly effective against several HIV isolates (Wild et al., 1993; Wild et al. 1994). T-20 was developed by Trimeris, a company founded by the scientists who discovered the compound. In 2003, the drug was licensed and obtained marketing approval by the FDA.

The main efforts in antibody-based HIV vaccine design focus on eliciting neutralising antibodies as immune response to the gp120/ gp41 complex. However, the main problem is that antibodies against the most immunogenic epitopes do not exhibit neutralising activity. For example, the fusion peptide of HIV (as a good target) is not even accessible before receptor binding. Moreover, it turned out that vaccine trials using monomeric gp120 gave disappointing results and antibody responses are more often directed against linear epitopes than correctly folded gp120 (Chan & Kim, 1998). Therefore, antibody-based vaccine design for HIV still remains a big challenge.

Pseudo-typed retroviral particles (see section 1.4.1) that display the processed mature, C-terminally truncated, gp120/ gp41 complex on their surface could offer an alternative for immunisation and induction of a strong B-cell response (Siegert et al., 2005; Jegerlehner et al., 2002; Lechner et al., 2002). Subsequent screening of isolated B-cells or hybridoma cells derived from these B-cells in a functional assay combined with droplet-based microfluidic technology should allow a revolutionary approach for the screening of neutralising antibody activity, instead of binding properties. One part of this doctoral thesis focused on establishing such a functional assay suitable for microfluidic HTS systems.

1.2 ANGIOTENSIN-CONVERTING ENZYME

Another aim of this work was to show the principle of screening for functionality instead of binding for enzyme inhibition. For this purpose, the clinical relevant angiotensin-converting enzyme (ACE) was chosen. ACE is part of the rennin-angiotensin system (RAS), a series of reactions that control and regulate extracellular volume and blood pressure.

1.2.1 STRUCTURE & FUNCTION

ACE is an extracellular exopeptidase (EC 3.4.15.1) and exists in two isozymes, a somatic and germinal form. Somatic ACE is present in endothelial cells, primarily in pulmonary and renal tissue and responsible for blood pressure control. Testicular (germinal) ACE is found exclusively in the testis and is involved in male fertility. ACE is a type I integral membrane protein and is converted into a soluble isoform by membrane protein secretases (Hooper et al., 1997). Somatic soluble ACE consists of two homologous catalytic domains, the so called N- and C-domain, whereas testis ACE comprises only one single active domain, identical to the C-domain of somatic ACE (structure of testis ACE or C-domain, respectively, see Figure 50; Natesh et al., 2003).
Both, the N- and C-domain, have a functional active site and hydrolyse the same peptides (angiotensin I and bradykinin). However, each of them has different substrate specificities and catalytic properties as well as different affinities for competitive inhibitors (Wei et al., 1992, Danilov et al., 1994). The C-domain of somatic ACE is the dominant angiotensin-converting site, thus suggested to be necessary and sufficient to control blood pressure (Junot et al., 2001; Natesh et al., 2003). Somatic soluble ACE was used in this study as a model drug target and therefore is subject of further discussion.

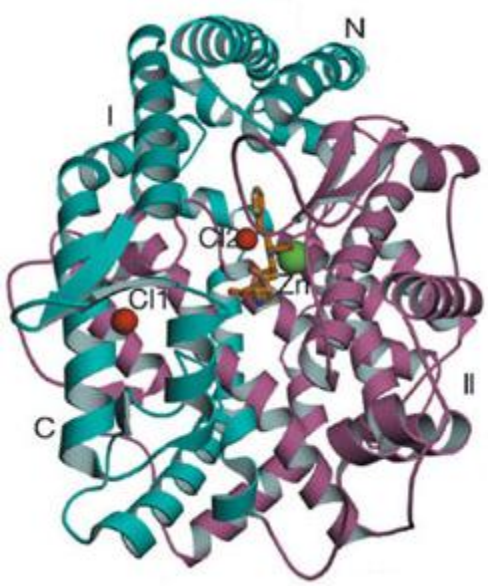

Figure 50: **Crystal structure of testis ACE.** The molecule has two secondary elements, subdomain I and II (cyan and pink, respectively). N indicates the N-terminus and C the C-terminus. The active-site zinc ion and an inhibitor molecule, lisinopril, are shown in green and yellow, respectively. The two chloride ions are shown in red. (Natesh et al., 2003)

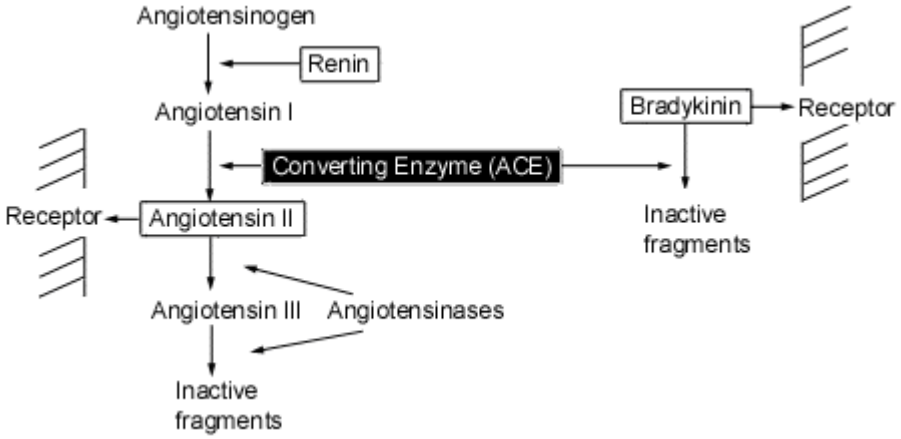

Figure 51: **Renin-Angiotensin system.** Processing of angiotensin I and bradykinin by ACE (black box; Lima, 1998).

Angiotensin-converting enzyme is a zinc-dependent metallopeptidase and exhibits two major functions in blood pressure regulation within the renin-angiotensin system (RAS). When blood pressure decreases, first the enzyme renin is released from the kidneys. Renin (an angiotensinogenase) activates RAS by cleaving angiotensinogen into angiotensin I (Figure 51 and Figure 52). Then, ACE cleaves the carboxy terminal dipeptide His-Leu from the decapeptide angiotensin I, resulting in the most potent vasopressor known, angiotensin II (Figure 52; Lima, 1998). The second function of

ACE is to inactivate the vasodilatory peptide bradykinin (Figure 51; Lima, 1998). At the end of the RAS cascade, angiotensinases destruct angiotensin II into angiotensin III and inactive fragments to limit an excess of generated angiotensin II and its vasopressoric activity.

The role of ACE in the metabolism of both vasoactive peptides (angiotensin I and bradykinin) provides a potential target to develop specific ACE inhibitors for the treatment of hypertension and congestive heart failure (Williams et al., 1994).

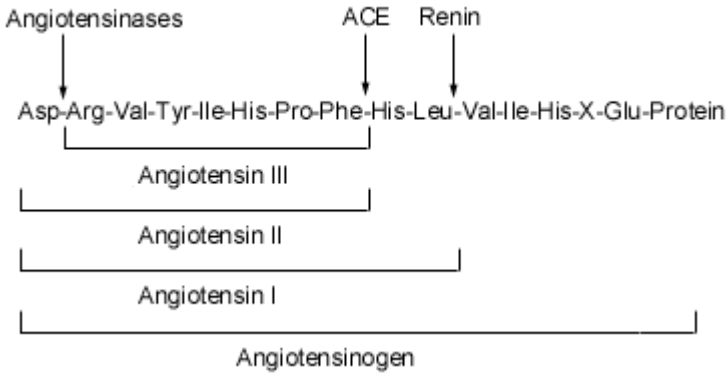

Figure 52: Sequence and enzymatic cleavage of human angiotensinogen within the rennin-angiotensin system. (Lima, 1998).

1.2.2 ACE INHIBITORS

Currently recommended standard therapies for hypertension include two types of inhibitors of the renin-angiotensin system, angiotensin II receptor blockers (ARBs) and ACE inhibitors. ARBs, a recently developed drug class (peptide or non-peptide angiotensin II antagonists), directly block the vasoconstrictory effect of angiotensin II at the receptor level by preventing the interaction of angiotensin II and its G-protein coupled receptor AT_1 (Hebert et al., 2003). ACE inhibitors (usually competitive small molecules) prevent the conversion of angiotensin I to angiotensin II, therefore decreasing angiotensin II levels in the blood. This also leads to increased levels of the vasodilatory active bradykinin enhancing the ACE inhibitor effect (Hebert et al., 2003).

The first ACE inhibitor was the small molecule drug captopril, a compound developed by the pharmaceutical company Bristol-Myers Squibb and marketed in 1981. Subsequently, several new ACE inhibitors were developed, usually designed by structure-based drug modelling, to improve pharmacokinetic properties and decreased

adverse effects (Lima, 1998). Recently, a vaccination strategy, based on virus-like particles, for the treatment of hypertension was reported (Ambuehl et al., 2007; Tissot et al., 2008). This new approach showed that immunotherapy using angiotensin II-derived peptides coupled on virus-like particles represents an efficient alternative to conventional (ARBs and ACE inhibitors) pharmacological inhibition.

Therefore, it seems to be possible to implement monoclonal antibodies as ACE inhibitors to treat hypertension. This approach was used in this work intending to set up a system for screening antibody activity against ACE in droplet-based microfluidics.

1.3 SCREENING OF MONOCLONAL ANTIBODIES

Today, passive antibody therapy provides a specific tool for transplant rejection prevention, cancer therapy, treatment of auto-immune disorders and inflammation. Moreover, monoclonal antibodies are used against microorganisms responsible for human disease.

Over many decades, several antibodies were reported, showing potential for efficient treatment of viral infection (Gallagher, 1935; Hattwick et al., 1976; Frickenhofen et al., 1990; Groothuis et al., 1993; Sáez-Llorens et al., 1998; McGory et al., 1996; Eren et al., 2005; Galun et al., 2001; Boeckh et al., 2001). XTL Biopharmaceuticals Ltd. reported on clinical trials with antibodies against the Hepatitis B and C virus (Eren et al., 2005; Galun et al., 2001). Serveral broadly neutralising antibodies for HIV could be identified implicating therapeutic and prophylactic applications as well as reverse-engineering of HIV vaccines (Mo et al., 1997; Parren et al., 1998; Gorny & Zolla-Pazner, 2004). Surprisingly, so far only one antibody for an infectious disease was approved by the FDA and licenced. Since 1998, MedImmune Inc. is marketing Palivizumab, a monoclonal antibody against the respiratory syncytial virus (RSV) disease in children (Groothuis et al., 1993; Sáez-Llorens et al., 1998). Moreover, clinical studies for a cytomegalovirus-specific monoclonal antibody (Sevirumab, Protein Design Labs) were halted as efficacy could not be verified (Boeckh et al., 2001). It occurs that the development of neutralising antibodies against viruses is a challenging task as the successful elimination of a viral infection is complex and requires a number of events such as inhibition of cell infection, viral replication, viral release and cell-cell

transmission as well as mediation of cell death of infected cells (Brekke & Sandlie, 2003; Parren & Burton, 2001; Burton, 2002).

When looking at enzyme inhibition, conventional antibodies are quite rare, although the immune system is the preferred tool to generate specific inhibitors because of the omnipotence of the antibody repertoire (Lauwereys et al., 1998; Paul, 1993). Usually, competitive inhibitors for enzymes are small molecules that have structural similarity to the original substrate but cannot be converted by the enzyme (substrate analogues). Two possible reasons could give an explanation for the fact that enzyme inhibitors are usually chemical compounds rather than antibodies. First, strategies to develop enzyme inhibitors are often based on the synthesis of transition state anlogues (Miles et al., 1998; Ringia et al., 2006; Lauwereys et al., 1998). Second, the surface topography of enzymes and antibodies is seemingly incompatible as the binding sites of both molecules have a concave shape. The active site of an enzyme is often characterised by a particular large and deep cleft (Laskowski et al., 1996). The structure of the antigen-binding site within the antibody depends on the antigen type and can be categorised in three classes: cavity (interaction with hapten), groove (interaction with peptide, DNA, carbohydrate) or planar (interaction with protein) (Webster et al., 1994). Therefore, the mechanism of enzyme inhibition is rarely due to a direct interaction of the antibody with the catalytic site but rather by steric hindrance (Arnon, 1975).

Taking these facts into account, there is a substantial need to establish HTS technologies that are suitable and sensitive enough to select rare antibodies which have the functionality to neutralise viruses or inhibit enzymes.

Screening of monoclonal antibodies is either based on the production of recombinant monoclonal antibodies by display technologies, such as phage display (*in vitro* process), or the selection of generated hybridoma cells (*in vivo* process). Both methods are explained more in detail in the following sections.

1.3.1 PHAGE DISPLAY

In 1985, George P. Smith presented phage display for the first time (Smith, 1985). Phages (baceriophages) are viruses that infect bacteria. Phage display is a screening technique that uses phage display vectors consisting of the gene for the phage coat

protein gIIIp or gVIIIp, respectively, and a 'foreign' DNA sequence. By expressing this fusion protein the desired protein or peptide is displayed on the surface of bacteriophage. This procedure ensures the connection of phenotype and genotype. Phage display for antibody screening was demonstrated by displaying antibody variable domains on the surface of bacteriophages (McCafferty et al., 1990). An extantion of this method enabled also to isolate fully human antibodies (Marks et al., 1991).

Today, most antibody libraries for phage display are sythetically generated using e.g. HuCAL (Human Combinatorial Antibody Library) technology (Knappik et al., 2000), This concept creates more than 45 billion antibody specificities by combining highly variable CDRs (complenentary-determining region) with 7 heavy and 6 light chain variable region genes. Subsequently, the antibody library is transferred into *E. coli* suitable vectors carrying the gene of the gIIIp protein. Then, *E. coli* is transformed with the display library and infected with helper phages to release the phage particles, expressing each one antibody variant on their surface. After this, the phage library can be screened for protein-protein, protein-peptide, protein-DNA and other binding properties by affinity selection (Figure 53A). Affinity selection is based on selecting a library of antibodies by their binding affinity to an immobilised antigen. Non-bound phage antibodies are washed away, whereas bound antibodies are recovered and enriched by repeating selection rounds.

In phage display, antibody libraries of up to 10^{12} variants are presented on the surface of phage particles that can be selected for the binding to a desired antigen (Figure 53A; Brekke et al., 2003). In several selection rounds, antibodies with the strongest antigen interaction are enriched. Usually screening of recombinant monoclonal antibodies is performed by ELISA (enzyme-linked immunoabsorbent assay) in a microarray fashion. In phage display, as phenotype and genotype (e.g. the binding properties of an antibody and its encoding nucleic acid) are coupled in the phage particles, selected variants can be identified by standard nucleic acid sequencing.

Antibody phage display is frequently used in the pharmaceutical industry for drug discovery and development. The first phage display-derived fully human antibody was Adalimumab (HUMIRA). HUMIRA, an anti-inflammatory drug directed against TNF-α, was discovered by Cambridge Antibody Technology. The antibody was

developed and marketed by Abbott Laboratories and is FDA approved since 2002. It is one of the most successful monoclonal antibodies that achieved blockbuster status and its sales is projected to surpass 4 billion dollar in 2010 (Lawrence, 2007).
Evidently, display systems have proven to be extremely powerful for affinity-based selections. However, the affinity does not directly correlate with any inhibitory property (e.g. neutralising or inhibitory activity). Hence, there is no guarantee that the affinity-selected antibodies show any therapeutic effects. To overcome this problem hybridoma cells can be used alternatively for antibody screening.

1.3.2 HYBRIDOMA CELLS

In contrast to phage display, where antibodies are selected for their binding properties, hybridoma cells can be directly tested in assays that determine the functional activity of monoclonal antibodies, for example neutralisation properties against viral cell-entry or enzyme inhibition (Barer & Millership, 1990; Polonis et al., 2008).
The generation of hybridoma cells is based on the fusion of antigen exposed B-cells with myeloma cells to create immortal hybridomas (Koehler & Milstein, 1975; Figure 53B from Brekke et al., 2003). Five steps can be defined: immunisation, fusion and selection, screening, characterisation and further development (Nelson et al., 2000). To obtain human monoclonal antibodies, a specific antigen is induced into transgenic mice and several weeks later, responding B-cells are isolated (immunisation). Subsequently, these cells are fused with myeloma cells resulting in hybridoma cells, and cultured in selective medium that leads to cells death of unfused myeloma cells (fusion and selection). In addition, unfused B-cells can not devide indefinetly and therefore only fused hybridomas remain alive. Subsequently, these hybridoma cells are screened individually for the release of antibodies with the desired properties. This normally requires clonal expansion for 5-10 days in culture (usually in 96 or 384 well plates) to produce sufficient concentrations of antibodies for the following screening assay (screening). This time-consuming procedure and the generation process itself strongly restrict the number of hybridoma clones that can be screened to ~ 1000, which represents only a tiny fraction (ca. $1/10^4$) of the available antibody repertoire in a mouse

and about $1/10^{6}$ of the human immune repertoire. Further analysis of the selected antibody (hybridoma clone) allows profiling of reactivity, specificity and cross-reactivity (characterisation). Once identified, monoclonal antibodies might need to be processed, e.g. for commercial exploitation (further development).

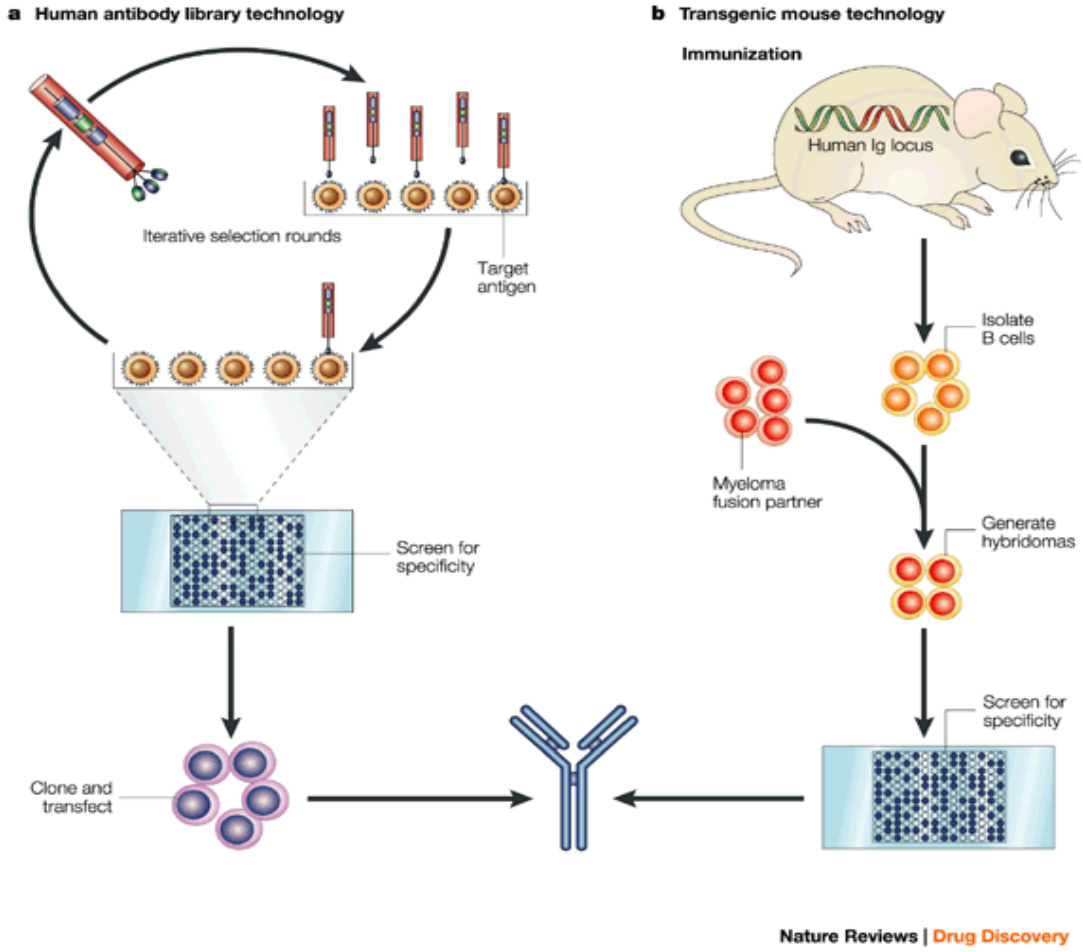

Figure 53: **Phage display (*in vitro*) and hybridoma technology (*in vivo*). (A)** The *in vitro* process is based on selecting a library of antibodies by affinity to an immobilised antigen. Non-bound phage antibodies are washed away, whereas recovered antibodies are amplified by infection in *E. coli*. Selection rounds are repeated several times to enrich the desired specificity. **(B)** The *in vivo* process is based on the immunisation of transgenic mice. The mice are genetically engineered for the expression of human immunoglobulins. B-cells isolated after immunisation are immortalised by fusion with myeloma cells. The resulting hybridoma cells release high amounts of antibodies which can be screend for functional properties. (Brekke et al., 2003)

The first FDA approved human monoclonal antibody derived by hybridoma technology was Pantitumumab (approved in 2006), an antibody for the treatment of epidermal

growth factor receptor (EGFR) expressing metastatic coloretal cancer (Cohenuram & Saif, 2007).

Phage display and hybridoma technology are undeniably two powerful screening methods. However, in phage display only binding properties are selected, whereas the generation of hybridoma cells results in a loss of immune repertoire diversity. There is certainly a huge lack in available antibody screening methods that allow for high throughput screening and selection for functional activity at the same time. A possible solution could be the development of functional assays in combination with droplet-based microfluidics for screening neutralising antibodies.

1.4 INHIBITION ASSAYS

In drug discovery, HTS methods are based on either biochemical or cell-based assays (Gad, 2005). Biochemical assays use well characterised and purified drug targets but do not represent the cellular environment. Therefore, these assays might result in the selection of molecules that, under physiological conditions, have lower efficacy or even adverse effects. Cell-based assays on the other hand are able to reflect the mechanisms involved in diseases and provide a native (physiological) environment for drug targets. Moreover, detailed knowledge about the drug target is not required as the physiological context offers several potential working points.

Cell-based assays typically use quantification of changes in light adsorption/ transmittance, luminescence or fluorescence for detection of drug effects (Chen et al., 2000; Holland et al., 2004; Pozzo et al., 2008; Westby et al., 2005). For viral inhibition assays, most of the systems are based on reporter genes (e.g. green fluorescent protein (GFP), luciferase and β-galactosidase) that are expressed upon viral infection (Westby et al., 2005). Therefore, a decreased reporter signal in a sample can be interpreted as the presence of a potent inhibitor. However, the negative linking of viral cell-entry with the reporter signal results in misleading information and potential selection of false positives. The lower signal could also result from cytotoxic effects of the drug compound or other adverse events that affect cell viability. Hence, a positive coupling of inhibition and the readout signal seems to be much more advantageous (Clausell-Tormos et al., 2010).

This doctoral study focused on two different approaches for functional assays (assays to screen neutralising/ inhibiting antibodies) which were assessed for their suitability for the microfluidic platform: (1) a cell-based viral cell entry inhibition assay (performed in virus-cell or cell-cell fusion fashion coupling the inhibition with a positive fluorescence signal) and (2) a biochemical enzyme inhibition assay for screening antibodies inhibiting enzymatic activity. In the first approach, the patented novel viral inhibition assay was adjusted and optimised for the screening of neutralising HIV antibodies (Clausell-Tormos et al., 2010; (WO/2006/082385) SCREENING METHOD). This cell-based selection assay could be performed using pseudotype viruses to simulate viral cell-entry (Chapter II, 3.1) or cell-cell fusion to mimic fusion of the cell and viral membrane (Chapter II, 3.2).

The mechanism of both approaches, viral cell-entry (Figure 54A, B) and cell-cell fusion (Figure 54C), is based on genetically engineered cells (indicator cells) that continuously generate a strong fluorescence signal (surface displayed tPA) unless transduced with pseudotype particles (effector particles) or fused with effector cells. Upon cell-entry or cell-cell fusion a vector encoding an shRNA abolishing the puromycin resistance of the indicator cells and/ or a suicide gene (thymidine kinase) are introduced into the indicator cells. Hence, the indicator cells die in presence of puromycin or ganciclovir (a thymidine kinase substrate that is converted into a cytotoxic product), leading to a shutdown of the reporter gene signal.

The second approach aimed to set up an assay for the inhibition of enzymes by specific antibodies. Angiotensin-converting enzyme (ACE) served as a model system (Chapter II, 3.3). Combining both assays with microfluidic technology should allow a novel high throughput approach for the screening of neutralising and/ or inhibiting antibodies.

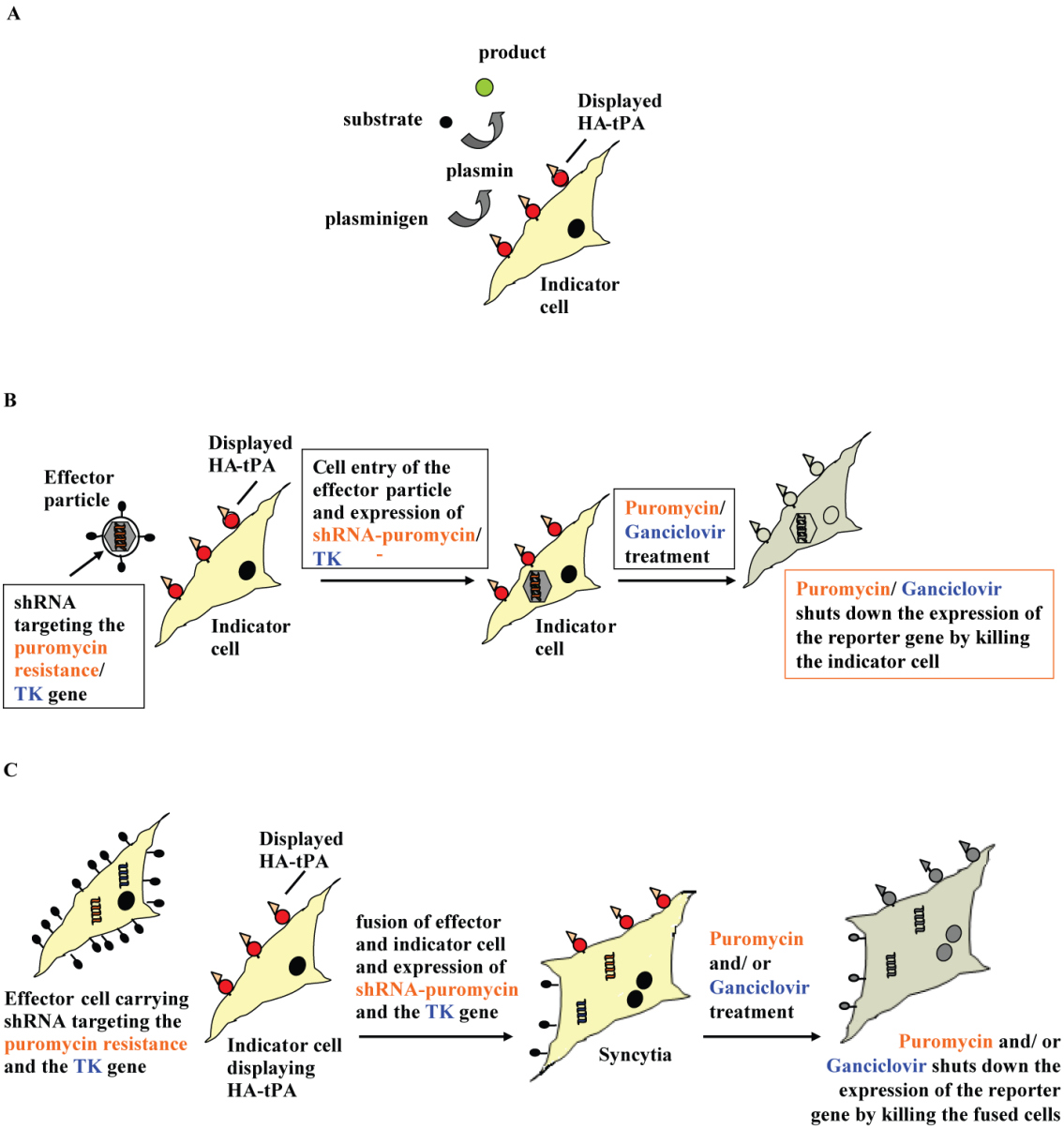

Figure 54: Viral inhibition assay. Indicator cells express the reporter gene tPA. (A) Cells constitutively stably expressing a membrane-bound and HA-tagged form of the human tissue plasminogen activator (HA-tPA) unless infected effector particles. HA-tPA cleaves plasminogen into plasmin which itself converts a non-fluorescent substrate (HDVLK-Amc) into a fluorescent product. **(B)** Virus-mediated assay using downregulation of the enzyme Puromycin-N-acetyltransferase in indicator cells by introducing a vector carrying an shRNA targeting the puromycin resistance. Puromycin addition leads to cell death. And virus-mediated assay using a suicide gene (thymidine kinase, TK) which is expressed upon cell-entry and leads to cell death when ganciclovir is added. **(C)** Cell-cell fusion assay using puromycin shRNA and TK gene to induce cell death and downregulate the tPA signal.

1.4.1 PSEUDOTYPED RETROVIRAL PARTICLES

The viral inhibition assay applied in this study uses effector particles (derived from murine leukaemia virus, MLV) pseudo-typed with the envelope proteins (env) of HIV, resulting in the host range tropism of this species (Siegert et al., 2005). In pseudo-typed vectors or viral particles the structural proteins (nucleocapsid, capsid and matrix protein) and the envelope protein originate from different viral species. Using this method the host tropism as well as the stability of the particle can be altered

MLV belongs to the family of retroviruses (Chapter II, 1.1). Retroviral vectors are the most widely used delivery vehicle in research and gene therapy due to their efficiency of integration (Bushman, 2007; Gene Therapy Clinical Trials Worldwide). Wildtype retroviral particles are capable of integrating their genome into the host cell genome, resulting in a productive infection (Figure 55A; Nikol & Hoefling, 1996). Replication-defective retroviral particles are based on separated transfer gene, gag/ pol and env vectors (Figure 55B; Nikol & Hoefling, 1996; Trajcevski et al., 2005). This non-replicative delivery system improves safety and allows pseudo-typing that can increase transfer efficiency.

Pseudo-typing of MLV was demonstrated successfully for different envelope proteins (Burns et al., 1993; Sung & Lai, 2002). The possibility of retroviral pseudo-typing broadened their host-cell range, increased viral titers, stability and transduction efficiency opening wider fundamental research and clinical applications. An important feature of pseudo-typing is the fact that the entry process can be separated from other steps of the viral life cycle offering a simple tool for screening entry inhibitors as well as viral receptors (Sanders, 2002).

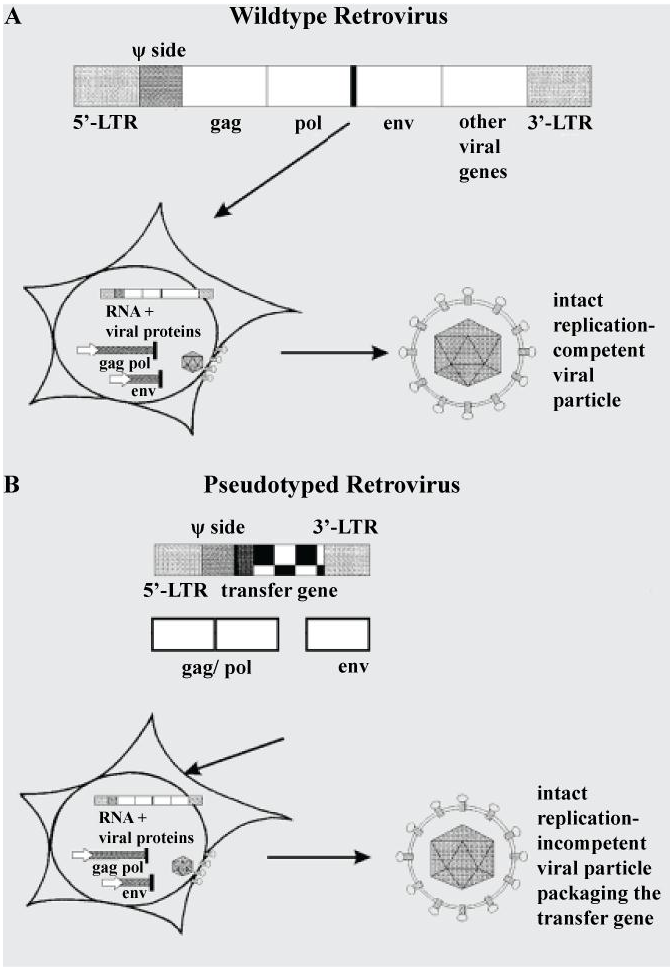

Figure 55: Retroviral particles. (A) Replication-competent wildtype particles. **(B)** Pseudotyped replication-incompetent retroviral particles. (Nikol & Hoefling, 1996).

1.4.2 RNA INTERFERENCE

In this study RNA interference (RNAi) was used in virus-cell and cell-cell fusion assays to abolish the puromycin resistance of the indicator cells by downregulating the enzyme Puromycin-N-acetyltransferase. RNAi is a very selective process and has a robust effect on gene expression. These features make the system quite useful as a research tool, as the introduction of synthetic RNA into cells can suppress specific genes.

RNA interference is a mechanism in living cells to control gene expression (gene silencing). It plays an important role in gene expression and development, but also serves as immune response to parasitic genes. The discovery of RNAi dates back to the 1980s and the phenomenon was reported by several groups (Izant & Weintraub, 1984; Ecker & Davis, 1986; Napoli et al., 1990; Nellen & Lichtenstein, 1993). In 1998,

Andrew Fire and Graig C. Mello found out that double-stranded RNA was substantially more effective at producing interference than was single stranded RNA (Fire et al., 1998). Eight years later, both shared the Nobel Price in Physiology or Medicine for their work (Daneholt, 2010).

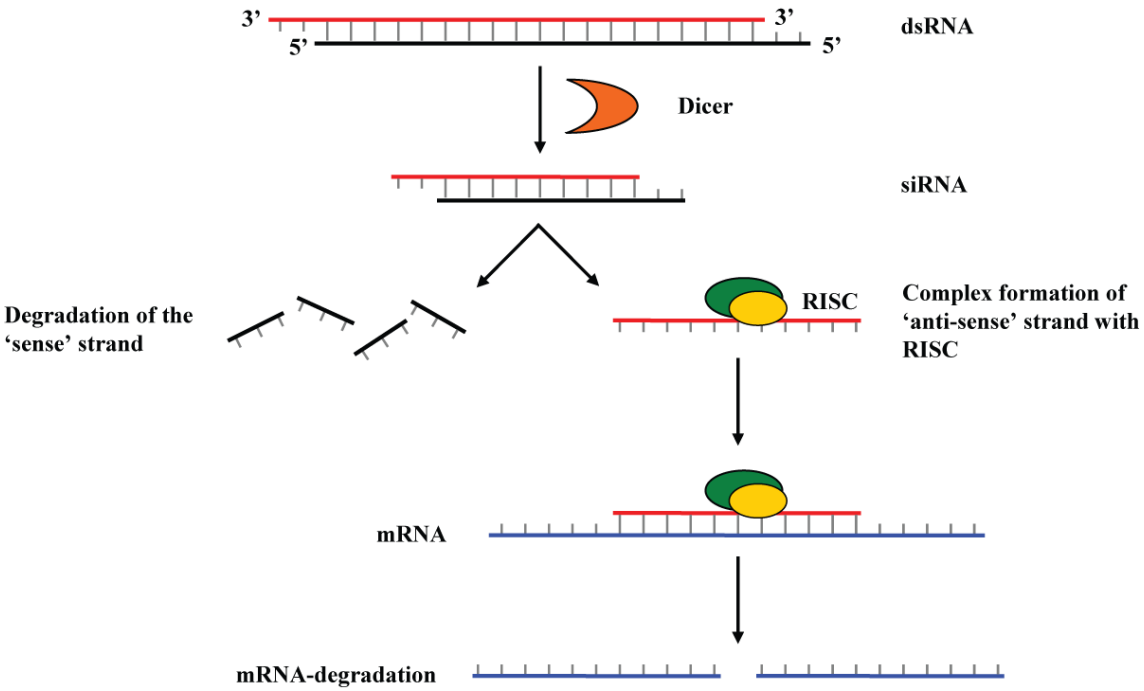

Figure 56: **Mechanism of RNA interference.** Double stranded RNA is cleaved by the protein Dicer. The RNA-induced silencing complex (RISC) binds to one of the single RNA strands and forms a complex that degrades the complementary target mRNA.

The mechanism of the gene silencing process starts with cleavage of double stranded RNA (dsRNA) into small interfering RNA (siRNA) by the ribonulease protein Dicer (Figure 56). Double stranded RNA is either endogenous or introduced into the cell, e.g. by retroviral delivery using RNA strands encoding two complementary sequences separated by a hairpin loop. Subsequently, the RNA-induced silencing complex (RISC) produces single strands of the siRNA molecule and binds to its anti-sense strand, whereas the sense strand is degraded. Then, the RISC/ anti-sense siRNA complex interacts with the complementary mRNA target sequence to prevent translation thereof by degradation of the messenger RNA.

2 MATERIAL & METHODS

2.1 PLASMIDS

The plasmid pOGP3, encoding MLV gag/ pol, and the MLV-packagable plasmid, encoding VSV-G (pMD-G) have been described elsewhere (Randow and Sale, 2006).

The MLV-packagable vector pCMVnls-*lacZ* encodes the β-galactosidase reporter gene (Merten et al., 2006d).

The Δct plasmid encodes for a C-terminally truncated version of the envelope proteins (env) of HIV (Siegert et al., 2005).

The MLV-packagable vector MP71 encodes a fusion gene (HSV-TK-CD34) of the herpes simplex virus thymidine kinase and CD34 (Fehse et al., 2002).

The MLV-packagable vector pSIREN-puro encodes an shRNA targeting the expression of puromycin N-acetyltransferase expression (Clausell-Tormos et al., 2010).

2.2 GENERATION OF CHEMICALLY COMPETENT BACTERIA & TRANSFORMATION OF THEREOF

To produce large amounts of plasmid DNA, *E.coli* was used for cellular plasmid amplification. Prior transformation of bacteria, the cells had to be treated to be competent for the uptake of foreign DNA.
100 µL of XL-10 Gold ultra-competent *E. coli* cells (Stratagene) were added to 100 mL fresh LB medium (Sigma) and the culture was incubated at 37 °C and 200 rpm (Incubator Shaker Innova 44**,** New Brunswick Scientific). When the bacteria reached the logarithmic growth phase, corresponding to an OD_{600} of about 0.3 - 0.4, the cell suspension was pelleted at 420 x g for 10 min at 4 °C. Subsequently, the cells were

resuspended in 1 mL chilled 1 M $CaCl_2$ and water was added to a final volume of 20 mL corresponding to a final concentration of 50 mM $CaCl_2$. After 20 min incubation on ice, the cells were pelleted (see above) and resuspended in 3 mL total volume of 50 mM chilled $CaCl_2$ solution and 450 µL glycerol. After 2.5 h on ice, aliquots of 100 µL in 1.5 mL sterile eppendorf tubes were frozen at - 80 °C.

For transformation, one aliquot was thawed on ice and approximately 100 ng of plasmid DNA (carrying an ampicillin resistance gene) were added. After 30 min on ice, a heat shock for 45 s at 42 °C and a further incubation step on ice for 2 min was performed. Subsequently, 900 µL LB medium were added and the bacteria suspension was incubated for 30 min at 37 °C, to allow expression of the ampicillin resistance gene. Afterwards, the cells were pelleted, resupended in 100 µL LB medium, plated onto a LB-AMP-plate (1 % (w/v) Bacto-Trypton, 0.5 % (w/v) yeast extract, 1 % NaCl, 50 µg/ mL ampicillin 1.5 % (w/v) agar) and grown over night (o/n) at 37 °C.

2.3 Preparation of Plasmid DNA for Transfection

To obtain large amounts of plasmid DNA for the production of viral pseudotype particles, plasmids were purified from bacteria using a QIAGEN Plasmid Maxi Kit. For this, 250 mL of LB-AMP medium were inoculated with transformed bacteria and cultivated o/n at 37 °C and 200 rpm. The next day, cells were centrifuged at 3000 x g for 15 min at 4 °C (Eppendorf 5810 R centrifuge) and the pellet was treated according to the manufacturer's instructions. The purification of DNA is based on binding of plasmid DNA to an anion-exchanger, purification from remaining cell debris and chromosomal DNA by a medium-salt wash and elution of the plasmid DNA by a high-salt wash. After isopropanol/ ethanol precipitation the final concentration and purity of the DNA was determined photometrically at 260 nm.

2.4 CELL CULTURE

2.4.1 CULTIVATION OF DIFFERENT CELL TYPES

In this project different cell lines were used. HEK293T cells (a human embryonic kidney cell line expressing the simian virus 40 large T-antigen) were used for viral pseudotype particle production, biocompatibility tests of surfactants, on-chip dilution experiments and cell survival experiments of adherent cells in drops and plugs. HEK293T-CD4/CCR5-tPA cells, expressing the HIV-1 cell-entry receptors CCR5 and CD4 and a membrane-bound, HA-tagged form of tissue plasminogen activator (tPA) were used for on-chip transduction experiments and cell-cell fusion assays. Jurkat cells (an immortalized line of T lymphocyte cells) were used for on-chip dilution experiments and cell survival experiments of suspension cells in drops and plugs. Starting from the NIH cell line CHO-WT (HIV-1 WT envelope), expressing wild type HIV-1 envelope glycoprotein, a stable cell line was generated expressing HSV-TK-CD34 and a vector encoding an shRNA against the puromycin resistance (Chapter, 2.4.4). This cell line was used for cell-cell fusion with HEK293T-CD4/CCR5-tPA cells. CRL-2153 hybridoma cells (a cell line producing monoclonal antibodies against human immunodeficiency virus 1 (HIV-1) gp120) were used for on-chip dilution experiments and their supernatant for cell-cell fusion inhibition assays. Supernatants of HB-10895 hybridoma cells (a cell line producing monoclonal neutralising antibodies against gp120 of HIV-1) were utilised in cell-cell fusion inhibition experiments. tACE-4E3 hybridoma cells (a cell line producing monoclonal antibodies against truncated ACE (tACE)) were used for surfactant biocompatibility tests and ACE inhibition assays. In Table 4 the cultivation medium and supplements of each cell line are summarised.

For cultivation, cells were split every second to third day. Adherent cells were trypsinised (0.25 % trypsin in PBS, GIBCO), resuspended in medium and centrifuged at 340 x g for 6 min at 4 °C. Subsequently, the pellet was resuspended in fresh medium and 1/5 of the cell suspension was seeded into a new culture flask. When passing

suspension cells, a fraction of 1/5 was transferred directly into a new culture flask. Cells were incubated at 37 °C under a 5 % CO_2 atmosphere saturated with water.

cell line	*Medium*	*supplements*
HEK293T	DMEM (GIBCO)	- 10 % FBS (GIBCO) - 1 % penicillin/streptomycin (GIBCO)
HEK293T-CD4/CCR5	DMEM (GIBCO)	- 10 % FBS (GIBCO) - 1 % penicillin/streptomycin (GIBCO)
HEK293T-CD4/CCR5-tPA	DMEM (GIBCO)	- 10 % FBS (GIBCO) - 1 % penicillin/streptomycin (GIBCO)
Jurkat	RPMI 1640 (GIBCO)	- 10 % FBS (GIBCO) - 1 % penicillin/streptomycin (GIBCO)
CHO-WT (HIV-1 WT envelope) (NIH Research & Reference Reagent Program)	GMEM-S	http://www.aidsreagent.org/pdf_images/2237_001.pdf
CHO-WT (HIV-1 WT envelope) -HSV-TK-CD34/ puromycin N-acetyltransferase shRNA	GMEM-S	http://www.aidsreagent.org/pdf_images/2237_001.pdf
CRL-2153 (ATCC)	Hybricare (ATCC)	- 10 % FBS (GIBCO) - 1 % penicillin/streptomycin (GIBCO)
HB-10895 (ATCC)	ATCC modified RPMI (ATCC)	- 15 % FBS (GIBCO) - 1 % penicillin/streptomycin (GIBCO)
tACE-4E3 (Naperova et al., 2008)	HyClone RPMI 1640 (Thermo Fischer)	- 10 % hybridoma tested FBS (SIGMA) - 1x non-essential amino acids (GIBCO) - 1 mM sodium pyruvat (SIGMA) - 1x RPMI 1640 vitamins (SIGMA) - 250 µL 0.1 M β-mercaptoethanol (SIGMA)

Table 4: Cultivation medium and supplements of the cell lines used in this work.

2.4.2 FREEZING & THAWING OF MAMMALIAN CELLS

To allow storage and re-cultivation of the cell lines, aliquots of approximately 1.5 x 10^6 cells/ mL were frozen and transferred to - 80 °C.

For freezing, first, in case of adherent cell lines, cells were trypsinised and resuspended in medium. Subsequently, cells (adherent as well as suspension cells) were pelleted at 340 x g for 6 min at 4 °C. Then the pellet was resuspended in freezing medium (90 %

FBS, 10 % DMSO), divided into aliquots of approximately 1.5 x 10^6 cells/ mL, frozen o/n at - 20 °C and the next day kept at - 80 °C.

For thawing, cryotubes were thawed in a water bath at 37 °C. To remove cytotoxic DMSO from the cells, 15 mL pre-warmed medium was added and the suspension was centrifuged at 340 x g for 6 min at 4 °C. Afterwards, the pellet was resuspended in fresh medium supplemented with an additional 20 % FBS, the cells were transferred into a cell culture flask and cultivated at 37 °C under a 5 % CO_2 atmosphere saturated with water.

2.4.3 PRODUCTION OF VIRAL PSEUDOTYPE PARTICLES

For the generation of pseudotyped replication-deficient retroviral particles, $CaPO_4$ transfection was used which was originally discovered by F. L. Graham and A. J. van der Eb in 1973 (Graham and van der Eb, 1973a). Calcium-phosphate mediated transfection is mostly used for transient expression of genes of interest. The negatively charged DNA interacts with the positively charged Ca^{2+} ions which are present in excess. The loose DNA/ Ca^{2+} complex forms a crystalline complex with PO_4^{3-} ions. Some of this insoluble DNA/ Ca^{2+}/ PO_4^{3-} precipitates are then taken up into the cells by a process that is not yet entirely understood. The protocol described here is a modification of a standard protocol for calcium-phosphate mediated transfection of HEK293T cells (http://www.genomics.sbg.ac.at/meth/cacl2_transfection.pdf). Different parameters, such as the pH value, amount of DNA, cell density, medium, complex formation time, transfection duration, different protein concentrations in the medium, temperature of solutions, fast or slow mixing and additives, like chloroquine, DMSO, glycerol or sodium butyrate, were tested to achieve a high transfection efficiency. The conditions allowing maximally efficient transfection are listed in Table 5.

One day prior transfection, 8.75 x 10^6 cells were seeded into a 175 cm^2 culture flask. The next day, the medium was removed 3 h before transfection and 31.5 mL fresh medium were added. 10.5 µg of the plasmid encoding gag/ pol, 10.5 µg of the plasmid encoding env and 21 µg of the plasmid encoding the transfer gene were added to 1.75 mL of 250 mM $CaCl_2$. When using VSV-G as env protein, a ratio of 18:6:18 (gag/ pol:env:transfer vector) was applied to avoid cytotoxic effects of VSV-G.

Afterwards, the $CaCl_2$/ DNA solution was gently mixed with 1.75 mL pre-warmed (37 °C) 2x HBS buffer and incubated for a maximum duration of 15 min at room temperature. Subsequently, 3.5 mL transfection mix were added to the cells seeded into a 175 cm^2 flask and incubated for 16 h at 37 °C and 8 % CO_2. Then, the transfection mix was removed and 12 mL fresh medium were added. 24 h later, the supernatant was collected and replaced by another 12 mL fresh medium. After centrifuging (340 x g for 6 min at 4 °C) and filtering (0.45 µm filter unit, MILLIPORE), the supernatant, containing the particles, was ultra-centrifuged at 154500 x g for 2 h at 4 °C (Optima L-100 XP, Beckman-Coulter) over a 2 mL 25 % sucrose cushion. To concentrate the viral pseudotype particles, the resulting pellet from 9.5 mL supernatant was resuspended in 300 µL fresh medium and kept at - 20 °C until used in transduction experiments. 24 h after the first harvest, particles were harvested a second time according to the above described procedure.

pH	7.1
amount of DNA	42 µg
cell density	8.75 x 10^6 cells
medium change before transfection	3 h before transfection
complex formation time	10 min
transfection duration	16 h
different protein concentrations in the medium	10 % FBS
temperature of solutions	- 2x HBS at 37 °C - $CaCl_2$ at 4 °C or room temperature
fast or slow mixing	no effect observed
Additives	no effect observed

Table 5: Best conditions for $CaPO_4$ transfection of HEK293T cells for the production of viral pseudotype particles using a 175 cm^2 culture flask.

1 L of 2x HBS buffer	**100 mL of 2.5 M $CaCl_2$**
- 50 mM HEPES (11.92 g) - 280 mM NaCl (16.36 g) - 1.5 mM Na_2HPO_4 (= 100 mL 10x Na_2HPO_4) (10x Na_2HPO_4 = 1.064g to 500 mL) - pH adjusted exactly to 7.1 with NaOH	**- 27.75 g $CaCl_2$** **- solution steril filtered and put to -20 °C** **- for transfection 2.5 M $CaCl_2$ solution diluted 1:10, results in a solution of 250 mM**

Table 6: Formulation of 2x HBS buffer and $CaCl_2$ solution used for calcium-phosphate mediated transfection of HEK293T cells.

2.4.4 VIRAL TRANSDUCTION

In contrast to transfection, viral transduction offers a long-term expression of genes in host cells. Retrovirus-mediated gene transfer results in the stable integration of transfer vectors into the genome of transduced cells. HEK293T cells were transfected with plasmids encoding capsid, env and transfer genes as described above. Subsequently, target cells (cells, carrying the corresponding receptor for the env protein) were transduced with the resulting particles.

Viral transduction was used to generate cell lines stably expressing a gene of interest for cell-cell fusion assays. For this, 2 x 10^4 cells were seeded in a 96-well plate (Becton Dickinson) and 24 h later incubated with 100 µL of concentrated viruses (~ 2.5 x 10^7 i.U./ mL) for 3 h. Subsequently, cells were cultivated for 3 days, the transduction step was repeated and two weeks later, cells were selected or tested for gene expression (e.g. ganciclovir titration (Chapter II, 2.6).

HEK293T-CD4/CCR5-tPA cells expressing a membrane-bound and HA-tagged form of tissue plasminogen activator were obtained by retroviral transduction of HEK293T-CD4/CCR5 cells with MLV-VSV-G pseudotype particles packaging the tPA-encoding vector. High-expressing cells were selected with a fluorescence-activated cell sorter (MoFlo, BD) using goat polyclonal antibodies raised against tissue plasminogen activator (tPA, Abcam).

CHO-WT (HIV-1 WT envelope) stably expressing thymidine kinase and an shRNA against the puromycin N-acetyltransferase expression were produced by transduction with MLV-VSV-G particles having packaged the HSV-TK-CD34 vector or the vector encoding for the shRNA abolishing the puromycin resistance. Thymidine kinase expression was tested by ganciclovir titration of transduced CHO cells over 96 h (Chapter II, 2.6).

In this study, transduction was also carried out before on-chip single cell analysis (Chapter I, 2.10) and in on-chip transduction experiments (Chapter II, 2.5).

2.4.5 VIRAL TITER DETERMINATION

To calculate the transduction efficiency, viral titers have been determined by X-gal assays (Stitz et al., 2001). After transduction of the cells with viral particles, cells were further incubated for 48 h to 72 h, to allow expression of the transfer vector. Subsequently, cells were fixed by treatment with 2 % formaldehyde and 0.5 % glutaraldehyde for a few minutes. Then, the cells were incubated with staining solution (4 mM potassium ferricyanide, 4 mM potassium ferrocyanide, 2 mM $MgCl_2$ and 80 µg/ ml X-Gal (SIGMA), in PBS) at 37 °C o/n. The next day, blue colonies were counted under a light microscope and the viral titers were calculated by Equation 1.

$$\text{Viral titer} = n_S * \frac{A_{\text{well of microtiter plate}}}{A_{\text{microscope field of view}}} * \frac{V_{\text{total}}}{V_{\text{virus}}}$$

Equation 1: Computation formula to calculate the transduction efficiency.

The average number of stained blue cells per field of view under the microscope is denoted by the symbol n_S. $A_{\text{well of microtiter plate}}/ A_{\text{field of view}}$ stands for the magnification factor (A = area), V_{total} represents the total sample volume and V_{virus} is the volume of the particles used in the sample.

2.5 ON –CHIP TRANSDUCTION

In on-chip transduction experiments the transduction efficiency of pseudotyped retroviral particles was explored, compared to off-chip transduction. For this purposes, effector particles (derived from murine leukaemia virus, MLV) with the envelope proteins (env) of HIV were generated, resulting in the host range tropism of this species (Siegert et al., 2005). As reporter gene, the *lacZ* vector encoding the enzyme β-galactosidase, was used. The expression of this vector in transduced cells was visualised by an X-gal assay.

To obtain comparable results for viral transduction in eppendorf tubes, in 24 well plates and 660 pL droplets, HEK293T-CD4/CCR5-tPA cells were adjusted to a density of 2.5 x 10^6 cells/ mL, one day before encapsulation/ transduction. 4 mL of this suspension

were seeded into a 25 cm^2 culture flask and 125 µL per well were seeded into a 24 well plate. 24 h later, the cells within the 25 cm^2 culture flask were detached and suspended in 4 mL fresh medium to obtain a similar density as adjusted one day before. 125 µL of this suspension were transferred into a 1.5 mL eppendorf tube and the remaining suspension into a 5 mL syringe. The cells within the syringe were encapsulated into drops as described in Chapter I, 2.5. Instead of an additional stream of sterile medium, a MLV-Δct-*LacZ* particle suspension was added with the same flow rate as the cells, resulting in 1:1 dilution with viral particles. From the obtained drops, three emulsions with each 500 mL were collected within a 15 mL centrifuge tube through a punched sealing and incubated for 3 h within a CO_2 incubator (5 % CO_2, saturated with H_2O) at 37 °C. At the same time, 125 µL of MLV-Δct-*LacZ* were added to 125 µL cell suspension in an eppendorf tube. Another 125 µL of MLV-Δct-*LacZ* and additional 125 µL fresh medium were added to the seeded cells in a 24 well plate, after removing the medium. Of both samples, triplets were incubated within the same conditions as the emulsions. To ensure equal cell density for the readout of different samples, after 3 h of incubation, cells from 250 µL emulsion were re-covered and re-cultivated for 9 days in a 6 well plate. Samples from 1.5 mL eppendorf tubes and 24 well plates were seeded into a 6 well plate, after 3 h of transduction. 6 days later, both samples have been transferred into a 25 cm^2 culture flask. After 9 days of total re-cultivation, an X-gal assay was performed for all samples to calculate and determine the transduction efficiency.

2.6 CELL-CELL FUSION ASSAY

To perform the viral inhibition assay (described in 1.4, Figure 54) using cell-cell fusion, CHO cells expressing HIV env instead of MLV(HIV env) particles were used. For this, a stable CHO(HIV env) cell line expressing an shRNA against puromycin and expressing a thymidine kinase (HSV-TK-CD34) was generated. Both vectors have the ability to kill the cell, hence abolishing the reporter gene signal (tPA) generated in HEK293T-CD4/CCR5-tPA cells. Upon cell-cell fusion and addition of puromycin or ganciclovir the fluorescence signal of tPA is decreased due to induced cell death.

To perform cell-cell fusion assays, CHO-WT (HIV-1 WT envelope)-HSV-TK-CD34/ puromycin N-acetyltransferase shRNA cells and HEK293T-CD4/CCR5tPA cells were seeded 1 : 5 in a 96 well plate, with a total number of 8 x 10^4 cells per well (day 0) usually allowing fusion within 24 h (Rusche et al., 1988; Wild et al., 1992; Jiang et al., 2004). For cultivation during the cell-cell fusion assay, Hybricare medium (Table 4) was used to ensure viable conditions for both cells lines. To inhibit cell-cell fusion, 100 nM T20 (NIH Research & Reference Reagent Program), a well known HIV fusion inhibitor, were added. After 24 h (day 1) and 72 h (day 3), T20 was renewed. The effective concentrations for puromycin and ganciclovir (at which effectors cells die, but indicator cells still survive) were identified in titrations. It turned out that 100 % of CHO/HIVenv cells died at 10 µg/ mL puromycin, whereas HEK293T/CD4/CCR5/tPA cells showed high viability until 15 µg/ mL, as confirmed in corresponding bright-field microscopy images. At 20 µg/ mL puromycin HEK293T/CD4/CCR5/tPA cells changed the morphology and the cultures showed increasing numbers of dead cells. Thus, for the assay concentrations of 10 µg/ mL, 15 µg/ mL and 20 µg/ mL puromycin were tested. Ganciclovir was used in concentration of 40 µM and 400 µM, since CHO/HIVenv cells died within this range up to 100 %. Indicator cells, on the other hand were not affected by 40 µM ganciclovir but started to show cell death at 400 µM. Both compounds were added toghether with T20 on day 1 and day 3. On day 4, the fluorescent readout assay was performed. For this, the cell medium was removed completely and 100 µL PBS containing HDVLK-Aminocoumarin (Bachem) and Plasminogen (Roche) at a final concentration of 1 mM and 19.76µM, respectively, were added. Subsequently, all samples were measured in a microplate reader at 37 °C with excitation and emission wavelengths of 370 nm and 450 nm, respectively.

2.7 ACE Inhibition Assay

2.7.1 ACE Inhibition by Purified Antibodies

Bulk assays. The Angiotensin I-converting enzyme (ACE) assay was performed using a human recombinant enzyme (R&D Systems, Inc.) and the fluorogenic peptide substrate

Mca-Arg-Pro-Pro-Gly-Phe-Ser-Ala-Phe-Lys(Dnp)-OH (Mca-RPPGFSAFK(Dnp), R&D Systems, Inc.). In a 96 well plate, a total volume of 100 µL assay buffer (50 mM MOPS, (3-(N-morpholino)propanesulfonic acid), pH 6.5), an enzyme concentration of 0.2 ng/ mL and a substrate concentration of 10 µM were used. Kinetics of the samples were measured at 37 °C in a plate reader at excitation and emission wavelength of 320 nm and 405 nm, respectively.

Before starting all ACE experiments, enzyme and substrate stability tests were performed. Incubation of the enzyme before substrate addition over time at 4 °C, room temperature and 37 °C did not have any effect on the reaction efficiency. The same results were obtained when incubation the substrate at these temperatures and then adding it to a fresh enzyme solution. Therefore, the enzyme seemed to be stable enough to be incubated over several hours at 37 °C which was required for off-chip co-incubation together with hybridoma cells (Chapter II, 2.7.2).

The enzymatic reaction and the inhibition thereof by a purified ACE antibody (tACE-4E3) were tested in different assay buffers and solutions to identify conditions allowing maximum activity and inhibition. Moreover, the effect of different incubation times of ACE with the tACE-4E3 antibody, before substrate addition, was investigated.

To prove the specificity of tACE-4E3, different antibodies (Ab's) were tested for their ACE-neutralising activity (Table 7). For inhibition experiments, Ab's were used at an initial concentration of 40 µg/ mL in 50 µL enzyme solution (0.4 ng/ mL). The antibody and the enzyme concentration were diluted to 20 µg/ mL and 0.2 ng/ mL, respectively, and 50 µL of a 20 µM substrate solution were added.

Antibody	***Specificity***
ab39172 (Abcam)	carboxy end of carboxyterminal catalytic ACE domain
ab28313 (Abcam)	amino end of carboxyterminal catalytic ACE domain
tACE-4E3 (Naperova et al., 2008)	truncated ACE
ab82249 (Abcam)	tissue plasminogen activator (tPA)

Table 7: Antibodies tested in inhibition experiments for their inhibitory effects against ACE.

Assays in drops. For ACE inhibition experiments in 530 pL droplets, ACE (0.8 ng/ mL) was encapsulated with purified tACE-4E3 antibody (80 µg/ mL) (Naperova et al., 2008) by 1:1 on-chip dilution. For control purpose ACE was encapsulated 1:1 together with PBS instead of purified tACE-4E3. Directly after droplet

generation (0 h), 3 h and 6 h later, 200 µL emulsion were broken by the addition of 15 % 1H,1H,2H,2H-Perfluoro 1-octanol. 50 µL of the upper aqueous phase were transferred into a 96 well plate and 50 µL substrate solution were added. The samples were measured in a plate reader for 30 min at 37 °C at excitation and emission wavelength of 320 nm and 405 nm, respectively.

To determine the activity of ACE within emulsions, the enzyme (0.4 ng/ mL, without antibody) was encapsulated together with a 20 µM substrate solution by 1:1 into 530 pL droplets. Directly after encapsulation, 100 µL of the emulsion and 100 µL supernatant of a broken emulsion were measured at 37 °C in a plate reader at excitation and emission wavelength of 320 nm and 405 nm, respectively, to investigate the effect of the breaking process.

2.7.2 ACE INHIBITION BY HYBRIDOMA CELLS

Hybridoma cells producing a monoclonal antibody against truncated ACE (tACE-4E3) (Naperova et al., 2008), were used for inhibition experiments based on crude cell culture supernatants instead of purified tACE-4E3 antibodies. The aim was to determine the incubation time necessary to produce sufficient amounts of the antibody for ACE inhibition. For this, hybridoma cells were washed with PBS before adjusting to a density of 1.52×10^6 cells/ mL which was theoretically equivalent to 660 pL droplets hosting each one single cell. The cells were co-incubated with ACE (0.4 ng/ mL) within a CO_2 incubator (5 % CO_2, saturated with H_2O) at 37 °C. After different incubation times, 0 h, 2 h, 4 h and 6 h, samples of 250 µL were filtered through a 0.45 µm filter tip (MILLIPORE). To each 50 µL of the filtrate, another 50 µL of a 20 µM substrate solution were added and the samples measured in a plate reader (at 37 °C, excitation 320 nm/ emission 405 nm).

3 RESULTS

3.1 VIRAL INHIBITION ASSAY (ON-CHIP TRANSDUCTION)

The first approach, to set up a functional assay for screening neutralising antibody activity, intended to combine a patented novel viral inhibition assay (Figure 54; Clausell-Tormos et al., 2010; (WO/2006/082385) SCREENING METHOD) with the microfluidic system. The assay uses genetically engineered cells (indicator cells, HEK293T/CD4/CCR5/tPA; Chapter II, 2.4.1) continuously generating a strong fluorescence signal unless transduced with recombinant pseudotype particles (effector particles). These effector particles have packaged a vector encoding an shRNA abolishing the puromycin resistance of the indicator cells (by downregulating the expression of the enzyme Puromycin-N-acetyltransferase). Hence, the indicator cells die in presence of puromycin, leading to a shutdown of the reporter gene signal. Thus, viral cell-entry results in a decreased reporter gene signal, whereas non-transduced cells show the maximum signal intensity. Alternatively, a vector encoding a suicide gene (thymidine kinase) could be used which upon the addition of the corresponding substrate (Ganciclovir) mediates cell death of the indicator cells, also resulting in the efficient shut down of the reporter gene upon cell-entry.

To check the feasibility of this approach for use in combination with the developed droplet-based microfluidic platform, the transduction efficiency of MLV(HIV env) effector particles in droplets was assessed. For this, particles having packaged a vector encoding β-galactosidase were generated. These effector particles were incubated with indicator cells in 24 well plates, eppendorf tubes and drops using the same cell density for all samples, during the transduction as well as the readout. After incubation and re-cultivation, the viral titers were determined by X-Gal assay (Figure 57). Transduction in 24 well plates and eppendorf tubes was chosen for comparison with transduction in drops and for evaluation of the transduction efficiency in different systems. In drops, a titer of 2.17×10^6 i.U./ mL (infectious units per millilitre) was determined. This value is lower compared to the viral titers obtained in 24 well plates (4.12×10^6 i.U./ mL) and

eppendorf tubes (3.88 x 10^6 i.U./ mL). However, when assuming a cell recovery rate from drops of just 25 % (a typical value after 3 h of incubation in droplets) 2.17 x 10^6 i.U./ mL corresponds to 8.68 x 10^6 i.U./ mL when extrapolating for a recovery rate of 100 %. This value is approximately two-times higher than the viral titer for transduction in 24 well plates or eppendorf tubes. This clearly shows that MLV particles pseudotyped with HIV gp160 (MLV(HIV env)) co-encapsulated in drops efficiently enter their host cells.

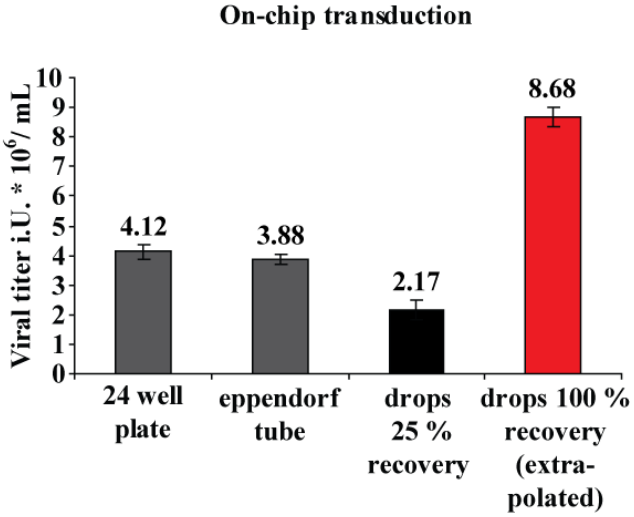

Figure 57: Comparison between off-chip and on-chip transduction efficiencies. MLV(HIV env) particles were incubated for 3h with corresponding host cells in 24 well plates, 1.5 mL eppendorf tubes and 660 pL drops, at the same cell densities. The recovery of cells from drops was typically ~ 25 %. The viral titer for this percentage (black bar) was extrapolated to 100 % recovery (red bar) to compare viral titers between the different samples (gray bars).

Having a viral titer of 4.12 x 10^6 i.U./ mL in 24 well plates corresponds to ~ 2.7 particles per 660 pL drop. This also means, in one drop one cell is surrounded by 2.7 viral particles under single cell conditions. Pseudo particles, used in this study, were always concentrated by ultra-centrifugation. Non-concentrated virus preparations would be insufficient for the experiments since the obtained titers would correspond to 0.08 i.U./ drops or 0.12 x 10^{-3} i.U./ mL, respectively (calculated from concentrated viruses, 2.7 particles per drop, divided by the concentration factor of 35). Therefore, particle concentration was required for efficient transduction in droplets. It turned out that HIV pseudotyped particles have low transduction efficiencies when concentrated

by ultracentrifugation. This could be explained by the high sensitivity of the envelope protein to the centrifugal forces. The surface glycoprotein gp120 (SU) is assumed to dissociate from the transmembrane glycoprotein (TM) resulting in non-infective particles. This phenomenon is called 'shedding' and was reported by several groups (Schneider et al, 1986; Pyle et al., 1987). To circumvent this problem other techniques, like concentration of particles by magnetic beads or the use of polybrene to accumulate viruses have been investigated, but did not succeed (data not shown). Therefore, a cell-cell fusion assay using CHO cells expressing HIV env instead of MLV(HIV env) particles was established.

3.2 CELL-CELL FUSION ASSAY

In a second approach a cell-cell fusion assay was set up using the tools of the patented viral inhibition assay. The first step was to identify cell lines and conditions for efficient cell-cell fusion.

For this purpose, a stable CHO(HIV env) cell line (effector cells) expressing an shRNA against puromycin and expressing thymidine kinase (mimicking the function of effector particles) was generated. CHO(HIV env) and HEK293T/HIVenv (HEK293T cells transient expressing HIVenv) were tested for their use as effector cells. HIV-permissive HEK293T-CD4/CCR5-tPA cells and Jurkat cells (expressing a membrane-bound form of tissue plasminogen activator, tPA) served as indicator cells and were investigated for their fusion ability.

The results of the cell-cell fusion experiments after co-cultivation for three days are presented in Figure 58. Cell-cell fusion between CHO/HIVenv and HIV-permissive HEK293T/tPA cells resulted in a complete layer of fused cells (Figure 58A). In contrast, CHO/HIVenv incubated with HIV-permissive Jurkat/tPA cells showed only little syncytia formation (Figure 58B). As expected, experiments with CHO/HIVenv and non HIV-permissive HEK293T/tPA cells (Figure 58C, negative control) did not lead to any cell-cell fusion.

In parallel, HEK293T cells transiently transfected with a plasmid encoding HIVenv were co-cultivated with the same indicator cells as tested in combination with CHO/HIVenv cells. These HEK293T/HIV/env cells formed bigger syncytia when

co-cultivated with HIV-permissive HEK293T/tPA (Figure 58D) compared to the co-cultivation with Jurkat/tPA cells (Figure 58E). Once again, incubation with non HIV-permissive HEK293T/tPA cells served as negative control and did not result in cell-cell fusion (Figure 58F).

Based on these results, the co-cultivation of CHO/HIVenv cells with HIV-permissive HEK293T/tPA cells was identified as the most suitable model for cell-cell fusion assays and used for all following experiments.

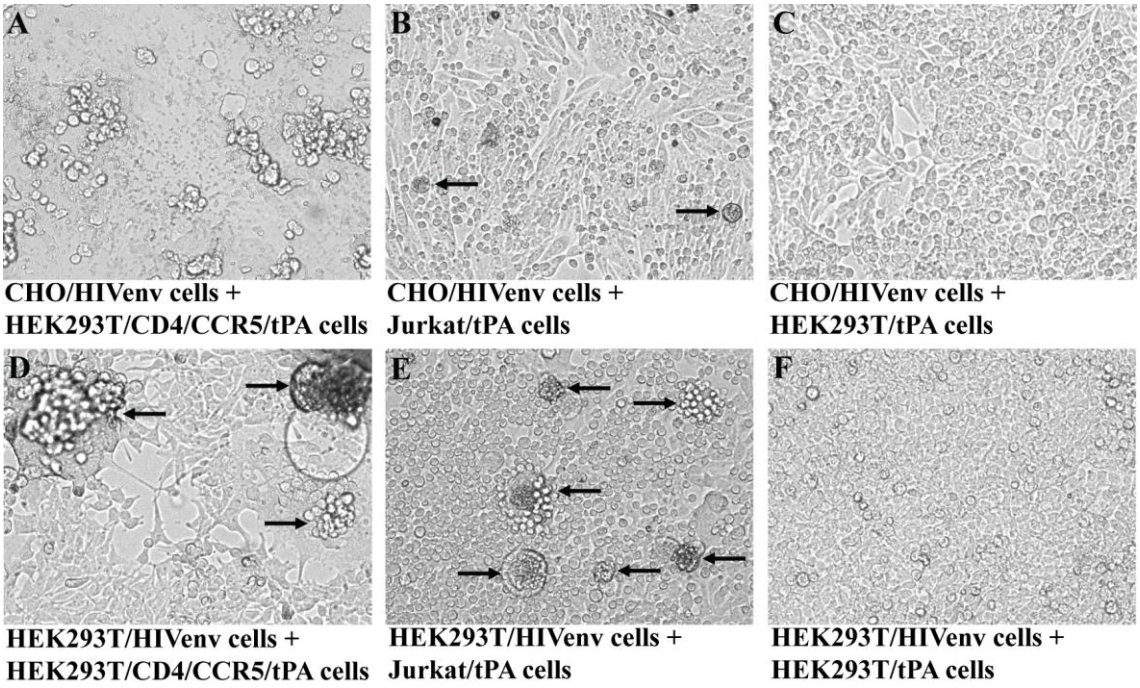

Figure 58: Cell-cell fusion between different cell lines. Cells were co-cultivated in a ratio of 1:4 (HIVenv expressing cells to HIV-permissive cells) **(A)** CHO/HIVenv and HIV-permissive HEK293T/tPA cells. **(B)** CHO/HIVenv and HIV-permissive Jurkat/tPA cells. **(C)** CHO/HIVenv and non HIV-permissive HEK293T/tPA cells (negative control). **(D)** HIV/env transduced HEK293T and HIV-permissive HEK293T/tPA cells. **(E)** HIV/env transduced HEK293T and HIV-permissive Jurkat/tPA cells. **(F)** HIV/env transduced HEK293T and non HIV-permissive HEK293T/tPA cells (negative control).
Black arrows indicate syncytia.

After choosing the cell lines, the optimal assay medium for long-term cultivation was determined. As the fusion assay requires at least 5 days of incubation, a medium was needed that ensures cell viability for both, CHO/HIVenv and HEK293T/CD4/CCR5/tPA cells. For this, both cell lines where tested separately in four different media, CHO, DMEM, ATCC RPMI and Hybricare medium (Figure 59).

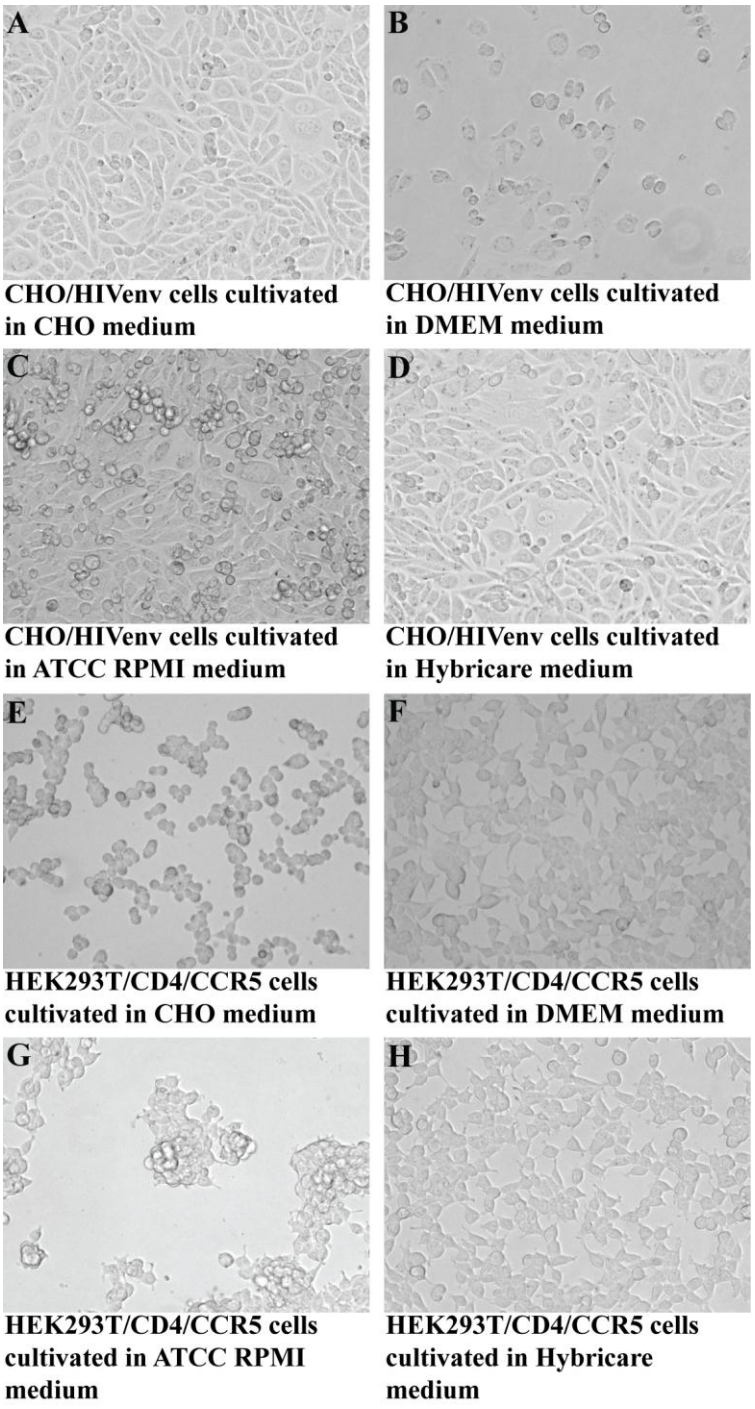

Figure 59: **Identification of suitable assay media for cell-cell fusion between CHO/HIVenv and HIV-permissive HEK293T/tPA cells. (A)**, **(B)**, **(C)** and **(D)** CHO/HIVenv cells cultivated in CHO, DMEM, ATCC RPMI and Hybricare medium. **(E)**, **(F)**, **(G)** and **(H)** HIV-permissive HEK293T/tPA cells cultivated in CHO, DMEM, ATCC RPMI and Hybricare medium.

As expected, CHO/HIVenv as well as HEK293T/CD4/CCR5/tPA cells showed best viability in the media specifically recommended for their cultivation (CHO for

CHO/HIVenv cells, Figure 59A and DMEM for HIV-permissive HEK293T/tPA cells, Figure 59H). However, both cell lines showed also good cell viability in Hybricare medium, as usually used for hybridoma cell cultivation. Hence, Hybricare medium was used as assay medium for all subsequent cell-cell fusion experiments.

3.2.1 INHIBITION OF CELL-CELL FUSION AND DOWNREGULATION OF THE REPORTER GENE SIGNAL

After identification of cell lines and conditions for efficient cell-cell fusion, the next step was to demonstrate its inhibition by using the well known HIV fusion inhibitor T20 (Enfuvirtide) as model system. T20 binds to gp41, blocking the fusion of cell and viral membranes and therefore preventing entry of the viral capsid into the cell. Moreover, a neutralising antibody inhibiting cell-cell fusion of effector and indicator cells and an antibody only binding HIVenv without any inhibitory activity needed to be identified as further controls to prove the concept of antibody selection for inhibitory properties.

The effective T20 concentration for inhibiting fusion between CHO/HIVenv cells and HIV-permissive cells was determined. According to Pang et al., 2008, a T20 concentration of 100 nM is sufficient (for HIV-1 envelope proteins) to block syncytia formation up to 100 %. Even though cell-cell fusion inhibition depended on the cell line, 100 nM was chosen as initial T20 concentration. In the assay, the samples were incubated for 5 days probably having an effect on the anti-fusion activity of T20. The inhibitor could either be degraded by the cells or hydrolysed over time. Therefore, higher concentrations and repeated addition of T20 during the fusion assay were investigated. The probable activity loss over time counts for antibodies as well, therefore repeated addition was also tested for hybridoma cell supernatants, used to suppress cell fusion.

The results are displayed in Figure 60. Clearly, 100 nM T20 (Figure 60B) and HB-10895 cell supernatant (Figure 60D) added on day 0 and renewed on day 1 and day 3, blocked fusion completely. In contrast, in absence of any inhibitor (Figure 60A) and presence of CRL-2153 cell supernatant (Figure 60C) cells fused and formed a confluent layer of syncytia.

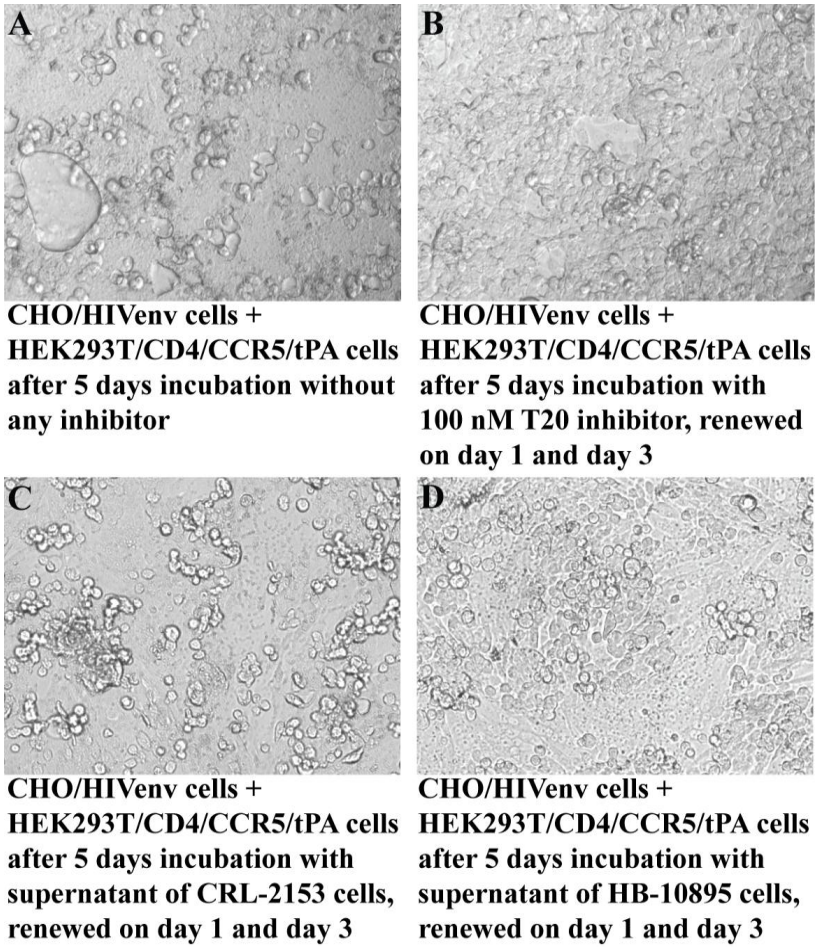

Figure 60: Demonstration of cell-cell fusion inhibition between CHO/HIVenv and HIV-permissive HEK293T/tPA cells using different inhibitors. (A) Sample without any inhibitor. **(B)** Fusion inhibited by 100 nM T20 when renewed 1 day and 3 days after fusion (day 0). **(C)** Fusion in presence of CRL-2153 cell supernatant. **(D)** Supernatant of HB-10895 cells blocked cell-to-cell fusion between CHO/HIVenv and HEK293T/CD4/CCR5/tPA cells.

Consequently, a concentration of 100 nM T20 and frequent renewal of the media (containing this concentration of the drug) allowed the inhibition of cell-cell fusion between effector and indicator cells. As expected, HB-10895 hybridoma cells produce a neutralising antibody against HIV-1 that could block cell fusion, whereas antibodies produced by CRL-2153 hybridoma cells seemed to only exhibit binding properties.

After the successful establishment of assays for cell-cell fusion and its inhibition, the next task was to perform a fluorescence readout of samples with and without. The CHO/HIVenv cells express an shRNA abolishing the puromycin resistance of the indicator cells (HEK293T/CD4/CCR5/tPA cells) and a vector encoding a suicide gene

(thymidine kinase). Therefore, upon fusion and addition of puromycin and/ or ganciclovir the reporter gene signal (tPA) should be downregulated resulting from cell death of the indicator cells (Figure 54C).

Different puromycin (10 µg/ mL, 15 µg/ mL and 20 µg/ mL) and ganciclovir (40 µM and 400 µM) concentrations were tested for their effect to induce cell death and therefore decreasing the reporter gene signal.

The optimal time points for pyromycin/ ganciclovir addition and for the fluorescent readout were used, according to the viral inhibition assay reported in Clausell-Tormos et al., 2010. Here the addition of these compounds on day 1 and day 3 and subsequent tPA-based fluorescence readout of the samples on day 4 resulted in the highest signal to background ratios (16.5 for puromycin treatment and 9.3 for ganciclovir addition). Moreover, addition of the compounds on day 1 and day 3 is well compatible with the renewal of T20 during the cell-cell fusion assay.

However, for the cell-cell fusion assays different results were obtained. At a puromycin concentration of 10 µg/ mL (Figure 61, black bars), an signal to background ratio of just 1.2 was obtained. For 15 µg/ mL (Figure 61, dark grey bars) and 20 µg/ mL (Figure 61, light grey bars) puromycin the ratios were similar, 1.35 and 1.41, respectively.

Although, a difference between fused and non-fused samples was obvious, it could not be considered as a significant signal to background ratio caused by the downregulation of the reporter gene. Moreover, besides the desired effect of puromycin the lower fluorescence signal in syncytia-forming samples could also be due to retarded proliferation. Obviously, cells proliferated quicker in non-fused populations, for which reason HEK293T/CD4/CCR5/tPA cells showed higher fluorescence signals. An additional fact could be that in syncytia the expression of the shRNA abolishing the puromycin resistance of the indicator cells is not efficient.

In absence of puromycin (Figure 61, red bars), both, samples with and without T20, had a lower signal than in presence of puromycin. After five days of incubation, samples without puromycin were more confluent and the fluorescence signal was decreased.

With increasing puromycin concentrations, up to 15 µg/ mL, the fluorescence signal increased in non-fused populations. The most likely explanation is that the addition of puromycin resulted in death of CHO/HIVenv cells, resulting in additional space for proliferating HEK293T/CD4/CCR5/tPA cells in presence of T20. With higher

puromycin concentrations (20 µg/ mL), also HEK293T/CD4/CCR5/tPA cells seemed to be affected by the compound. For samples without inhibitor this effect was less obvious, most likely due to missing proliferation in fused cells.

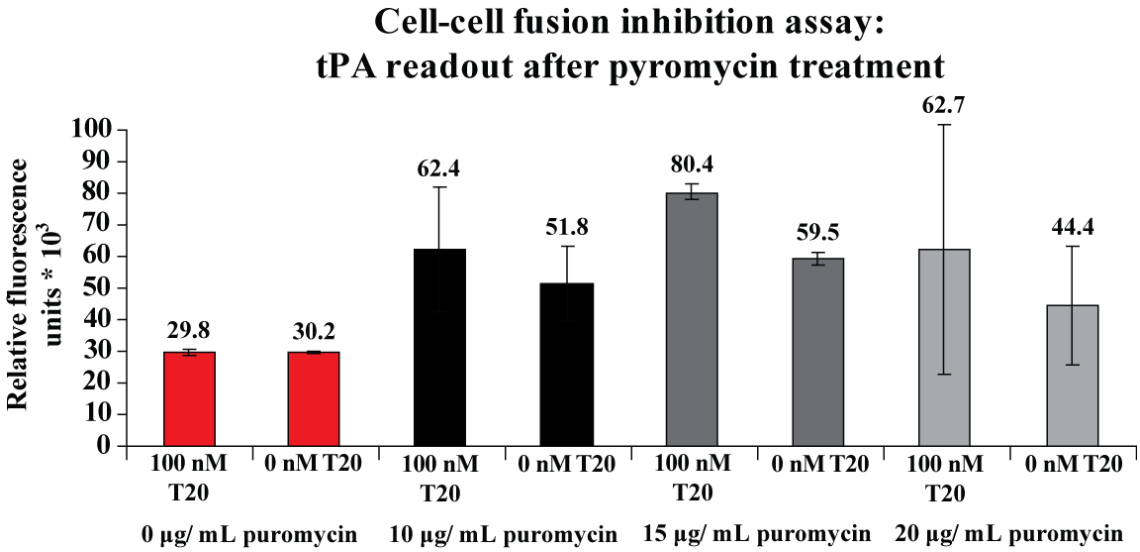

Figure 61: Fluorescent tPA readout after co-cultivation of CHO/HIVenv cells together with HIV-permissive cells, in presence and absence of T20 and puromycin. Comparison of the reporter gene activity at different puromycin concentrations between fused and non-fused samples.

Using thymidine kinase and ganciclovir for the downregulation of the tPA reporter gene (Figure 62), the ratio was 1.05 for 40 µM ganciclovir and 0.9 for 400 µM. Once again, these ratios could not be considered as significant signal to background ratios, since also in this scenario syncytia formation could be likely to stop cell proliferation. It is obvious that non-fused cells (100 nM T20) at 400 µM ganciclovir (Figure 62, grey bars) give a lower signal than non-fused cells at 40 µM (Figure 62, black bars) and 0 µM (Figure 62, red bars), whereas, for fused cells (samples without T20), this could not be observed. This effect could be explained by the fact that the thymidine kinase/ ganciclovir system indirectly affects HEK293T/CD4/CCR5/tPA cells. Its mechanism of action involves phosphorylation by kinases, resulting in a nuclesid-analogue that leads to chain termination in the DNA replication process and subsequent cell death by apoptosis. Nonetheless, also cells which do not express thymindine kinase can be affected by the cytotoxic product of ganciclovir, produced in thymindine kinase expressing cells. This phenomenon is called the ‘bystander effect’ and is based on the transfer of toxic

nuclesid-analogues through cellular channels (gap junctions) or phagocytosis of apoptotic vesicles (Dilber et al., 1997; Dilber & Smith, 1997).

In absence of ganciclovir, fused samples showed a lower fluorescence signal than non-fused samples. This might just be an artefact but could also support the fact that retarded proliferation in syncytia-forming samples let to lower fluorescence signals. Moreover, it seemed that also here syncytia formation did not allow sufficient expression of the thymidine kinase gene, for which reason ganciclovir was not extensively converted into a cytotoxic product and the fluorescence signal was not significantly decreased by cell death.

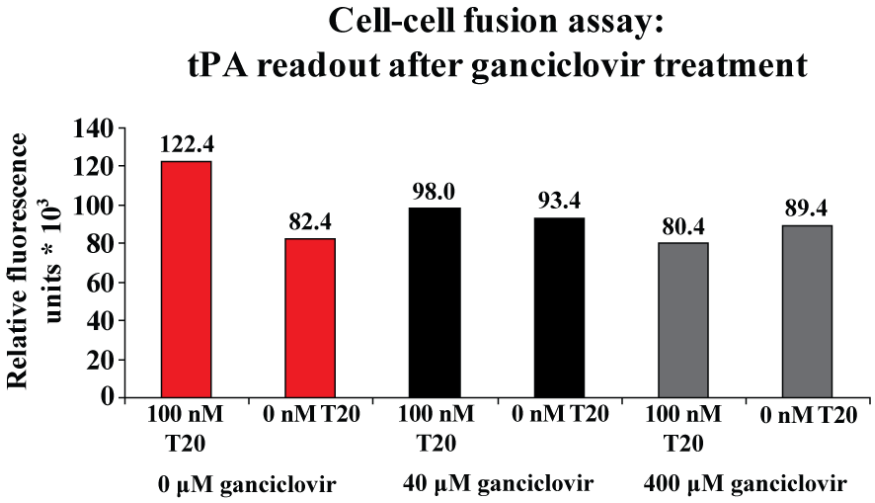

Figure 62: Fluorescent tPA readout after co-cultivation of CHO/HIVenv cells together with HIV-permissive cells, in presence and absence of T20 and ganciclovir. Comparison of the reporter gene signal at different ganciclovir concentrations between fused and non-fused samples. In independent sets of experiments, single data points were measured for each sample. Therefore descriptive error bars as for puromycin treated samples (Figure 61) are not represented.

When repeating these experiments several times, untreated samples (no puromycin/ ganciclovir addition) did not show coherent fluorescence signals (compare Figure 61 and Figure 62 red bars). In some cases, very low fluorescence signals for all samples were obtained and corresponding bright-field microscopy images confirmed cells death in all of them (data not shown). One explanation for these differences could be the limited accuracy (assumed to be ± 10%) of the number of cells seeded into each well when starting the assay. Increased densities could potentially result in higher confluency and cell death before the end of the assay, whereas decreased cell densities allowed

proliferation and therefore a higher fluorescence signal (Saeki et al., 1997; Song et al., 2009). However, as long as cells were still alive at the end of the assay, the differences in the fluorescence intensities between samples with and without inhibitor were reproducible.
It seemed that the downregulation of the tPA signal by puromycin/ ganciclovir induced cell death is not efficient when performing cell fusion.

3.3 ENZYME INHIBITION ASSAY

Besides the viral inhibition and cell-cell fusion assay, a third kind of assay aimed to explore the feasibility of monitoring the inhibition of enzymatic reactions by specific antibodies within microcompartments. Taking account of our previous results, obtained using a cell-cell fusion assay, a biochemical assay seemed much more feasible. Moreover, this kind of assay would also circumvent the problem of encapsulating different cell types into one drop. For this purpose, an enzyme of therapeutic interest, Angiotensin-converting enzyme (ACE), was chosen. A neutralising mAb (purified) and hybridoma cells producing this antibody were obtained from a collaborating group (Irina Baliasnikova; Naperova et al., 2008). To develop this system for the microfluidic platform, cell-compatible oil/ surfactant mixtures were identified (Chapter I, 3.1). However, conditions in which reaction/ inhibition of ACE could be performed and hybridoma cells survived were optimized. In addition, the time required for the release of sufficient antibody concentrations by individually encapsulated cells was analysed for different drop sizes.

3.3.1 ACE REACTION & INHIBITION BY PURIFIED ANTIBODIES

Using recombinant human ACE, the conversion of a fluorogenic substrate (Mca-RPPGFSAFK(Dnp)) in MOPS buffer, PBS, RPMI Utility medium and Freestyle medium was compared. It turned out that in MOPS buffer and PBS the reaction occurred more efficient than in RPMI Utility medium and Freestyle medium (Figure 63A, B, C, D; black lines).

In addition, the inhibition efficiency of the neutralising antibody against ACE (tACE-4E3) was assessed in MOPS buffer, PBS, RPMI Utility and Freestyle medium (Figure 63A, B, C, D; red lines). Not only that the reaction in MOPS buffer (Figure 63A) and PBS (Figure 63B) gave a higher fluorescence signal but also the inhibition by tACE-4E3 was more efficient. For example the ACE reaction efficiency was decreased nearly by 73 % in MOPS buffer and 75 % in PBS. In contrast, the antibody did not inhibit the fluorescence reaction in RPMI Utility medium (Figure 63C) and Freestyle medium (Figure 63D), probably due to unspecific substrate hydrolysis by a compound within the medium.

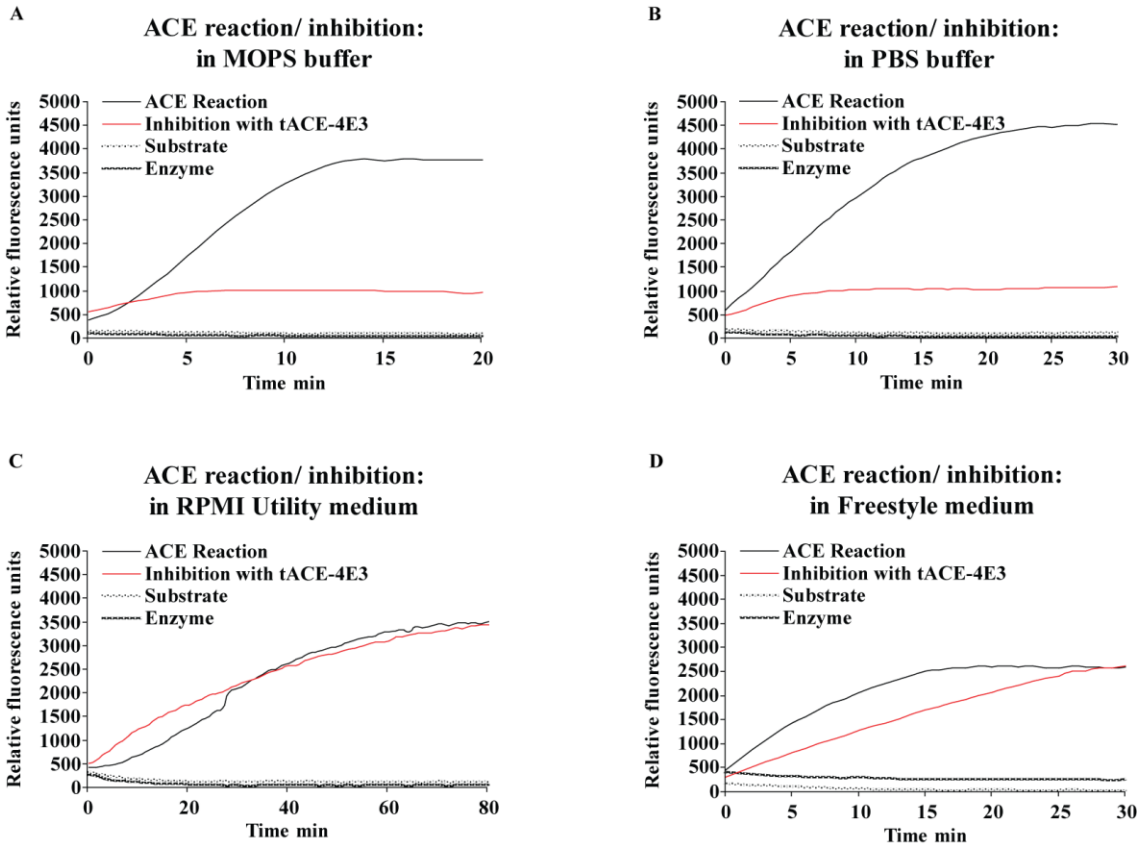

Figure 63: Efficiency of the ACE-catalysed reaction and its inhibition by a purified ACE antibody (tACE-4E3) in different solutions (MOPS buffer, PBS, RPMI Utility medium and Freestyle medium). The relative fluorescence is plotted against the reaction time. The black continuous line indicates the absence of antibodies; the red line corresponds to samples containing the tACE-4E3 antibody.

Based on these results, MOPS buffer and PBS were chosen for further optimization of the assay. For this, different incubation times were tested. An increased incubation time

of the enzyme together with the antibody up to 3 h enabled to decreasing ACE activity by 86 % (Figure 64B, continuous red line). This value was obtained only for PBS, but not for MOPS buffer (Figure 64A, continuous red line) and could also not be increased by longer incubation times or higher antibody concentrations. Hence, these results show that PBS offered the best conditions to perform the ACE reaction and inhibit the enzyme.

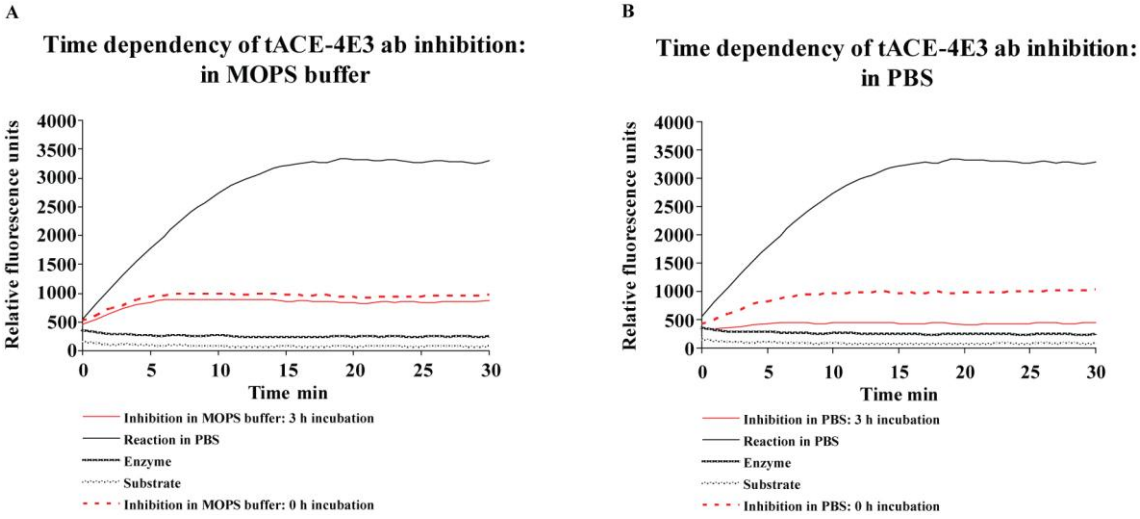

Figure 64: Time dependency of ACE inhibition in MOPS buffer and PBS. In PBS **(B)**, the ACE inhibition increased with longer incubation time (red continuous line), whereas in MOPS buffer **(A)** this effect could not be observed.

To demonstrate the specificity of tACE-4E3 and distinguish between neutralising antibodies and antibodies which just bind ACE, tACE-4E3 inhibition was compared to inhibitory properties of two other antibodies against ACE and one tPA antibody. The experiment was performed in the pre-defined conditions: PBS used as assay solution and 3 h incubation at 37 °C. Clearly only the tACE-4E3 antibody displayed neutralising activity against ACE (Figure 65, continuous red line; the continuous black line corresponds to the ACE reaction without antibody) proving its specificity for the Angiotensin-converting enzyme.

In a next step, ACE and the tACE-4E3 antibody were encapsulated into drops in order to explore the activity of the enzyme and the efficiency of its inhibition within droplets. In a first experiment, the enzyme in presence and absence of the antibody was encapsulated and incubated for 3 h within a CO_2 incubator (5 % CO_2, saturated with

H_2O) at 37 °C. Then, the emulsion was broken using 15 % 1H,1H,2H,2H-Perfluoro-1-octanol and the activity of ACE within the supernatant was determined. For both, samples with and without antibody no fluorescence signal was obtained in the readout (data not shown).

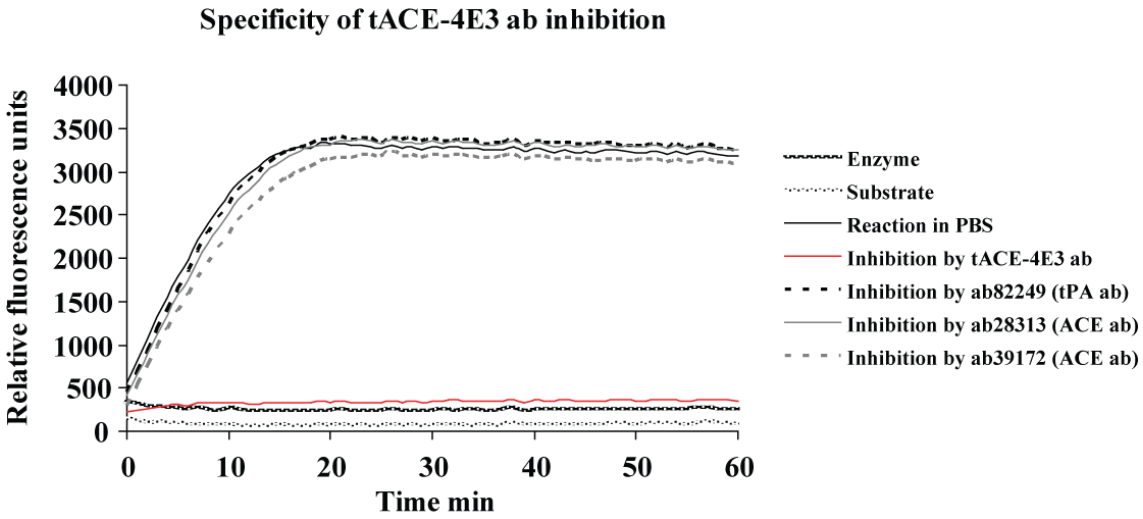

Figure 65: Specific ACE inhibition by purified ACE antibody (tACE-4E3). Incubation of ACE with tACE-4E3, two other anti-ACE antibodies and an anti-tPA antibody.

In a second experiment, to exclude that the breaking process decreased the enzymatic activity, only the enzyme (without antibody) was encapsulated together with the substrate. Afterwards, one part of the emulsion was measured directly in a plate reader, another part was first broken and then the content of the drops was measured. Compared to the ACE reaction in bulk both measurements did not show any fluorescence signal (data not shown). This was probably due to the fact that the used surfactant (DMP-PFPE) is not biocompatible with the ACE reaction. This effect of DMP-PFPE was already observed for alcohol dehydrogenase (Mazutis, (PhD) 2009) where the surfactant slowed down the reaction of the enzyme in droplets compared to its activity in bulk. A possible explanation could be impurities in the surfactant in form of heavy metals. In the synthesis of DMP-PFPE heavy metals are involved in the coupling process between the Krytox tail and the head group. Since ACE is a zinc-containing enzyme, the presence of other metal ions than zinc could inhibit the activity of ACE. Therefore, others surfactants should be considered to be used for measuring ACE activity in droplets.

3.3.2 ACE INHIBITION BY HYBRIDOMA CELLS

After establishing the ACE model system in bulk using purified tACE-4E3 antibody, the next task was to assess the incubation time of tACE-4E3 hybridoma cells which is required for obtaining sufficient amounts of antibody to inhibit ACE activity.

First, since the reaction and inhibition of ACE was established in PBS, the survival of hybridoma cells in this assay solution was investigated. Cultivation of tACE-4E3 hybridoma cells in PBS over 8 h resulted in normal cell morphology up to 6 h (as determined by microscopical analysis, data not shown). Therefore, experiments were performed for a maximum duration of 6 h.

Second, a cell density corresponding to single-cells within 660 pL droplets was adjusted (1.51×10^6 cells/ mL). Hybridoma cells were incubated together with ACE within a CO_2 incubator (5 % CO_2, saturated with H_2O) at 37 °C over 6 h. Samples were taken at t = 0 h, 2 h, 4 h and 6 h, the substrate was added and the fluorescence readout was performed in a plate reader. In addition, the ACE activity in absence of any antibody and its inhibition with purified antibody were determined by measuring fluorescence signals after 6 h of incubation.

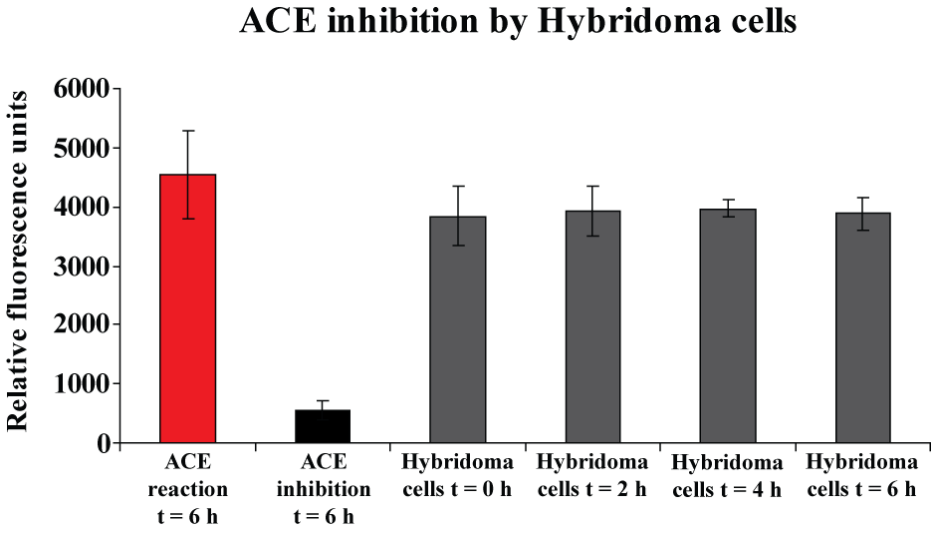

Figure 66: **ACE inhibition by hybridoma cells.** Co-incubation of 1.51×10^6 cells/ mL and recombinant ACE. Samples were taken after the indicated incubation times, then the substrate was added and fluorescence (corresponding to the enzymatic activity) was measured in a plate reader.

The resulting data shows that co-incubation of hybridoma cells together with ACE over 6 h did not result in significant inhibition of the enzyme (Figure 66). A likely explanation could be that at a cell density of 1.51 x 10^6 cells/ mL the concentration of the released antibody in the medium was not high enough to inhibit ACE. Therefore, the next step would be to increase the cell density, corresponding to smaller drops, e.g. d = 7.575 * 10^6 cells/ mL for 132 pL.

DISCUSSION & PERSPECTIVES

This work has focused on developing a droplet-based microfluidic platform for screening functional antibody activity. For this purpose, we established a microfluidic system that can be utilised for cell-based screens and allows for post-incubation fluorescence readout of individual compartments. In parallel, we were interested in the development of assays for the functional screening of monoclonal antibodies (mAb) screening compatible with microfluidic HTS technology. In particular, we investigated assays for the inhibition of viral cell-entry (e.g. HIV) and the inhibition of enzymatic reactions (e.g. ACE).

We have used droplet-based microfluidic systems to create miniaturised reaction vessels in which, both adherent and non-adherent, cells can survive for several days. In principal almost any volume, from picoliters to nanoliters, can be generated by changing the channel sizes and flow rates, or by splitting relatively large microcompartments through a T-junction into smaller units (Adamson et al., 2006). Therefore, tailored microcompartments either for the encapsulation of small objects, like single cells or compartments big enough to host multicellular organisms like *C. elegans* can be generated. For some functional assays it is necessary to encapsulate single cells per drop, whereas other assay designs require emulsions with 100 % occupied drops. Thus it is essential being able to control the number of cells per drop. In good agreement with a position distribution, cell densities corresponding to λ between 0.4 and 0.5 lead to less than one cell per drop on average (~ 30 % single cells per drop), whereas λ higher than 4 result in emulsions in which each drop hosts at least one cell. These results are independent of the drop size and hence demonstrate how the number of cells per drop can be adapted for different assay types. The microfluidic platforms described here allow the encapsulation step to occur at rates of more than 800 droplets per second. As the number of cells per drop follows a Poission distribution, the optional encapsulation of single cells causes the generation of empty drops, thus decreasing the resulting encapsulation rate to ~ 300 cells per second. Nevertheless, to obtain emulsions with < 1 % empty drops methods like controlled or high-throughput encapsulation can be used (Edd et al., 2008; Chabert et al., 2008). Furthermore, the drop size and therefore

the drop volume can be adjusted according to the assay duration. The cell density was found to inversely correlate with the survival time of encapsulated cells. Larger compartments are hence preferential for long-term assays, especially since encapsulated cells proliferate within the microcompartments. Consequently, even proliferation assays (e.g., for screening cytostatic drugs) should be possible as long as the chosen volume is big enough to guarantee sufficient supply of nutrition. On the other hand, small volumes might be advantageous for other applications, for example to minimise reagent costs or to rapidly obtain high concentrations of secreted cellular factors such as antibodies. A collaborating group demonstrated that detectable antibody concentrations were obtained from single encapsulated hybridoma cells after just six hours of incubation (Köster et al., 2008).

Besides the volume, additional factors, notably the biocompatibility of the surfactants and the gas permeability of the storage system, have a major impact on cell survival. All of the non-ionic surfactants described here allowed for cell survival and proliferation, whereas the two ionic surfactants mediated cell lysis. Even though there is no direct proof of correlation, it seemed quite striking that poly-L-lysine, a compound widely used to improve cell attachment to surfaces (Budd et al., 1989), mediated membrane disruption when used as a head group of an ionic surfactant. Long-term incubation also requires sufficient gas exchange. This can be ensured either by using open reservoirs or channels or tubing made of gas-permeable materials such as fluorinated polymers. Efficient gas exchange is also helped by the fact that perfluorocarbon carrier fluids can dissolve more than 20-times the amount of O_2, and three-times the amount of CO_2, than water and have been shown to facilitate respiratory gas delivery to both prokaryotic and eukaryotic cells in culture (Lowe et al., 1998).

The possibility of re-injecting microcompartments into a chip after the incubation step opens the way for integrated droplet-based microfluidic systems for cell-based HTS. As we have shown, a fluorescence-based readout of the expression of a cellular reporter gene can be performed in individual compartments at frequencies of 500 Hz. Hence, a wide range of commercially available fluorescence-based assays (Gonzalez and Negulescu, 1998; Sundberg, 2000) can potentially be performed in a high-throughput fashion. The fact that possible coalescence of individual drops does not necessarily bias the readout is noteworthy. As shown, coalesced drops with higher volumes can easily be

identified and excluded from the data analysis. In theory, the use of gates also allows for the analysis of only those compartments hosting a specific number of (fluorescent) cells. In contrast to conventional FACS analysis, the assay readout does not have to be based on fluorophores that remain in, or on the surface of, the cells (e.g., GFP or fluorescent antibodies). Using compartmentalisation, we have been able to measure the activity of an intracellular reporter enzyme (β-galactosidase) by using a fluorescent product that is highly membrane permeable (fluorescein).

We have demonstrated post-incubation fluorescence readout of individual compartments at 500 Hz, and additional droplet manipulation procedures (such as fusion, splitting, and sorting) can be performed at similar rates (Link et al., 2004, 2006; Ahn et al., 2006). The integration of further microfluidic modules into the microfluidic platforms shown here should allow the application range to be expanded. Integrating a microfluidic sorting module (Baret et al., 2009a; Ahn et al., 2006; Fu et al., 2002) could, for example, enable the screening of drug candidates. In the simplest case, the candidates could be genetically encoded by the encapsulated cells themselves (starting with a cell library), e.g. antibodies released by hybridoma cells or even B-cells. Hence, the collection of sorted positive drops would allow for the identification of hits by DNA sequencing. Alternatively, the sorting module could be used to screen synthetic compounds fixed on beads (e.g., one-bead-one-compound libraries) co-encapsulated in the drops. After the sorting step, beads that mediated the desired effect could be recovered from the drops for a subsequent decoding step (e.g., by mass spectroscopy). Using optical barcodes encoding the compound identity might even allow the decoding step to be performed in real time (without the need for a sorting module) (Battersby et al., 2002; Pregibon et al., 2007). For example, different fluorescence channels could be used for the assay and label readout. The fact that the optical barcode does not even have to be directly linked to the test compound when using droplet-based microfluidics is noteworthy: the label can simply be mixed with the test compound prior to the encapsulation step.

The throughput of a single integrated, droplet-based microfluidic system for cell-based screening could potentially be 500 times higher than conventional robotic microtiter plate-based HTS technologies that can perform a maximum of ~ 100.000 assays per day, or ~ 1 s^{-1}. Using compartments as small as 660 pL, the volume of each assay, and

hence the cost of reagents for screening, could be reduced by > 1.000-fold compared to the smallest assay volumes in microtiter plates (1–2 µL). This may allow many high-throughput biochemical screens to be replaced by more physiologically relevant cell-based assays (Chapman, 2004; Johnston and Johnston, 2002), including assays with highly valuable cells, e.g., primary human cells (which are arguably the most physiologically relevant model systems, but which generally cannot be obtained on the scale required for HTS) or mature antigen-activated B-cells.

Recently, RainDance Technologies presented automated quantitative in-droplet analysis of cell survival similar to the off-chip readout presented here. The group demonstrated an integrated biological assay using a stable pre-made optically encoded droplet library (Brouzes et al., 2009). In 2010, Agresti and co-workers demonstrated the power of droplet-based microfluidic systems by directed evolution of horseradish peroxidase (HPR). HPR is extensively used in biochemical applications and therefore already very efficient. Thus its improvement is a challenging task. In the reported system, based on encapsulated yeast cells (yeast display), > 10^7 individual reactions in total were screened resulting in 1.000-fold increase in speed and a 1-million-fold reduction in costs compared to state-of-the-art robotic screening systems (Agresti et al., 2010).

Aqueous microcompartments can be used as miniaturised vessels for chemical and biological reactions (Tawfik and Griffiths, 1998; Kelly et al., 2007; Griffiths and Tawfik, 2006), thus offer a novel technology for high throughput screening. We have shown how this approach can also be utilised for cell-based applications. In parallel to establishing our microfluidic platform we developed functional assays for screening inhibiting antibodies and assessed their suitability for droplet-based microfluidics. In three different approaches we investigated a viral cell-entry assay, a cell-cell fusion assay and an enzyme inhibition assay.

In this study we have aimed to establish an assay to screen for neutralising human immunodeficiency virus 1 (HIV-1) antibodies. HIV has the ability to mutate, evolve and develop a wide-spread resistance to existing drugs used in HIV standard therapies. This and the lack of a universal HIV vaccine point out the tremendous need of continuous development of new antivirals to treat HIV infections.

Promising approaches in HIV vaccine research and development use virus-like particles (Hammonds et al., 2007). These pseudovirions are able to recapitulate the native trimeric structure of HIV env and therefore represent an effective epitope presentation platform for inducing a neutralising antibody response (Hicar et al., 2010). Using MLV particles pseudotyped with HIV gp120 and gp41, we showed that pseudoparticles efficiently enter their host cells when co-encapsulated in droplets. Even though HIV pseudotyped particles exhibit a great potential to induce neutralising antibody responses, they are difficult to prevent from shedding of the gp120 env protein when concentrated using ultracentrifugation. Therefore, HIV env pseudoparticles showed less transduction efficiency in our experiments, as concentration is essential for the use in droplets to obtain at least one particle per drop. Therefore, we decided to investigate an alternative approach that mimicks the cell-virus fusion step of HIV infection. Instead of HIV env pseudotyped particles (effector particles), we used CHO cells expressing wild type HIV env proteins (effector cells) resulting in cell-cell fusion.

To reduce the number of false positives, we have chosen an inhibition assay that couples a positive fluorescence signal with the presence of potent inhibitors, instead of viral cell-entry. This assay also allows for exclusion of cytotoxic compound (or concentrations thereof) and specifically selects cells prevented from viral-cell entry (Clausell-Tormos et al., 2010; (WO/2006/082385) SCREENING METHOD). This assay was optimised in our lab for the use of MLV-(VSV-G) pseudoparticles and we assumed it to be transferable to cell-cell fusion assays using HIV-permissive, tPA expressing cells (indicator cells) and HIV env expressing cells (effector cells).

The tools of the patented viral inhibition assay were adjusted to the use for cell-cell fusion. We established a system that allows for simulating the fusion of the HIV envelope with the target cell membrane and inhibition thereof using T20 as a model inhibitor. We determined an initial effective T20 concentration of 100 nM for inhibiting cell-cell fusion which is in agreement with a previous report (Pang et al., 2008). Pang and co-workers described that a T20 concentration of 100 nM over 6 h is effective to inhibit HIV-1-mediated membrane fusion. As the complete inhibition assay, described here, takes place over 5 days, the model inhibitor had to be renewed after 24 h and after 72 h to maintain the inhibitory activity of T20 ($t_{1//2}$ = 1.83 h; Kilby et al., 1998). The reason for the activity loss could either be hydrolysis of the peptide or a decline of the

T20 concentration in the assay medium by cell uptake and subsequent degradation. In addition to T20, antibodies against HIV were tested for their ability to neutralise cell-cell fusion in our system. We found that the hybridoma cell line HB-10895 (commercially available from ATCC) is suitable for this assay. The conditions determined for the fusion and its inhibition were in good agreement with the conditions already optimised for the viral inhibition assay (Clausell-Tormos et al., 2010). Addition and renewal of T20 and HB-10895 supernatant could be adjusted to the addition of puromycin and ganciclovir and the readout time point, without any effect on syncytia formation or its inhibition. For the fluorescent readout, no significant difference between samples with and without inhibitor could be seen, even though syncytia formation was observed in absence of an inhibitor. This could be explained by decreasing cell viability due to long assay duration. To allow contact between cells for fusion, a minimum cell density was required. This limited the subsequent cultivation time to maximum three days, as with longer incubation cells died. In contrast, for sufficient downregulation of the reporter gene signal the assay demands at least five days. Moreover, both transfer genes, shRNA against the puromycin resistance and thymidine kinase (that would direct the downregulation of the reporter signal), might have low expression and/ or co-expression levels in CHO cells and/ or in syncytia (Fehse et al., 2002). Therefore, the cell-cell fusion assay does not seem to be compatible with the downregulation of the tPA reporter gene signal.

To set up a cell-based assay for drug discovery, the screening requires consideration of several factors, such as choosing an endpoint, characterising assay responsiveness, determining dose and duration of compound exposure, reagent stability, sensitivity of detection and most important reproducibility of data (Riss, 2005). Since cell-based assays (as described here) turned out to be difficult, especially as for antibody screens at least 2 different cells per drop have to be co-encapsulated, we focused on biochemical assays. In a second approach we aimed to develop an enzyme inhibition assay, using Angiotensin I-converting enzyme, to prove the concept of antibody screening in microdroplets.

For this purpose, an assay was established that allows for maximum inhibition of ACE, using a purified antibody directed against the C-domain of the enzyme (Naperova et al.,

2008). Naperova and co-workers reported decreased ACE activity by nearly 40 %. In our hands, we could even demonstrate an activity decrease of up to 85 %.

In a next step, first attempts were made to combine the assay with the use of hybridoma cells, producing the ACE-inhibiting antibody, instead of purified antibodies. Investigations of the incubation time of hybridoma cells, required for sufficient antibody production in 660 pL droplets, did not lead to any significant ACE inhibition. Further studies should focus for example on cell density increase (corresponding to smaller droplet volumes) or longer incubation times (> 6 h). Whereupon, in doing the latter, another assay medium than PBS should be identified as hybridoma cells showed normal cell morphology only up to 6 h of incubation. Moreover, it has not been proved that normal antibody production is provided when using PBS as assay medium. Therefore, identifying a cell culture medium compatible with the ACE reaction and its inhibition as well as ensuring viability of the hybridoma cells is an important step towards establishing a system demonstrating the inhibition of ACE-1 by antibodies released from single encapsulated cells.

The second obstacle that needs to be overcome would be the possible inhibition of the ACE reaction itself by the used surfactant. DMP-PFPE, even though very biocompatible with cells, seems to affect the ACE reaction within droplets. As shown by our experiments, co-encapsulation of the enzyme together with the substrate did not result in any fluorescence signal, indicating loss of activity. A possible solution could be the use of Jeffamine®-PFPE or PEG-PFPE as droplet stabiliser; like DMP-PFPE, both surfactants showed good cell biocompatibility. Moreover, PEG-PFPE has also been proved to be biocompatible with enzymatic reactions in droplets, for example alcohol dehydrogenase or horseradish peroxidase (Mazutis, (PhD) 2009; Agresti et al., 2010).

As an alternative system we initiated the set-up of Acetylcholine esterase (AChE, EC 3.1.1.7) as model target for antibodies released by single encapsulated cells. Acetylcholine esterase hydrolyses the neurotransmitter acetylcholine to choline and an acetate group. AChE is used as a drug target for the treatment of Alzheimer's disease (cholinergic-based strategies; Francis et al., 1999). Even though there are also other hypotheses explaining the cause of the disease, AChE inhibition will remain valid as one approach for rational drug development against Alzheimer's disease (Terry & Buccafusco, 2003). Using the inhibitory antibody Elec-403 that supresses the AchE

activity by 99 % (Simon et al., 1999), we are currently investigating the suitability of this target as a model system for the microfluidic screening of therapeutic antibodies.

In conclusion, we established a droplet-based microfluidic platform to generate miniaturised reaction compartments in which cells survive for several days. Additionally, we demonstrated controlled encapsulation of individual cells and analyses of individual compartments thus allowing single cell assays to be performed at very high throughput (500 samples can be analysed per second). Antibodies released from single cells (hybridoma cells) were found to reach detectable concentrations in microdroplets (Köster et al., 2008). Antibodies inhibiting an enzymatic drug target (ACE) exist and are at hand. Further assay optimisation is required but should ultimately allow the screening of individual cells (hybridoma cell) for the release of therapeutic antibodies. After proving the feasibility of this concept within microdroplets, even B-cells could be screened and selected for the release of neutralising antibodies, circumventing the need for hybridoma cells and drastically increasing throughput. Once established, this system could be used for the screening/ selection of many more therapeutic antibodies.

Résumé de Thèse en Français

Développement de tests fonctionnels pour le criblage de l'activité anticorps dans un système microfluidique en gouttelettes

Les méthodes de criblage à haut-débit permettent de contrôler l'effet de millions de composés dans un test donné. Elles nécessitent de petits volumes afin de réduire les coûts et permettre une manipulation rapide des échantillons. Les systèmes traditionnels sont généralement basés sur des mesures en microplaques, mais une miniaturisation supplémentaire avec ces tests rencontrerait des problèmes. En effet, pour des volumes inférieurs au microlitre, le comportement des liquides est dominé par l'évaporation et les forces capillaires qui vont, par exemple, conduire à la formation de ponts entre les puits. Dans notre laboratoire, nous développons des systèmes basés sur la microfluidique en gouttes. Dans ces systèmes, de minuscules microgouttelettes aqueuses entourées d'huile (émulsion d'eau dans l'huile) agissent comme des microréacteurs indépendants qui permettent de surmonter les limitations des systèmes conventionnels en microplaques. Ces micro-compartiments ont des volumes plus de 1000 fois plus petits et permettent d'avoir un débit ~ 500 fois plus grand. Le but de cette étude était de développer des tests fonctionnels pour le criblage d'anticorps monoclonaux (mAc) compatibles avec la technologie microfluidique de criblage à haut débit. Nous nous sommes intéressés particulièrement à des tests pour l'inhibition de l'entrée virale dans les cellules et/ou des cibles de médicaments avec une forte importance clinique comme le Virus de l'immunodéficience humaine (le VIH) et l'Enzyme de conversion d'Angiotensine (ACE).

Les approches pour la sélection des mAc sont généralement basées sur des technologies de présentation (comme le phage display) ou sur utilisation d'hybridomes. « Phage display » permet la sélection de banques d'anticorps avec une forte diversité génétique (jusqu'à 10^{12} variants) pour leur activité de liaison. Cependant, l'affinité n'est

directement corrélée avec une propriété inhibitrice. Pour surmonter ce problème, les hybridomes peuvent être utilisés pour la sélection des mAc. Les hybridomes sont des cellules-B immortalisées qui sont mises en culture pour obtenir des concentrations suffisantes d'anticorps sécrétés pour des criblages basés sur des tests fonctionnels (par exemple la neutralisation de virus, l'inhibition de cibles médicamenteuses). Cependant, l'inconvénient de cette approche est d'une part le temps nécessaire à la génération des hybridomes et d'autre par le peu de clones pouvant être sélectionnés (pas plus de 1000) ce qui correspond seulement à $1/10^4$ du répertoire immunité total d'une souris.

Ces limitations pourraient être dépassées par la miniaturisation, en utilisant des microréacteurs suffisamment assez petits pour directement obtenir des concentrations détectables d'anticorps à partir d'une seule cellule relargant des anticorps. Pour cela, nous avons décrit une plateforme de microfluidique en goutte dans laquelle les cellules sont mises en culture dans des micro-compartiments aqueux (Clausell-Tormos et al., 2008). La synthèse et l'identification de tensio-actifs biocompatibles a permis aux cellules humaines de survivre et de proliférer dans les micro-compartiments pendant plusieurs jours. En outre, un groupe de collaborateurs a démontré que des concentrations détectables d'anticorps pouvaient être obtenues après seulement six heures d'incubation (Köster et al., 2008). Par la suite, nous nous sommes concentrés sur la mise en place de tests fonctionnels pour l'inhibition de différentes cibles médicamenteuses, appropriés à notre plateforme microfluidique en gouttes. Nous avons en particulier optimisé un test d'inhibition virale (Clausell-Tormos et al., 2010) et avons développé un test pour l'inhibition de cibles enzymatiques médicamenteuses.

La première étape du projet était le développement d'une plateforme microfluidique permettant l'encapsulation et la culture de cellules humaines dans des micro-compartiments aqueux. Une étape cruciale fut d'identifier des surfactants biocompatibles pour la production de gouttelettes. Les étapes suivantes ont été d'encapsuler une cellule unique ou de produire des émulsions dans lesquelles toutes les gouttes étaient occupées. Les méthodes pour récupérer les cellules encapsulées et pour la remise en culture ont été développées. De plus, le taux de survie des cellules dans les micro-compartiments après encapsulation et incubation ainsi que le taux de récupération ont été déterminés.

Pour l'encapsulation des cellules humaines nous avons développé un dispositif en PolyDiMethylSiloxane (PDMS) dans lequel des gouttes de 660 pL sont produites par la rencontre d'un flux de phase aqueuse et d'un flux de phase inerte d'huile perfluoro-carbonée. Pour obtenir de plus grosses gouttes, la largeur et la profondeur des canaux et ont été changés respectivement de 75 µm x 100 µm (gouttes de 660 pL) à 255 µm x 100 µm (des gouttes de 2120 pL) et 255 µm x 200 µm (gouttes de 5960 pL).
Dans certains tests fonctionnels, il est nécessaire d'encapsuler une seule cellule par goutte tandis que d'autres tests exigent une émulsion avec un taux de remplissage de 100 %.
Pour contrôler le nombre de cellules par goutte, des expériences de dilution sur-puce ont été exécutées. En ajustant les débits d'injection d'une suspension cellulaire (Jurkat ou des hybridomes) et en co-injectant du milieu stérile, nous avons pu moduler la densité cellulaire et ainsi observer que le nombre de cellules par goutte suivait une distribution de Poisson.
Ainsi, le nombre de cellules par goutte peut facilement être ajusté et permet même l'encapsulation de phase aqueuse d'une cellule unique. Par exemple, en utilisant une densité cellulaire correspondant à moins d'une cellule par goutte en moyenne ($\lambda = 0.425$), 63.3 % des gouttelettes sont vides, 31.7 % contiennent exactement une cellule humaine et seulement très peu de gouttelettes sont occupées par deux cellules ou plus (5 %). Ces résultats sont indépendants de la taille des gouttes et démontrent de là comment le nombre de cellules par goutte peut être adapté pour différents types de tests.
Pour que les cellules restent vivantes dans les gouttelettes, la biocompatibilité du tensio-actif utilisé pour la stabilisation des gouttelettes s'est avéré être crucial. Dans notre groupe nous avons synthétisé plusieurs tensio-actifs perfluoro-polyether (PFPE) qui différent seulement par leur tête hydrophile. Pour analyser la biocompatibilité, nous avons déposé des cellules HEK293T sur la surface d'une couche d'huile perfluoro-carbonée en présence (0.5 % w/w) et en l'absence de différents tensio-actifs. En l'absence de tensio-actif les cellules sont restées intactes et ont même proliférées. Par contre, le sel d'ammonium du carboxy-PFPE et du poly-L-lysine-PFPE (PLL-PFPE) a entrainé la mort des cellules.Néanmoins, deux tensio-actifs biocompatibles ont pu être identifiés, le Jeffamine®-PFPE et le dimorpholinophosphate-PFPE (DMP-PFPE), qui n'ont pas affecté l'intégrité de la membrane cellulaire et ont même permis leur

prolifération. Bien que, le Jeffamine®-PFPE et DMP-PFPE aient des biocompatibilités comparables, les tests de stabilité ont révélé que le « DMP-PFPE » produirait des émulsions plus stables que le « Jeffamine®-PFPE ».

Pour l'étape suivante, nous avons déterminé les taux de survie (cellules vivantes / le nombre total de cellules récupérées) pour différents temps d'incubation dans différentes tailles de micro-compartiments contenant des nombres différents de cellules.

Le même comportement a été observé pour les cellules adhérentes et pour les cellules en suspension. Pendant les deux premiers jours le nombre de cellules vivantes est resté stable ou a légèrement augmenté (prolifération), suivie par une diminution de leur nombre en raison de l'épuisement des substances nutritives disponibles. En comparant les cellules HEK293T aux cellules Jurkat, on observe une moindre prolifération des premières comparées aux deuxièmes due probablement au manque du support solide. Le taux de récupération des cellules HEK293T à partir des gouttes était de 20 % et de 30 % pour les cellules Jurkat. Et pourront ainsi remises en culture.

En parallèle, pour mettre en place la plateforme microfluidique nous avons développé des tests fonctionnels pour le criblage d'anticorps inhibiteurs et avons évalué s'ils étaient utilisables pour la microfluidique en gouttelettes. En utilisant trois approches différentes, nous avons évalué un test d'entrée virale cellulaire, un essai de fusion cellule-cellule et un test d'inhibition d'enzymatique. La première approche visait à combiner un nouvel essai breveté d'inhibition virale (Clausell-Tormos et al., 2010; (WO/2006/082385) SCREENING METHOD) avec le système microfluidique. Le test utilise des cellules modifiées génétiquement (cellules indicatrices) produisant un fort signal de fluorescence de manière continue à moins qu'elles ne soient transformées avec des particules de pseudotype recombinantes (particules effectrices). Ces particules effectrices ont empaqueté un vecteur codant pour un « shRNA » supprimant la résistance à la puromycine des cellules indicatrices (en régulant négativement l'enzyme Puromycin-N-acetyltransferase). Ainsi les cellules indicatrices meurent en présence de puromycin, menant à une extinction du signal rapporteur du gène, tandis que les cellules non-transformées montrent une intensité de signal maximale. Alternativement, un gène codant pour un gène de suicide (thymidine kinase) a été utilisé. L'addition du substrat correspondant (Ganciclovir) entraine la mort des cellules indicatrices, aboutissant également à l'inactivation efficace du gène rapporteur en réponse à une entrée

cellulaire. Lors de nos expériences, nous avons produit des particules d'effectrices (dérivées du virus de la leucémie murine, MLV) pseudotypées avec les protéines de l'enveloppe du VIH (env), la résultante à un tropisme équivalent à cette espèce, comme décrit par Siegert et al., 2005.

Pour identifier la faisabilité de cette approche pour notre plateforme microfluidique en gouttelettes, nous avons tout d'abord évalué l'efficacité de la transduction des particules effectrices de MLV (VIH env) dans des gouttelettes. Pour cela, nous avons produit des particules ayant empaqueté un vecteur codant pour l'enzyme ß-galactosidase. Après incubation des particules effectrices avec les cellules indicatrices dans les gouttes, un titre de 2.17×10^6 i.U./ mL a été déterminé (unités infectieuses par millilitre). Cette valeur est inférieure à celle obtenue dans les microplaques de 24 puits et à celle mesurée en tube eppendorf et qui sont respectivement de 4.12×10^6 i.U./ mL et 3.88×10^6 i.U./ mL. Cependant, en considérant un taux de récupération des cellules des gouttes de seulement 30 % (une valeur typique avec le processus de cassage de gouttes) 2.17×10^6 i.U./ mL correspond à 6.51×10^6 i.U./ mL en extrapolant pour un taux de récupération de 100 %. Cela montre clairement que les particules MLV pseudotypées avec le VIH gp160 (MLV – (VIH env)) co-encapsulées dans les gouttes pénètrent efficacement dans leurs cellules hôtes.

Dans une deuxième approche nous avons mis en place un test de fusion cellulaire utilisant des cellules CHO exprimant la protéine enveloppe VIH env au lieu des particules de MLV (le VIH env). Pour cela, une lignée stable de cellules CHO (le VIH env) (cellules effectrices) exprimant le shRNA anti-puromycin et la thymidine kinase a été produite. Les conditions pour la fusion cellule-cellule (par exemple le milieu de culture, la quantité de cellules pour une fusion efficace) et la détection du signal rapporteur (par exemple la concentration, le temps d'incubation et la répétition d'ajout de puromycine et de Ganciclovir, le moment de mesure) ont été défini et optimisé. En outre, T20, un inhibiteur de VIH bien connu, a été utilisé comme système modèle pour l'inhibition de la fusion. Tandis qu'en absence de n'importe quelle drogue la formation de « syncytia » a été observée, l'addition de 100 nM de T20 a réprimé cet effet. La fusion cellule-cellule pourrait aussi être inhibée par le surnagent d'une lignée cellulaire d'hybridomes produisant un anticorps ciblant VIH env gp120 (HB-10895, ATCC). Pour

la mesure de fluorescence, aucune différence significative entre des échantillons avec et sans inhibiteurs n'a été détectée, bien que la formation de « syncytia » ait été observée en l'absence d'inhibiteur. Ceci pourrait s'expliquer par la diminution de la viabilité cellulaire due à la longue durée de l'essai. Pour permettre le contact entre les cellules pour la fusion, une densité cellulaire minimale a été requise. Cela a limité le temps de culture ultérieure à trois jours maximum, comme avec temps d'incubation plus long les cellules mourraient. Ce pendant, pour suffisamment diminuer le signal du gène rapporteur le test exige au moins cinq jours. Le test de fusion cellule-cellule ne semble donc pas être compatible avec la régulation négative du gène rapporteur.Le troisième type de test visait à explorer la faisabilité de l'inhibition des anticorps de réactions enzymatiques dans des micro-compartiments. Pour cela, une enzyme d'intérêt thérapeutique, ACE, a été choisie. Pour développer ce système pour la plate-forme microfluidique, un mAc neutralisant, un substrat fluorogénique et un mélange d'huile biocompatible/surfactant ont été identifiés. Les conditions pour lesquelles les cellules survivent et pour lesquelles l'inhibition d'ACE peut être réalisée ont été optimisés. Nous étudions actuellement, le temps d'incubation nécessaire pour la production suffisante d'anticorps dans des gouttelettes de 660 pL.

Pour conclure, nous avons établi une plateforme microfluidique en gouttes pour créer des compartiments réactionnels miniaturisés dans lesquels les cellules survivent pendant plusieurs jours. De plus, nous avons démontré l'encapsulation contrôlée de cellules individuelles et les analyses de compartiments individuels permettant ainsi à des tests sur cellule unique d'être réalisés à très haut débit (500 échantillons peuvent être analysés par seconde). L'utilisation d'hybridomes sert de système modèle pour le criblage d'anticorps à l'échelle de la cellule unique. En outre, un test d'anticorps inhibiteurs pour l'enzyme de conversion de l'Angiotensine a été optimisé. Une fois la faisabilité de ce concept prouvée, l'étape suivante sera d'encapsuler des cellules-B de souris immunisées avec l'ACE humain et les sélectionner pour le relargage d'anticorps neutralisants. Ce serait le tout premier criblage fonctionnel d'anticorps basé sur des cellules-B primaires, ce qui permet de contourner le besoin de produire des hybridomes et ainsi augmenter considérablement le débit. Une fois établi, ce système pourrait être utilisé pour le criblage/sélection de beaucoup plus d'anticorps thérapeutiques.

LITERATURE

Abate, A. R.; Poitzsch, A.; Hwang, Y.; Lee, J.; Czerwinska, J. & Weitz, D. A. (2009). Impact of inlet channel geometry on microfluidic drop formation. *Phys Rev E Stat Nonlin Soft Matter Phys, 80, 026310.*

Adamson, D. N.; Mustafi, D.; Zhang, J. X. J.; Zheng, B. & Ismagilov, R. F. (2006). Production of arrays of chemically distinct nanolitre plugs via repeated splitting in microfluidic devices. *Lab Chip,* 6, 1178-1186.

Agresti, J. J.; Antipov, E.; Abate, A. R.; Ahn, K.; Rowat, A. C.; Baret, J.-C.; Marquez, M.; Klibanov, A. M.; Griffiths, A. D. & Weitz, D. A. (2010). Ultrahigh-throughput screening in drop-based microfluidics for directed evolution. *Proc Natl Acad Sci U S A, 107, 4004-4009.*

Ahn, K.; Kerbage, C.; Hunt, T. P.; Westervelt, R. M.; Link, D. R. & D. A. Weitz (2006). Dielectrophoretic manipulation of drops for high-speed microfluidic sorting devices. *Appl Phys Lett, 88, 024104.*

Ambuehl, P. M.; Tissot, A. C.; Fulurija, A.; Maurer, P.; Nussberger, J.; Sabat, R.; Nief, V.; Schellekens, C.; Sladko, K.; Roubicek, K.; Pfister, T.; Rettenbacher, M.; Volk, H.-D.; Wagner, F.; Müller, P.; Jennings, G. T. & Bachmann, M. F. (2007). A vaccine for hypertension based on virus-like particles: preclinical efficacy and phase I safety and immunogenicity. *J Hypertens, 25, 63-72.*

Anna, S. L.; Bontoux, N. & Stone, H. A. (2003). Formation of dispersions using 'flow-focusing' in microchannels. *Applied Physics Letters, 82, 364-366.*

Aris, R. (1956). On the Dispersion of a Solute in a Fluid Flowing through a Tube. *Proc R. Soc Lond A, 235, 67.77.*

Arnon, R. (1975a). Enzyme inhibition by antibodies. *Acta Endocrinol Suppl (Copenh), 194, 133-153.*

Aumiller, G. D.; Chandross, E. A.; Tomlinson, W. J. & Weber H. P. (1974). Submicrometer resolution replication of relief patterns for integrated optics. *J Appl Phys*, 45, *4557-4562.*

Barer, M. R. & Millership, S. E. (1990). Direct selection of monoclonal antibodies neutralising the cytotoxic activity of Aeromonas sobria. *FEMS, 59, 311-314.*

Baret, J.-C.; Miller, O. J.; Taly, V.; Ryckelynck, M.; El-Harrak, A.; Frenz, L.; Rick, C.; Samuels, M. L.; Hutchison, J. B.; Agresti, J. J.; Link, D. R.; Weitz, D. A. & Griffiths, A. D. (2009a). Fluorescence-activated droplet sorting (FADS): efficient microfluidic cell sorting based on enzymatic activity. *Lab Chip, 9, 1850-1858.*

Barré-Sinoussi, F.; Chermann, J. C.; Rey, F.; Nugeyre, M. T.; Chamaret, S.; Gruest, J.; Dauguet, C.; Axler-Blin, C.; Vézinet-Brun, F.; Rouzioux, C.; Rozenbaum, W. & Montagnier, L. (1983). Isolation of a T-lymphotropic retrovirus from a patient at risk for acquired immune deficiency syndrome (AIDS). *Science, 220, 868-871.*

BBC NEWS (2009). http://news.bbc.co.uk/2/hi/8272113.stm.

Berg, M.; Undisz, K.; Thiericke, R.; Zimmermann, P.; Moore, T. & Posten, C. (2001). Evaluation of Liquid Handling Conditions in Microplates. *J Biomol Screen, 6, 47.*

Blazej, R. G.; Kumaresan, P. & Mathies, R. A. (2006). Microfabricated bioprocessor for integrated nanoliter-scale Sanger DNA sequencing. *Proc Natl Acad Sci U S A, 103, 7240-7245.*

Boeckh, M.; Bowden, R. A.; Storer, B.; Chao, N. J.; Spielberger, R.; Tierney, D. K.; Gallez-Hawkins, G.; Cunningham, T.; Blume, K. G.; Levitt, D. & Zaia, J. A. (2001). Randomized, placebo-controlled, double-blind study of a cytomegalovirus-specific monoclonal antibody (MSL-109) for prevention of cytomegalovirus infection after allogeneic hematopoietic stem cell transplantation. *Biol Blood Marrow Transplant, 7, 343-351.*

Boedicker, J. Q.; Li, L.; Kline, T. R. & Ismagilov, R. F. (2008). Detecting bacteria and determining their susceptibility to antibiotics by stochastic confinement in nanoliter droplets using plug-based microfluidics. *Lab Chip, 8, 1265-1272.*

Brekke, O. H. & Sandlie, I. (2003). Therapeutic antibodies for human diseases at the dawn of the twenty-first century. *Nat Rev Drug Discov, 2, 52-62.*

Brezden, C. B. & Rauth, A. M. (1996). Differential cell death in immortalized and non-immortalized cells at confluency. *Oncogene, 12, 201-206.*

Bringer, M. R.; Gerdts, C. J.; Song, H.; Tice, J. D. & Ismagilov, R. F. (2004). Microfluidic systems for chemical kinetics that rely on chaotic mixing in droplets. *Philos Transact A Math Phys Eng Sci, 362, 1087-1104.*

Brody, J. P.; Yager, P.; Goldstein, R. E. & Austin, R. H. (1996). Biotechnology at low Reynolds numbers. *Biophys J, 71, 3430-3441.*

Brouzes, E.; Medkova, M.; Savenelli, N.; Marran, D.; Twardowski, M.; Hutchison, J. B.; Rothberg, J. M.; Link, D. R.; Perrimon, N. & Samuels, M. L. (2009). Droplet microfluidic technology for single-cell high-throughput screening. *Proc Natl Acad Sci U S A, 106, 14195-14200.*

Burns, J. C.; Friedmann, T.; Driever, W.; Burrascano, M. & Yee, J. K. (1993). Vesicular stomatitis virus G glycoprotein pseudotyped retroviral vectors: concentration to very high titer and efficient gene transfer into mammalian and nonmammalian cells. *Proc Natl Acad Sci U S A, 90, 8033-8037.*

Burton, D. R. (2002). Antibodies, viruses and vaccines. *Nat Rev Immunol, 2,* 706-713.

Bushman, F. D. (2007). Retroviral integration and human gene therapy. *J Clin Invest, 117, 2083-2086.*

Battersby, B. J.; Lawrie, G. A.; Johnston, A. P. R. & Trau, M. (2002a). Optical barcoding of colloidal suspensions: applications in genomics, proteomics and drug discovery. *Chem Commun (Camb), 1435-1441.*

Cardo, D. M.; Culver, D. H.; Ciesielski, C. A.; Srivastava, P. U.; Marcus, R.; Abiteboul, D.; Heptonstall, J.; Ippolito, G.; Lot, F.; McKibben, P. S. & Bell, D. M. (1997a). A case-control study of HIV seroconversion in health care workers after percutaneous exposure. Centers for Disease Control and Prevention Needlestick Surveillance Group. *N Engl J Med, 337, 1485-1490.*

Casadevall, A.; Dadachova, E. & Pirofski, L. (2004). Passive antibody therapy for infectious diseases. *Nat Rev Microbiol, 2, 695-703.*

Chabert, M. & Viovy, J.-L. (2008). Microfluidic high-throughput encapsulation and hydrodynamic self-sorting of single cells. *Proc Natl Acad Sci U S A, Institut Curie, 105, 3191-3196.*

Chaga, G. S. (2008). Antibody arrays for determination of relative protein abundances. *Methods Mol Biol, 441, 129-151.*

Chan, D. C. & Kim, P. S. (1998b). HIV entry and its inhibition. *Cell, 93, 681-684.*

Chapman, T. (2004). Drug discovery: the leading edge. *Nature, 430, 109-115.*

Chen, D. L. & Ismagilov, R. F. (2006). Microfluidic cartridges preloaded with nanoliter plugs of reagents: an alternative to 96-well plates for screening. *Curr Opin Chem Biol, 10, 226-231.*

Chen, D. S. & Davis, M. M. (2006). Molecular and functional analysis using live cell microarrays. *Curr Opin Chem Biol, 10, 28-34.*

Chen, D. L. & Ismagilov, R. F. (2006). Microfluidic cartridges preloaded with nanoliter plugs of reagents: an alternative to 96-well plates for screening. *Curr Opin Chem Biol, 10, 226-231.*

Chen, G.; Way, J.; Armour, S.; Watson, C.; Queen, K.; Jayawickreme, C. K.; Chen, W. & Kenakin, T. (2000). Use of Constitutive G Protein-Coupled Receptor Activity for Drug Discovery. *Mol Pharm, 57:125–134.*

Clausell-Tormos, J.; Lieber, D.; Baret, J.-C.; El-Harrak, A.; Miller, O. J.; Frenz, L.; Blouwolff, J.; Humphry, K. J.; Köster, S.; Duan, H.; Holtze, C.; Weitz, D. A.; Griffiths, A. D. & Merten, C. A. (2008). Droplet-based microfluidic platforms for the encapsulation and screening of Mammalian cells and multicellular organisms. *Chem Biol, 15, 427-437.*

Clausell-Tormos, J.; Griffiths, A. D. & Merten, C. A. (2010). Coupling the inhibition of viral transduction with a positive fluorescence signal. *Comb Chem High Throughput Screen, 13, 352-357.*

Cohen, A. A.; Geva-Zatorsky, N.; Eden, E.; Frenkel-Morgenstern, M.; Issaeva, I.; Sigal, A.; Milo, R.; Cohen-Saidon, C.; Liron, Y.; Kam, Z.; Cohen, L.; Danon, T.; Perzov, N. & Alon, U. (2008). Dynamic proteomics of individual cancer cells in response to a drug. *Science, 322, 1511-1516.*

Cohenuram, M. & Saif, M. W. (2007a). Panitumumab the first fully human monoclonal antibody: from the bench to the clinic. *Anticancer Drugs, 18, 7-15.*

Daneholt, B. (2010). Advanced Information: The 2006 Nobel Prize in Physiology or Medicine. http://nobelprize.org/nobel_prizes/medicine/laureates/2006/adv.html

Danilov, S.; Jaspard, E.; Churakova, T.; Towbin, H.; Savoie, F.; Wei, L. & Alhenc-Gelas, F. (1994). Structure-function analysis of angiotensin I-converting enzyme using monoclonal antibodies. Selective inhibition of the amino-terminal active site. *J Biol Chem, 269, 26806-26814.*

Dilber, M. S.; Abedi, M. R.; Christensson, B.; Björkstrand, B.; Kidder, G. M.; Naus, C. C.; Gahrton, G. & Smith, C. I. (1991). Gap junctions promote the bystander effect of herpes simplex virus thymidine kinase in vivo. *Cancer Res, 57, 1523-1528.*

Dilber, M. S. & Smith, C. I. (1997). Suicide genes and bystander killing: local and distant effects. *Gene Ther, 4, 273-274.*

Ecker, J. R. & Davis, R. W. (1986a). Inhibition of gene expression in plant cells by expression of antisense RNA. *Proc Natl Acad Sci U S A, 83, 5372-5376.*

Edd, J. F.; Carlo, D. D.; Humphry, K. J.; Köster, S.; Irimia, D.; Weitz, D. A. & Toner, M. (2008). Controlled encapsulation of single-cells into monodisperse picolitre drops. *Lab Chip, 8, 1262-1264.*

Eren, R.; Landstein, D.; Terkieltaub, D.; Nussbaum, O.; Zauberman, A.; Ben-Porath, J.; Gopher, J.; Buchnick, R.; Kovjazin, R.; Rosenthal-Galili, Z.; Aviel, S.; Ilan, E.; Shoshany, Y.; Neville, L.; Waisman, T.; Ben-Moshe, O.; Kischitsky, A.; Foung, S. K. H.; Keck, Z.-Y.; Pappo, O.; Eid, A.; Jurim, O.; Zamir, G.; Galun, E. & Dagan, S. (2006). Preclinical evaluation of two neutralizing human monoclonal

antibodies against hepatitis C virus (HCV): a potential treatment to prevent HCV reinfection in liver transplant patients. *J Virol, 80, 2654-2664.*

Fallah et al., 2010, unpublished data.

Fehse, B.; Kustikova, O. S.; Li, Z.; Wahlers, A.; Bohn, W.; Beyer, W. R.; Chalmers, D.; Tiberghien, P.; Kühlcke, K.; Zander, A. R. & Baum, C. (2002). A novel 'sort-suicide' fusion gene vector for T cell manipulation. *Gene Ther, 9, 1633-1638.*

Fidalgo, L. M.; Whyte, G.; Ruotolo, B. T.; Benesch, J. L. P.; Stengel, F.; Abell, C.; Robinson, C. V. & Huck, W. T. S. (2009). Coupling microdroplet microreactors with mass spectrometry: reading the contents of single droplets online. *Angew Chem Int Ed Engl, 48, 3665-3668.*

Fire, A.; Xu, S.; Montgomery, M. K.; Kostas, S. A.; Driver, S. E. & Mello, C. C. (1998). Potent and specific genetic interference by double-stranded RNA in Caenorhabditis elegans. *Nature, 391, 806-811.*

Fischl, M. A.; Richman, D. D.; Grieco, M. H.; Gottlieb, M. S.; Volberding, P. A.; Laskin, O. L.; Leedom, J. M.; Groopman, J. E.; Mildvan, D. & Schooley, R. T. (1987). The efficacy of azidothymidine (AZT) in the treatment of patients with AIDS and AIDS-related complex. A double-blind, placebo-controlled trial. *N Engl J Med, 317, 185-191.*

Francis, P. T.; Palmer, A. M.; Snape, M. & Wilcock, G. K. (1999). The cholinergic hypothesis of Alzheimer's disease: a review of progress. *J Neurol Neurosurg Psychiatry, 66, 137-147.*

Frenz, L.; Harrak, A. E.; Pauly, M.; Bégin-Colin, S.; Griffiths, A. D. & Baret, J.-C. (2008). Droplet-based microreactors for the synthesis of magnetic iron oxide nanoparticles. *Angew Chem Int Ed Engl, 47, 6817-6820.*

Frickhofen, N.; Abkowitz, J. L.; Safford, M.; Berry, J. M.; de Mayolo, J. A.; Astrow, A.; Cohen, R.; Halperin, I.; King, L. & Mintzer, D. (1990). Persistent B19 parvovirus infection in patients infected with human immunodeficiency virus type 1 (HIV-1): a treatable cause of anemia in AIDS. *Ann Intern Med, 113, 926-933.*

Fu, A. Y.; Chou, H.-P.; Spence, C.; Arnold, F. H. & Quake, S. R. (2002c). An integrated microfabricated cell sorter. *Anal Chem, 74, 2451-2457.*

Gad, S. (2005). Drug Discovery Handbook. 1st Edition. Published by John Wiley & Sons, Inc., Hoboken, New Jersy.

Gallagher, J. R. (1935a). Use of Convalescent Measles Serum to Control Measles in a Preparatory School. *Am J Public Health Nations Health, 25, 595-598.*

Galun, E.; Eren, R.; Safadi, R.; Ashour, Y.; Terrault, N.; Keeffe, E. B.; Matot, E.; Mizrachi, S.; Terkieltaub, D.; Zohar, M.; Lubin, I.; Gopher, J.; Shouval, D. & Dagan, S. (2002). Clinical evaluation (phase I) of a combination of two human monoclonal antibodies to HBV: safety and antiviral properties. *Hepatology, 35, 673-679.*

González, J. E. & Negulescu, P. A. (1998). Intracellular detection assays for high-throughput screening. *Curr Opin Biotechnol, 9, 624-631.*

Gorny, M. K. & Zolla-Pazner, S. (2004). Human monoclonal antibodies that neutralize HIV-1. In: Korber, B. T. M.; Brander, C.; Haynes, B, F.; Koup, R.; Moore, J. P.; Walker, B. D.; Watkins, D. I. editors. *HIV Immunology and HIV/SIV Vaccine Databases 2003, pp. 37-51.*

Gottlieb, M. S.; Schanker, H. M.; Fan, P.T.; Saxon, A. & Weisman, J.D. (1981a). Pneumocystis pneumonia-Los Angeles. *MMWR Morb Mortal Wkly Rep, 30, 250-252.*

Gottlieb, M. S.; Schroff, R.; Schanker, H. M.; Weisman, J. D.; Fan, P. T.; Wolf, R. A. & Saxon, A. (1981b). Pneumocystis carinii pneumonia and mucosal candidiasis in previously healthy homosexual men: evidence of a new acquired cellular immunodeficiency. *N Engl J Med, 305, 1425-1431.*

Gottschalk, U. (2009). Process Scale Purification of Antibodies. 1st Edition. Published by John Wiley & Sons, Inc., Hoboken, New Jersy.

Graham, F. L. & van der Eb, A. J. (1973). A new technique for the assay of infectivity of human adenovirus 5 DNA. *Virology, 52, 456-467.*

Griffiths, A. D. & Tawfik, D. S. (2006). Miniaturising the laboratory in emulsion droplets. *Trends Biotechnol, 24, 395-402.*

Groothuis, J. R.; Simoes, E. A.; Levin, M. J.; Hall, C. B.; Long, C. E.; Rodriguez, W. J.; Arrobio, J.; Meissner, H. C.; Fulton, D. R. & Welliver, R. C. (1993). Prophylactic administration of respiratory syncytial virus immune globulin to high-risk infants and young children. The Respiratory Syncytial Virus Immune Globulin Study Group. *N Engl J Med, 329, 1524-1530.*

Haber, C. (2006). Microfluidics in commercial applications; an industry perspective. *Lab Chip, 6, 1118-112.*

Hammonds, J.; Chen, X.; Zhang, X.; Lee, F. & Spearman, P. (2007). Advances in methods for the production, purification, and characterization of HIV-1 Gag-Env pseudovirion vaccines. *Vaccine, 25, 8036-8048.*

Harris, L. J.; Larson, S. B.; Hasel, K. W.; Day, J.; Greenwood A. & McPherson, A. (1992). The three-dimensional structure of an intact monoclonal antibody for canine lymphoma. *Nature 360, 369 – 372.*

Hattwick, M. A.; Corey, L. & Creech, W. B. (1976a). Clinical use of human globulin immune to rabies virus. *J Infect Dis, 133 Suppl, A266-A272.*

He, M.; Edgar, J. S.; Jeffries, G. D. M.; Lorenz, R. M.; Shelby, J. P. & Chiu, D. T. (2005a). Selective encapsulation of single cells and subcellular organelles into picoliter- and femtoliter-volume droplets. *Anal Chem, 77, 1539-1544.*

Hebert, P. R.; Foody, J. M. & Hennekens, C. H. (2003). The renin-angiotensin system: the role of inhibitors, blockers, and genetic polymorphisms in the treatment and prevention of heart failure. *Curr Vasc Pharmacol, 1, 33-39.*

Hicar, M. D.; Chen, X.; Briney, B.; Hammonds, J.; Wang, J.-J.; Kalams, S.; Spearman, P. W. & Crowe, J. E. (2010). Pseudovirion particles bearing native HIV envelope trimers facilitate a novel method for generating human neutralizing monoclonal antibodies against HIV. *J Acquir Immune Defic Syndr, 54, 223-235.*

HIV Sequence Compendium. (2008).
http://www.hiv.lanl.gov/content/sequence/HIV/COMPENDIUM/2008/frontmatter.pdf.

Holland, A. U.; Munk, C.; Lucero, G. R.; Nguyen, L. D. & Landau, N. R. (2004). Alpha-complementation assay for HIV envelope glycoprotein-mediated fusion. *Virology, 319, 343-352.*

Holtze, C.; Rowat, A. C.; Agresti, J. J.; Hutchison, J. B.; Angilè, F. E.; Schmitz, C. H. J.; Köster, S.; Duan, H.; Humphry, K. J.; Scanga, R. A.; Johnson, J. S.; Pisignano, D. & Weitz, D. A. (2008). Biocompatible surfactants for water-in-fluorocarbon emulsions. *Lab Chip, 8, 1632-1639.*

Hooks, M. A.; Wade, C. S. & Millikan, W. J. (1991). Muromonab CD-3: a review of its pharmacology, pharmacokinetics, and clinical use in transplantation. *Pharmacotherapy, 11, 26-37.*

Hooper, N. M.; Karran, E. H. & Turner, A. J. (1997). Membrane protein secretases. *Biochem J, 321 (Pt 2), 265-279.*

http://www.abbottdiagnostics.de/images/content/file/MS_09_17658A_AACC_ScienceBook_booklet6_061709.pdf

http://www.aidsreagent.org/pdf_images/ 2237_001.pdf

http://www.fluidigm.com

http://www.genomics.sbg.ac.at/meth/cacl2_transfection.pdf

http://www.wiley.co.uk/genetherapy/clinical/

Huebner, A.; Srisa-Art, M.; Holt, D.; Abell, C.; Hollfelder, F.; deMello, A. J. & Edel, J. B. (2007). Quantitative detection of protein expression in single cells using droplet microfluidics. *Chem Commun (Camb), 1218-1220.*

Huebner, A.; Sharma, S.; Srisa-Art, M.; Hollfelder, F.; Edel, J. B. & Demello, A. J. (2008). Microdroplets: a sea of applications?. *Lab Chip, 8, 1244-1254.*

Hung, P. J.; Lee, P. J.; Sabounchi, P.; Lin, R. & Lee, L. P. (2005). Continuous perfusion microfluidic cell culture array for high-throughput cell-based assays. *Biotechnol Bioeng, 89, 1-8.*

Huang, W.-H.; Ai, F.; Wang, Z.-L. & Cheng, J.-K. (2008). Recent advances in single-cell analysis using capillary electrophoresis and microfluidic devices. *J Chromatogr B Analyt Technol Biomed Life Sci, 866, 104-122.*

Irish, J. M.; Hovland, R.; Krutzik, P. O.; Perez, O. D.; Bruserud, Ø.; Gjertsen, B. T. & Nolan, G. P. (2004). Single cell profiling of potentiated phospho-protein networks in cancer cells. *Cell, 118, 217-228.*

Izant, J. G. & Weintraub, H. (1984). Inhibition of thymidine kinase gene expression by anti-sense RNA: a molecular approach to genetic analysis. *Cell, 36, 1007-1015.*

Jegerlehner, A.; Tissot, A.; Lechner, F.; Sebbel, P.; Erdmann, I.; Kündig, T.; Bächi, T.; Storni, T.; Jennings, G.; Pumpens, P.; Renner, W. A. & Bachmann, M. F. (2002a). A molecular assembly system that renders antigens of choice highly repetitive for induction of protective B cell responses. *Vaccine, 20, 3104-3112.*

Jiang, S.; Lin, K.; Strick, N. & Neurath, A. R. (1993b). HIV-1 inhibition by a peptide. *Nature, 365, 113.*

Jiang, S.; Lu, H.; Liu, S.; Zhao, Q.; He, Y. & Debnath, A. K. (2004). N-substituted pyrrole derivatives as novel human immunodeficiency virus type 1 entry inhibitors that interfere with the gp41 six-helix bundle formation and block virus fusion. *Antimicrob Agents Chemother, 48, 4349-4359.*

Joanicot, M. & Ajdari, A. (2005). Applied physics. Droplet control for microfluidics. *Science, 309, 887-888.*

Johnston, K. P.; Harrison, K. L.; Clarke, M. J.; Howdle, S. M.; Heitz, M. P.; Bright F. V.; Carlier, C. & Randolph, T. W. (1996). Water-in-Carbon Dioxide Microemulsions: An Environment for Hydrophiles Including Proteins. *Science, Vol. 271. no. 5249, pp. 624 – 626.*

Johnston, P. A. & Johnston, P. A. (2002). Cellular platforms for HTS: three case studies. *Drug Discov Today, 7, 353-363.*

Judice, J. K.; Tom, J. Y.; Huang, W.; Wrin, T.; Vennari, J.; Petropoulos, C. J. & McDowell, R. S. (1997).

Inhibition of HIV type 1 infectivity by constrained alpha-helical peptides: implications for the viral fusion mechanism. *Proc Natl Acad Sci U S A, 94, 13426-13430.*

Junot, C.; Gonzales, M. F.; Ezan, E.; Cotton, J.; Vazeux, G.; Michaud, A.; Azizi, M.; Vassiliou, S.; Yiotakis, A.; Corvol, P. & Dive, V. (2001a). RXP 407, a selective inhibitor of the N-domain of angiotensin I-converting enzyme, blocks in vivo the degradation of hemoregulatory peptide acetyl-Ser-Asp-Lys-Pro with no effect on angiotensin I hydrolysis. *J Pharmacol Exp Ther, 297, 606-611.*

Kartalov, E. P.; Zhong, J. F.; Scherer, A.; Quake, S. R.; Taylor, C. R. & Anderson, W. F. (2006). High-throughput multi-antigen microfluidic fluorescence immunoassays. *BioTechniques, 40, 85-90.*

Kelly, B. T.; Baret, J.-C.; Taly, V. & Griffiths, A. D. (2007). Miniaturizing chemistry and biology in microdroplets. *Chem Commun (Camb), 1773-1788.*

Kilby, J. M.; Hopkins, S.; Venetta, T. M.; DiMassimo, B.; Cloud, G. A.; Lee, J. Y.; Alldredge, L.; Hunter, E.; Lambert, D.; Bolognesi, D.; Matthews, T.; Johnson, M. R.; Nowak, M. A.; Shaw, G. M. & Saag, M. S. (1998c). Potent suppression of HIV-1 replication in humans by T-20, a peptide inhibitor of gp41-mediated virus entry. *Nat Med, 1302-1307.*

Knappik, A.; Ge, L.; Honegger, A.; Pack, P.; Fischer, M.; Wellnhofer, G.; Hoess, A.; Wölle, J.; Plückthun, A. & Virnekäs, B. (2000). Fully synthetic human combinatorial antibody libraries (HuCAL) based on modular consensus frameworks and CDRs randomized with trinucleotides. *J Mol Biol, 296, 57-86.*

Koehler, G. & Milstein, C. (1975). Continuous cultures of fused cells secreting antibody of predefined specificity. *Nature 256, 495-497.*

Koshiba, T. & Chan, D. C. (2003b). The prefusogenic intermediate of HIV-1 gp41 contains exposed C-peptide regions. *J Biol Chem, 278, 7573-7579.*

Köster, S.; Angilè, F. E.; Duan, H.; Agresti, J. J.; Wintner, A.; Schmitz, C.; Rowat, A. C.; Merten, C. A.; Pisignano, D.; Griffiths, A. D. & Weitz, D. A. (2008). Drop-based microfluidic devices for encapsulation of single cells. *Lab Chip, 8, 1110-1115.*

Kopp, M. U.; Mello, A. J. & Manz, A. (1998). Chemical amplification: continuous-flow PCR on a chip. *Science, 280, 1046-1048.*

Laskowski, R. A.; Luscombe, N. M.; Swindells, M. B. & Thornton, J. M. (1996a). Protein clefts in molecular recognition and function. *Protein Sci, 5, 2438-2452.*

Lauwereys, M.; Ghahroudi, M. A.; Desmyter, A.; Kinne, J.; Hölzer, W.; Genst, E. D.; Wyns, L. & Muyldermans, S. (1998). Potent enzyme inhibitors derived from dromedary heavy-chain antibodies. *EMBO J, 17, 3512-3520.*

Lawrence, S. (2007). Billion dollar babies--biotech drugs as blockbusters. *Nat Biotechnol, 25, 380-382.*

Lechner, F.; Jegerlehner, A.; Tissot, A. C.; Maurer, P.; Sebbel, P.; Renner, W. A.; Jennings, G. T. & Bachmann, M. F. (2002). Virus-like particles as a modular system for novel vaccines. *Intervirology, 45, 212-217.*

Lewis, T. (1974). The Lives of a Cell: Notes of a Biology Watcher. *The Viking Press, Inc, New York, pp 5, 82.*

Li, L.; Mustafi, D.; Fu, Q.; Tereshko, V.; Chen, D. L.; Tice, J. D. & Ismagilov, R. F. (2006). Nanoliter microfluidic hybrid method for simultaneous screening and optimization validated with crystallization of membrane proteins. *Proc Natl Acad Sci U S A, 103, 19243-19248.*

Li, W.; Greener, J.; Voicu, D. & Kumacheva, E. (2009e). Multiple modular microfluidic (M3) reactors for the synthesis of polymer particles. *Lab Chip, 9, 2715-2721.*

Link, D. R.; Anna, S. L.; Weitz, D. A. & Stone, H. A. (2004). Geometrically mediated breakup of drops in microfluidic devices. *Phys Rev Lett, 92, 054503.*

Link, D. R.; Grasland-Mongrain, E.; Duri, A.; Sarrazin, F.; Cheng, Z.; Cristobal, G.; Marquez, M. & Weitz, D. A. 92006). Electric control of droplets in microfluidic devices. *Angew Chem Int Ed Engl, 45, 2556-2560.*

Lima, D. P. (1998). Synthesis of angiotensin-converting enzyme (ACE) inhibitors: an important class of antihypertensive drugsACE inhibitors are one of the most active classes of molecules that lower blood pressure. *Quím. Nova [online]. 1999, vol.22, n.3, pp. 375-381. ISSN 0100-4042.*

Love, J. C.; Ronan, J. L.; Grotenbreg, G. M.; van der Veen, A. G. & Ploegh, H. L. (2006). A microengraving method for rapid selection of single cells producing antigen-specific antibodies. *Nat Biotechnol, 24, 703-707.*

Lowe, K. C.; Davey, M. R. & Power, J. B. (1998). Perfluorochemicals: their applications and benefits to cell culture. *Trends Biotechnol, 16, 272-277.*

Maffia A. M.; Kariv I. & Oldenburg K. R. (1999). Miniaturization of a Mammalian Cell-Based Assay: Luciferase Reporter Gene Readout in a 3 Microliter 1536-Well Plate. *J Biomol Screen, 4, 137-142.*

Marcus, J. S.; Anderson, W. F. & Quake, S. R. (2006). Microfluidic single-cell mRNA isolation and analysis. *Anal Chem, 78, 3084-3089.*

Margulies, M.; Egholm, M.; Altman, W. E.; Attiya, S.; Bader, J. S.; Bemben, L. A.; Berka, J.; Braverman, M. S.; Chen, Y.-J.; Chen, Z.; Dewell, S. B.; Du, L.; Fierro, J. M.; Gomes, X. V.; Godwin, B. C.; He, W.; Helgesen, S.; Ho, C. H.; Ho, C. H.; Irzyk, G. P.; Jando, S. C.; Alenquer, M. L. I.; Jarvie, T. P.; Jirage, K. B.; Kim, J.-B.; Knight, J. R.; Lanza, J. R.; Leamon, J. H.; Lefkowitz, S. M.; Lei, M.; Li, J.; Lohman, K. L.; Lu, H.; Makhijani, V. B.; McDade, K. E.; McKenna, M. P.; Myers, E. W.; Nickerson, E.; Nobile, J. R.; Plant, R.; Puc, B. P.; Ronan, M. T.; Roth, G. T.; Sarkis, G. J.; Simons, J. F.; Simpson, J. W.; Srinivasan, M.; Tartaro, K. R.; Tomasz, A.; Vogt, K. A.; Volkmer, G. A.; Wang, S. H.; Wang, Y.; Weiner, M. P.; Yu, P.; Begley, R. F. & Rothberg, J. M. (2005c). Genome sequencing in microfabricated high-density picolitre reactors. *Nature, 437, 376-380.*

Marks, J. D.; Hoogenboom, H. R.; Bonnert, T. P.; McCafferty, J.; Griffiths, A. D. & Winter, G. (1991). By-passing immunization. Human antibodies from V-gene libraries displayed on phage. *J Mol Biol, 222, 581-597.*

Masur, H.; Michelis, M. A.; Greene, J. B.; Onorato, I.; Stouwe, R. A.; Holzman, R. S.; Wormser, G.; Brettman, L.; Lange, M.; Murray, H. W. & Cunningham-Rundles, S. (1981). An outbreak of community-acquired Pneumocystis carinii pneumonia: initial manifestation of cellular immune dysfunction. *N Engl J Med, 305, 1431-1438.*

Mazutis, L. (2009). Droplet-based microfluidics for protein evolution. Institut de Science et d'Ingénierie Supramoléculaires, Ph.D.: Université de Strasbourg (UdS), France.

Mazutis, L.; Baret, J.-C. & Griffiths, A. D. (2009a). A fast and efficient microfluidic system for highly selective one-to-one droplet fusion. *Lab Chip, 9, 2665-2672.*

McCafferty, J.; Griffiths, A. D.; Winter, G. & Chiswell, D. J. (1990). Phage antibodies: filamentous phage displaying antibody variable domains. *Nature, 348, 552-554.*

McClain, M. A.; Culbertson, C. T.; Jacobson, S. C.; Allbritton, N. L.; Sims, C. E. & Ramsey, J. M. (2003). Microfluidic devices for the high-throughput chemical analysis of cells. *Anal Chem, 75, 5646-5655.*

McDonald, J. C.; Duffy, D. C.; Anderson, J. R.; Chiu, D. T.; Wu, H.; Schueller, O. J. & Whitesides, G. M. (2000). Fabrication of microfluidic systems in poly(dimethylsiloxane). *Electrophoresis, 21, 27-40.*

McGory, R. W.; Ishitani, M. B.; Oliveira, W. M.; Stevenson, W. C.; McCullough, C. S.; Dickson, R. C.; Caldwell, S. H. & Pruett, T. L. (1996a). Improved outcome of orthotopic liver transplantation for chronic hepatitis B cirrhosis with aggressive passive immunization. *Transplantation, 61, 1358-1364.*

Merten, C. A.; Stitz, J.; Braun, G.; Medvedovska, J.; Cichutek, K. & Buchholz, C. J. (2006). Fusoselect: cell-cell fusion activity engineered by directed evolution of a retroviral glycoprotein. *Nucleic Acids Res, 34, e4.*

Miles, R. W.; Tyler, P. C.; Furneaux, R. H.; Bagdassarian, C. K. & Schramm, V. L. (1998). One-third-the-sites transition-state inhibitors for purine nucleoside phosphorylase. *Biochemistry, 37, 8615-8621.*

Miller, O. J.; Bernath, K.; Agresti, J. J.; Amitai, G.; Kelly, B. T.; Mastrobattista, E.; Taly, V.; Magdassi, S.; Tawfik, D. S. & Griffiths, A. D. (2006). Directed evolution by in vitro compartmentalization. *Nat Methods, 3, 561-570.*

Mo, H.; Stamatatos, L.; Ip, J. E.; Barbas, C. F.; Parren, P. W.; Burton, D. R.; Moore, J. P. & Ho, D. D. (1997). Human immunodeficiency virus type 1 mutants that escape neutralization by human monoclonal antibody IgG1b12. off. *J Virol, 71, 6869-6874.*

Naperova, I. A.; Baliasnikova, I. V.; Petrov, M. N.; Vakhitova, A. V.; Evdokimov, V. V.; Danilov, S. M. & Kost, O. A. (2008). Characteristics of monoclonal antibody binding with the C domain of human angiotensin converting enzyme. *Bioorg Khim, 34, 358-364.*

Napoli, C.; Lemieux, C. & Jorgensen, R. (1990). Introduction of a Chimeric Chalcone Synthase Gene into Petunia Results in Reversible Co-Suppression of Homologous Genes in trans. *Plant Cell, 2, 279-289.*

Natesh, R.; Schwager, S. L. U.; Sturrock, E. D. & Acharya, K. R. (2003). Crystal structure of the human angiotensin-converting enzyme-lisinopril complex. *Nature, 421, 551-554.*

National Institute of Allergy and Infectious Diseases (NIAID). (last updated March 2009). http://www.niaid.nih.gov/topics/HIVAIDS/Understanding/Biology/pages/structure.aspx; http://www.niaid.nih.gov/topics/HIVAIDS/Understanding/Biology/pages/hivreplicationcycle.aspx.

Nellen, W. & Lichtenstein, C. (1993). What makes an mRNA anti-sense-itive? *Trends Biochem Sci, 18, 419-423.*

Nelson, P. N.; Reynolds, G. M.; Waldron, E. E.; Ward, E.; Giannopoulos, K. & Murray, P. G. (2000). Monoclonal antibodies. *Mol Pathol, 53, 111-117.*

Nikol, S. & Hoefling, B. (1996). Aktueller Stand der Gentherapie. *Dt Aerztebl, 93, A-2620-2628.*

Nossal, G. J. & Lederberg, J. (1958). Antibody production by single cells. *Nature, 181, 1419-1420.*

Oldenburg, K. R.; Zhang, J.-H.; Chen, T.; Maffia, A. M.; Blom, K. F.; Combs, A. P. & Chung, T. D. Y. (1998). Libraries: A 9600-Well (0.2 Microliter) Assay System Assay Miniaturization for Ultra-High Throughput Screening of Combinatorial and Discrete Compound. *J Biomol Screen 1998; 3; 55.*

Pang, W.; Wang, R.-R.; Yang, L.-M.; Liu, C.-M.; Tien, P. & Zheng, Y.-T. (2008). Recombinant protein of heptad-repeat HR212, a stable fusion inhibitor with potent anti-HIV action in vitro. *Virology, 377, 80-87.*

Parren, P. W. & Burton, D. R. (2001a). The antiviral activity of antibodies in vitro and in vivo. *Adv Immunol, 77, 195-262.*

Parren, P. W.; Wang, M.; Trkola, A.; Binley, J. M.; Purtscher, M.; Katinger, H.; Moore, J. P. & Burton, D. R. (1998). Antibody neutralization-resistant primary isolates of human immunodeficiency virus type 1. *J Virol, 72, 10270-10274.*

Paul, W. E. (1993). Fundamental Immunology. 6th edition (2008). Lippincott Williams & Wilkins. Philadelphia, USA.

Pauling, L. (1940). A Theory of the Structure and Process of Formation of Antibodies. *Journal of the American Chemical Society, 62 (1940): 2643-2657.*

Pereira, D. A. & Williams, J. A. (2007). Origin and evolution of high throughput screening. *Br J Pharmacol, D, 152, 53-61.*

Polonis, V. R.; Brown, B. K.; Borges, A. R.; Zolla-Pazner, S.; Dimitrov, D. S.; Zhang, M.-Y.; Barnett, S. W.; Ruprecht, R. M.; Scarlatti, G.; Fenyö, E.-M.; Montefiori, D. C.; McCutchan, F. E. & Michael, N. L. (2008). Recent advances in the characterization of HIV-1 neutralization assays for standardized evaluation of the antibody response to infection and vaccination. *Virology, 375, 315-320.*

Popovic, M.; Sarngadharan, M. G.; Read, E. & Gallo, R. C. (1984c). Detection, isolation, and continuous production of cytopathic retroviruses (HTLV-III) from patients with AIDS and pre-AIDS. *Science, 224, 497-500.*

Pozzo, F. D.; Andrei, G.; Daelemans, D.; Winkler, M.; Piette, J.; Clercq, E. D. & Snoeck, R. (2008). Fluorescence-based antiviral assay for the evaluation of compounds against vaccinia virus, varicella zoster virus and human cytomegalovirus. *J Virol Methods, 151, 66-73.*

Pregibon, D. C.; Toner, M. & Doyle, P. S. (2007). Multifunctional encoded particles for high-throughput biomolecule analysis. *Science, 315, 1393-1396.*

Pyle, S. W.; Bess, J. W.; Robey, W. G.; Fischinger, P. J.; Gilden, R. V. & Arthur, L. O. (1987). Purification of 120,000 dalton envelope glycoprotein from culture fluids of human immunodeficiency virus (HIV)-infected H9 cells. *AIDS Res Hum Retroviruses, 3, 387-40.*

Randow, F. & Sale, J. E. (2006). Retroviral transduction of DT40. *Subcell Biochem, 40, 383-386.*

Remy, M. H.; Frobert, Y. & Grassi, J. (1995). Characterization of monoclonal antibodies that strongly inhibit Electrophorus electricus acetylcholinesterase. *Eur J Biochem, 231, 651-658.*

Ringia, E. A. T.; Tyler, P. C.; Evans, G. B.; Furneaux, R. H.; Murkin, A. S. & Schramm, V. L. (2006a). Transition state analogue discrimination by related purine nucleoside phosphorylases. *J Am Chem Soc, 128, 7126-7127.*

Riss, T. (2005). Selecting cell-based asays for drug discovery screening. *Promega Coporation, Cell Notes, 13.*

Rusche, J. R.; Javaherian, K.; McDanal, C.; Petro, J.; Lynn, D. L.; Grimaila, R.; Langlois, A.; Gallo, R. C.; Arthur, L. O. & Fischinger, P. J. (1988). Antibodies that inhibit fusion of human immunodeficiency virus-infected cells bind a 24-amino acid sequence of the viral envelope, gp120. *Proc Natl Acad Sci U S A, 85, 3198-3202.*

Sáez-Llorens, X.; Castaño, E.; Null, D.; Steichen, J.; Sánchez, P. J.; Ramilo, O.; Top, F. H. & Connor, E. (1998a). Safety and pharmacokinetics of an intramuscular humanized monoclonal antibody to respiratory

syncytial virus in premature infants and infants with bronchopulmonary dysplasia. The MEDI-493 Study Group. *Pediatr Infect Dis J, 17, 787-791.*

Sadtler, V.M.; Jeanneaux, F.; Krafft, M.P.; Rabai, J. & Riess, J.G. (1998). Perfluoroalkylated amphiphiles with monomorpholinophosphate or dimorpholinophosphate polar head group. *New J Chem 22, pp. 609–613.*

Saeki, K.; Yuo, A.; Kato, M.; Miyazono, K.; Yazaki, Y. & Takaku, F. (1997). Cell density-dependent apoptosis in HL-60 cells, which is mediated by an unknown soluble factor, is inhibited by transforming growth factor beta1 and overexpression of Bcl-2. *J Biol Chem, 272, 20003-20010.*

Saiki, R. K.; Scharf, S.; Faloona, F.; Mullis, K. B.; Horn, G. T.; Erlich, H. A. & Arnheim, N. (1985). Enzymatic amplification of beta-globin genomic sequences and restriction site analysis for diagnosis of sickle cell anemia. *Science, 230, 1350-1354.*

Sanders, D. A. (2002). No false start for novel pseudotyped vectors. *Curr Opin Biotechnol, 13, 437-442.*

Sanger, F.; Nicklen, S. & Coulson, A. R. (1977). DNA sequencing with chain-terminating inhibitors. *Proc Natl Acad Sci U S A, 74, 5463-5467.*

Schaerli, Y.; Wootton, R. C.; Robinson, T.; Stein, V.; Dunsby, C.; Neil, M. A. A.; French, P. M. W.; Demello, A. J.; Abell, C. & Hollfelder, F. (2009a). Continuous-flow polymerase chain reaction of single-copy DNA in microfluidic microdroplets. *Anal Chem, 81, 302-306.*

Schneider, J.; Kaaden, O.; Copeland, T. D.; Oroszlan, S. & Hunsmann, G. (1986). Shedding and interspecies type sero-reactivity of the envelope glycopolypeptide gp120 of the human immunodeficiency virus. *J Gen Virol, 67 (Pt 11), 2533-2538.*

Seo, J. K.; Kim, H. K.; Lee, T. Y.; Hahm, K.-S.; Kim, K. L. & Lee, M. K. (2005). Stronger anti-HIV-1 activity of C-peptide derived from HIV-1 89.6 gp41 C-terminal heptad repeated sequence. *Peptides, 26, 2175-2181.*

Siegal, F. P.; Lopez, C.; Hammer, G. S.; Brown, A. E.; Kornfeld, S. J.; Gold, J.; Hassett, J.; Hirschman, S. Z.; Cunningham-Rundles, C. & Adelsberg, B. R. (1981). Severe acquired immunodeficiency in male homosexuals, manifested by chronic perianal ulcerative herpes simplex lesions. *N Engl J Med, 305, 1439-1444.*

Siegert, S.; Thaler, S.; Wagner, R. & Schnierle, B. S. (2005). Assessment of HIV-1 entry inhibitors by MLV/HIV-1 pseudo-typed vectors. *AIDS Res Ther, 2, 7.*

Simon, S.; Goff, A. L.; Frobert, Y.; Grassi, J. & Massoulié, J. (1999). The binding sites of inhibitory monoclonal antibodies on acetylcholinesterase. Identification of a novel regulatory site at the putative "back door". *J Biol Chem, 274, 27740-27746.*

Smith, G. P. (1985). Filamentous fusion phage: novel expression vectors that display cloned antigens on the virion surface. *Science, 228, 1315-1317.*

Song, H.; Tice, J. D. & Ismagilov, R. F. (2003b). A microfluidic system for controlling reaction networks in time. *Angew Chem Int Ed Engl, 42, 768-772.*

Song, H.; Bringer, M. R.; Tice, J. D.; Gerdts, C. J. & Ismagilov, R. F. (2003). Experimental test of scaling of mixing by chaotic advection in droplets moving through microfluidic channels. *Appl Phys Lett, 83, 4664-4666.*

Song, I.-H.; Caplan, A. I. & Dennis, J. E. (2009). Dexamethasone inhibition of confluence-induced apoptosis in human mesenchymal stem cells. *J Orthop Res, 27, 216-221.*

Squires, T. M. & Quake, S. R. (2005). Microfluidics: Fluid physics at the nanoliter scale. *Rev Mod Phys, 77, 977-1026.*

Stephan, M. M. (2005). Microfluidics Meets its Market, Lab-on-a-chip companies gain momentum by a process of constant evolution. *The Scientist, 19(10):28.*

Stitz, J.; Mühlebach, M. D.; Blömer, U.; Scherr, M.; Selbert, M.; Wehner, P.; Steidl, S.; Schmitt, I.; König, R.; Schweizer, M. & Cichutek, K. (2001). A novel lentivirus vector derived from apathogenic simian immunodeficiency virus. *Virology, 291, 191-197.*

Sundberg, S. A. (200i). High-throughput and ultra-high-throughput screening: solution- and cell-based approaches. *Curr Opin Biotechnol, 11, 47-53.*

Sung, V. M. H. & Lai, M. M. C. (2002). Murine retroviral pseudotype virus containing hepatitis B virus large and small surface antigens confers specific tropism for primary human hepatocytes: a potential liver-specific targeting system. *J Virol, 76, 912-917.*

Tan, Y.-C.; Hettiarachchi, K.; Siu, M.; Pan, Y.-R. & Lee, A. P. (2006).Controlled microfluidic encapsulation of cells, proteins, and microbeads in lipid vesicles. *J Am Chem Soc, 128, 5656-5658.*

Tawfik, D. S. & Griffiths, A. D. (1998). Man-made cell-like compartments for molecular evolution. *Nat Biotechnol, 16, 652-656.*

Taylor, G. (1953). Dispersion of Soluble Matter in Solvent Flowing Slowly through a Tube. *Proc R Soc Lond A, 219, 186-20.*

Terry, A. V. & Buccafusco, J. J. (2003). The cholinergic hypothesis of age and Alzheimer's disease-related cognitive deficits: recent challenges and their implications for novel drug development. *J Pharmacol Exp Ther, 306, 821-827.*

Tewhey, R.; Warner, J. B.; Nakano, M.; Libby, B.; Medkova, M.; David, P. H.; Kotsopoulos, S. K.; Samuels, M. L.; Hutchison, J. B.; Larson, J. W.; Topol, E. J.; Weiner, M. P.; Harismendy, O.; Olson, J.; Link, D. R. & Frazer, K. A. (2009). Microdroplet-based PCR enrichment for large-scale targeted sequencing. *Nat Biotechnol, 27, 1025-1031.*

Thorsen, T.; Maerkl, S. J. & Quake, S. R. (2002) Microfluidic large-scale integration. *Science, 298, 580-584.*

Thorsen, T.; Roberts, R. W.; Arnold, F. H. & Quake, S. R. (2001). Dynamic pattern formation in a vesicle-generating microfluidic device. *Phys Rev Lett, 86, 4163-4166.*

Tissot, A. C.; Maurer, P.; Nussberger, J.; Sabat, R.; Pfister, T.; Ignatenko, S.; Volk, H.-D.; Stocker, H.; Müller, P.; Jennings, G. T.; Wagner, F. & Bachmann, M. F. (2008c). Effect of immunisation against angiotensin II with CYT006-AngQb on ambulatory blood pressure: a double-blind, randomised, placebo-controlled phase IIa study. *Lancet, 371, 821-827.*

Toriello, N. M.; Douglas, E. S.; Thaitrong, N.; Hsiao, S. C.; Francis, M. B.; Bertozzi, C. R. & Mathies, R. A. (2008). Integrated microfluidic bioprocessor for single-cell gene expression analysis. *Proc Natl Acad Sci U S A, 105, 20173-20178.*

Trajcevski, S.; Solly, S. K.; Frisén, C.; Trenado, A.; Cosset, F.-L. & Klatzmann, D. (2005). Characterization of a semi-replicative gene delivery system allowing propagation of complementary defective retroviral vectors. *J Gene Med, 7, 276-287.*

Umbanhowar, P. B.; Prasad, V. & Weitz, D. A. (2000). Monodisperse Emulsion Generation via Drop Break Off in a Coflowing Stream. *Langmuir, 16, 347-351.*

Villarino, A.; Bouvet, O. M.; Regnault, B.; Martin-Delautre, S. & PAD, G. (2000). Exploring the frontier between life and death in Escherichia coli: evaluation of different viability markers in live and heat- or UV-killed cells. *Res Microbiol, Aquabiolab, 151, 755-768.*

Viret, C. & Gurr, W. (2009). The origin of the "one cell-one antibody" rule. *J Immunol, 182, 1229-1230.*

Webster, D. M.; Henry, A. H. & Rees, A.R. (1994). Antibody-antigen interactions. *Curr Opin Struc Biol, 4, 123-129.*

Wei, L.; Clauser, E.; Alhenc-Gelas, F. & Corvol, P. (1992). The two homologous domains of human angiotensin I-converting enzyme interact differently with competitive inhibitors. *J Biol Chem, 267, 13398-13405.*

Westby, M.; Nakayama, G. R.; Butler, S. L. & Blair, W. S. (2005b). Cell-based and biochemical screening approaches for the discovery of novel HIV-1 inhibitors. *Antiviral Res, 67, 121-140.*

Wheeler, A. R.; Throndset, W. R.; Whelan, R. J.; Leach, A. M.; Zare, R. N.; Liao, Y. H.; Farrell, K.; Manger, I. D. & Daridon, A. (2003). Microfluidic device for single-cell analysis. *Anal Chem, 75, 3581-3586.*

Whitesides, G. M.; Ostuni, E.; Takayama, S.; Jiang, X. & Ingber, D. E. (2001). Soft lithography in biology and biochemistry. *Annu Rev Biomed Eng, 3, 335-373.*

Whitesides, G. M. (2006). The origins and the future of microfluidics. *Nature, 442, 368-373.*

Wild, C.; Oas, T.; McDanal, C.; Bolognesi, D. & Matthews, T. (1992). A synthetic peptide inhibitor of human immunodeficiency virus replication: correlation between solution structure and viral inhibition. *Proc Natl Acad Sci U S A, 89, 10537-10541.*

Wild, C.; Greenwell, T. & Matthews, T. (1993). A synthetic peptide from HIV-1 gp41 is a potent inhibitor of virus-mediated cell-cell fusion. *AIDS Res Hum Retroviruses, 9, 1051-1053.*

Wild, C. T.; Shugars, D. C.; Greenwell, T. K.; McDanal, C. B. & Matthews, T. J. (1994). Peptides corresponding to a predictive alpha-helical domain of human immunodeficiency virus type 1 gp41 are potent inhibitors of virus infection. *Proc Natl Acad Sci U S A, 91, 9770-9774.*

Williams, T. A.; Corvol, P. & Soubrier, F. (1994b). Identification of two active site residues in human angiotensin I-converting enzyme. *J Biol Chem, 269, 29430-29434.*

World Health Organization (2010). WHO report: HIV/AIDS programme highlights 2008-2009. *ISBN: 978 92 4 159945 0.*

Xia, Y. & Whitesides, G. M. (1998). Soft Litography. *Annu Rev Matter Sci, 28, 153-84.*

(WO/2006/082385) SCREENING METHOD.

Zheng, B.; Roach, L. S. & Ismagilov, R. F. (2003). Screening of protein crystallization conditions on a microfluidic chip using nanoliter-size droplets. *J Am Chem Soc, 125, 11170-11171.*